

# Taphonomic Markers and 3D-Modelling

A Non-Intrusive Method for Micromorphological  
Distinction of Metal and Stone Butchering Tools



**LUNDS**  
UNIVERSITET

**Gianni Bello Cifuentes**

ARKM23, Archaeology and Ancient History:

Master's Thesis - Historical Osteology

Supervisors: Adam Boethius and Giacomo Landeschi

Department of Archaeology and Ancient History

Lund University, Spring 2021

## Abstract

Digital tools in (zoo)archaeology have great potential for education, mediation, and research. Microphotogrammetric 3D-modeling offers new non-intrusive analytical approaches to old problems and questions. This thesis aimed to perform morphological differentiation between cut marks made from lithic and metal tool using qualitative and statistical quantitative approaches (Principal Component Analysis).

Osteoarchaeological material with cut marks from three Swedish sites were used: Huseby Klev (Mesolithic), Gamla Skogsby (Iron Age), and Falsterbo (Medieval). Modern material from lamb (*Ovis aries*) were subjected to experimental cutting (slicing action) using a steel knife, unretouched flint, uniface flint, and biface flint. All specimens were modelled using a digital camera with a macro lens, resulting models of the archaeological and modern material were compared to each other. Models of the modern material cut with flint tools were unusable for comparison, only steel cut marks yielded useful results. The archaeological material was qualitatively distinct from each other and from the steel knife cut marks. The PCA results demonstrates this distinction, displaying clear data clustering between the archaeological and modern specimens. The qualitative results also confirmed the archaeological cut marks to be the outcome of chopping action, not slicing action.

Despite a small sample size, inability to compare modern lithic tools, as well as acquisitional and experimental parameters which should be further refined to produce usable models, it is demonstrated that microphotogrammetry can be a viable method for differentiating cut marks made from different materials. It is a suitable analytical tool for sites and contexts in which metal and lithic cutting instruments may overlap.

**Keywords:** Osteology, Experimental Archaeology, 3D-modelling, Photogrammetry, Microphotogrammetry, Taphonomy, Bone Surface Modification, Cut Marks, Butchery Patterns, Digital Visualisation, Digital Zooarchaeology, Digital Osteology

## Acknowledgement

Many thanks to my supervisor Adam Boethius for valuable feedback, suggestions, and sense of direction, and to my co-supervisor Giacomo Landeschi for suggestions and technical advice. Thanks to Domenica Dininno and Fredrik Ekengren for help accessing the hardware, thanks to Linn Reinhold, Thomas Larsson, and Lina Andersson for help acquiring osteological material. Thanks to Daniel Forsberg and Filip Johnstone for helpful advice regarding the method. Many thanks to Henrik Bernro and Andra Tudor for company, support, and banter down in the osteology lab.

## Preface

With the benefit of hindsight, I realise that the words “3D-modelling” in the title are not the most representative. “Digital modelling” or “computer vision” would have been more suitable.

## List of Figures, Tables and Abbreviations

All pictures, models, and illustrations are by the author unless otherwise stated.

### **Figures, photographs, illustrations & screenshots**

**Figure 1.** Illustration depicting the anatomical distribution of cut marks commonly found on sheep (*Ovis aries*) from archaeological contexts. Based on the works of Larje (1992) and Kivikero (2019).

**Figure 2.** Collage of images from Walker & Long (1977) and Greenfield (1998). Cross-sectional view of cut mark grooves. A & B) Metal tools, C & D) Lithic tools.

**Figure 3.** Illustration depicting landmarks on the cut mark profile which were used for statistical analysis, these are the parameters set by Bello and Soligo (2008) but further refined and expanded. Image based on Maté-González et al (2016)

**Figure 4.** Collection of soft and hard hammers used for knapping experimental flint tools. Left to right: antlers from roe deer (*Capreolus capreolus*) and red deer (*Cervus elaphus*), hard hammer stone and abrader.

**Figure 5.** Collage of cutting instruments used in thesis experiment. A) All-purpose steel knife, B) unretouched heavy point/flake, C) uniface blade, D) biface drill/awl.

**Figure 6.** Fresh lamb radii and ribs on the day of procurement.

**Figure 7.** Collage of fresh cut marks. A and B) Cuts made transverse across the surface of the bone using steel and unretouched flint respectively, C) overhead view of cut marks. Photograph: Daniel Forsberg (A and B) and Gianni Bello Cifuentes (C, plus editing).

**Figure 8.** Collage of the archaeological bone material used as a basis for comparison, left to right: bear phalange from Huseby Klev, a hitherto unidentified long bone fragment from Gamla Skogsby, and bovine rib from Falsterbo.

**Figure 9.** Photograph depicting the acquisition set up: digital camera, lightbox, tripod, and improvised stand (lid from a boardgame on top of a book) to provide optimal distance between lens and object. Pictured is the Huseby Klev bear phalange. It was balanced on top of a piece of rubber eraser to provide better acquisition angle. A millimetre-scale (10x10mm) was placed on top of the bone, next to the cut mark.

**Figure 10.** Screenshot collage from Metashape showing the relative positioning of the camera during acquisition. Pictured is the cropped dense cloud of cut mark Steel #4.

**Figure 11.** Workflow for creating the photogrammetric models.

**Figure 12.** Screenshot of Cloud Compare where the upper envelope-line (green line) of the Gamla Skogsby cut mark's profile has been drawn and upon which three points of measurements have been selected. The data visible in this screenshot was not used as this

was a trial run to acquaint myself with the program. The final data that was used is provided in appendix II.

**Figure 13.** Illustration showing trigonometry used for calculating the depth of the incisions. Area is automatically given when placing the three measurements points in Cloud Compare.

**Figure 14.** Comparison between moderns cut marks: steel cut mark #8 (left) and unretouched flint cut mark #4 (right).

**Figure 15.** Example of cut marks with parallel grooves made by retouched flint tools. Uniface cutmark #2 on the left and biface cut marks #5 on the right.

**Figure 16.** Screenshots from Cloud Compare, two different angles of cut mark Steel #4's dense cloud which has prominent ridges/shoulders on both sides of the groove.

**Figure 17.** Screenshot collage from Cloud Compare of the unusable Data Point Clouds of the experimental cut marks. Upper envelope-lines have been rendered on both the X- and Y-axis of the cut mark for easier visualisation of the problems encountered regarding depth.

**Figure 18.** Screenshot collage - Comparison of the textured models

**Figure 19.** Comparison of the three archaeological cut marks profile. Same portion of where the 10 cross-sections were measured for the statistical analysis.

**Figure 20.** Graph - PCA scatter plot based on the average values from the 10 cross-sections on each specimen, using 4 components.

**Figure 21.** Graph - PCA scatter plot using 10 cross-sections using four components.

**Figure 22.** Graph - PCA scatter plot using 10 slices but only two components.

**Figure 23.** Graph - Non-PCA scatter plot using the WIS and Depth measurements.

## **Tables**

**Table 1.** Description of cutting instruments.

**Table 2.** Technical data of photographs used for point cloud and model creation.

**Table 3.** Summarised assessment of specimen Dense Point Clouds.

## **Abbreviations**

**DPC** – Dense Point Cloud

**PCA** – Principal Component Analysis

**WIS** – Width of the Incision at the Surface

**WIM** – Width of the Incision at the Mean

**WIB** – Width of the Incision at the Bottom

**OA** – Opening Angle of the incision

**LDC** – Left Depth of the incision Convergent

**RDC** – Right Depth of the incision Convergent

## Table of content

Abstract .....	ii
Acknowledgement.....	iii
Preface.....	iii
List of Figures, Tables and Abbreviations.....	iv
1. Introduction .....	1
1.1. Ethics, Posterity, and Legality.....	3
1.2. Aims, Purpose, Research Questions, and Limitation.....	5
1.3. Theoretical Framework and Perspective.....	6
1.4. Research History.....	8
1.4.1. Experimental Archaeology and Butchering Patterns .....	8
1.4.2. Osteological 3D-modelling .....	13
2. Material and Method.....	17
2.1. Experimental Material and Method .....	17
2.1.1. Archaeological material.....	20
2.2. Digital Material and Method .....	21
2.3. Quantifying Cut Mark Morphology .....	25
3. Results.....	28
3.1. Preliminary Ocular Assessment on the Macro Scale.....	28
3.2. Assessment of the Digital Models .....	30
3.3. Qualitative Comparisons of Dense Point Clouds.....	33
3.4. Quantitative Results – Principal Component Analysis .....	35
4. Discussion.....	38
4.1. Discussion of Methodology and Results.....	38
4.2. Sources of Error and Future Research.....	42
5. Conclusion.....	44
6. REFERENCES .....	46
PUBLISHED SOURCES .....	46
UNPUBLISHED/PENDING SOURCE .....	53
ONLINE RESOURCE .....	53
7. APPENDICES .....	54
Appendix I - HUSEBY KLEV DATABASE.....	54
Appendix II - CUT MARK MEASUREMENTS.....	55
Appendix III - SPSS PCA OUTPUT LOG.....	57
Appendix IV – Metashape Reports .....	77

## 1. Introduction

Osteology and archaeology are fast adopting digital tools for use in mediation, education, conservation, and research. At their core, these tools and their different uses are built around the same purpose: documentation. Digital recording methods has afforded us many new possibilities with which to conduct analysis. 3D-visualisations allows for data to be made more comprehensible and accessible. They may also be used for highlighting, contrasting and identifying features and landmarks, be it in a single excavation trench, an entire landscape, or on artefacts and bones (Verhoeven 2011; Edgeworth 2014; Forte *et al* 2015; Macheridis 2015; Wilhelmson & Dell'Unto 2015; Ostrowski & Hanus 2016; Dell'Unto *et al* 2017; Means 2017; Polig 2017; Dell'Unto 2018; Derudas *et al* 2018).

Digital tools may seem to be at odds with osteological research which is highly dependent on direct interaction with the material. Standardized methods and terminology exist for cataloguing, describing, and quantifying any observed pathologies and taphonomy (Behrensmeyer 1978; Buikstra & Dewitte 2019). Yet non-invasive and non-destructive methods are always preferable when conducting research on fragile material. The field of medicine frequently make use of such methods to peer inside a patient's body for diagnostic purposes. X-rays, computed tomography (CT) and Magnetic Resonance Imaging (MRI) are used diligently on a variety of archaeological material. In these cases, both pathological and taphonomic changes are captured. 3D-models based on these high-resolution techniques have great potential for both researchers and students. Although the cost and logistics of housing machines with such capabilities are often prohibitive for archaeologists, their usefulness when researching paleopathologies is undeniable (Ramsthaler, Kettner & Verhoff 2010; Micciché, Carotenuto & Sineo 2018; Ohno & Kawakubo 2019; Villa, Frohlich & Lynnerup 2019).

3D-visualisations technologies have been applied on animal and human remains for a variety of different purposes: morphologically distinguishing harp seal and ringed seal (Macāne 2012), attributing human skull trauma to a polar bear (Ryan *et al* 2014), creating reference 3D-models of extinct species of animals for educational purposes (Manzano *et al* 2015), morphologically identifying horses, donkeys and mules in archaeological context (Hanot *et al* 2016), morphometric analysis differentiating fossil remains of dogs and wolves (Drake *et al*



2017), quantifying the evolutionary morphology of bats (Giacomini *et al* 2019), identifying early reindeer domestication via forelimb morphology (Pelletier *et al* 2020). Case studies conducting quantitative micromorphological analysis of cut marks on animal remains have used different types of passive and active sensors when conducting 3D-data acquisition. The photogrammetric and laser scanning equipment vary between highly advanced optical 3D-imaging technology such as the Alicona 3D InfiniteFocus Imaging Microscope (Bello & Soligo 2008; Bello, Parfitt & Stringer 2009; Bello 2011; Bello *et al* 2011) and the Nanofocus  $\mu$ surf Mobile 3D Surface Measurement System (Otárola-Castillo *et al* 2017), to different types of metrological and structured light laser scanning devices (Maté-González *et al* 2015; Courtenay *et al* 2018). Even relatively simple methods such as using a tripod mounted digital camera coupled with a macro lens have been used with great success (Maté-González *et al* 2015; 2016).

Using non-invasive methods, as in the case studies presented above, is of vital interest in order to preserve the fragile material for future studies. Despite accurate recreation of taphonomic markers down to the microscopic level using silicon moulds, improper handling when applying any material for the purpose of making a cast may alter or even damage the morphology of the markers (Bello *et al* 2011). This concern is especially true in regard to fragile material. Anthropogenic climate change is a great challenge but also opportunity for archaeology to be employed for social good and to understand the changes from a historical perspective (Costanza *et al* 2007; Hudsun *et al* 2012). Climate change has also affected the conditions for preservation at many different locations. A few examples are the sites around the Ageröd basin. The osteological material from these sites have long held valuable information about the Scandinavian Mesolithic. The sites offered remarkable conditions for preservation until relatively recently when human induced climate change has provoked acidification in the soil in and around the Ageröd basin. Comparative studies of material excavated in the 1940's, 1970's and in 2019 have revealed rapid deterioration in the level of preservation of the osteological material (Boethius *et al* 2020). Continued alteration of soil conditions due to the extreme and erratic weather conditions brought upon by man-made climate change may render bones fragile and prone to disintegration when removed from situ. Hence the need for developing non-intrusive methodologies of equal or greater

analytical value than traditional methodologies which require direct handling of original material.

At the time of writing this thesis, the Covid-19 pandemic still halts much intra- and international travel, making the ability to investigate cultural heritage material first-hand difficult. Depending on where the material is located and stored it may be impossible. Osteology is particularly affected by this lack of primary engagement with material because standard osteological analysis is heavily dependent on sensory observation, predominantly visual and tactile observation though at times also aural. Morphological traits (both on the micro- and macro-scale) which are vital for analysis and diagnosis are difficult to both comprehend and to identify through visual means such as photographs. They are impossible to grasp, in the literal sense, through this medium. 3D-visualisation techniques brings us a step closer to the otherwise inaccessible materials. Direct handling of fragile material is reduced and the need for either research travels or shipping of material is minimised.

### 1.1. Ethics, Posterity, and Legality

Alongside the technical issues of accurately digitising osteological and archaeological material there are numerous ethical, legal and posterity concerns. These issues only come into play when striving for transparency and publishing the acquired data and results. The ethics of publicly sharing osteological remains online, issues of long-term storage and backwards-compatibility are in need of solutions. Concerns involving data ownership, copyright, and intellectual property is fraught with pitfalls that also require solutions. A deep dive into these topics and presenting solutions is beyond the scope of this thesis but still need to be addressed and discussed, albeit in short.

The digital age of course requires digitally available artefacts in order to reach a global audience. Interaction and communication in the digital space is an ever-expanding aspect of museums and research institutions (Galeazzi & Richards-Rissetto 2018). Yet, ethical guidelines and legal frameworks lag behind. The right to information and data accessibility are prime movers for much mediation of archaeological data though there is always a risk for decontextualization when this type of information and data is shared online. Ideally all stakeholders should be involved and consulted when archaeological data is shared, especially culturally sensitive data regarding the remains of dead individuals. Another sensitive issue is

that of publicly exhibiting human remains. This may be in direct violation of the wishes and/or tradition of the particular individual, their family and/or social group (Ulguim 2018a, 2018b).

Yet sharing data is crucial for research and collaboration, the need for which is also growing. The analytical potential of Big Data and machine learning when applied to archaeological data is great, data is also being generated at ever increasing speeds. Though this raises the question of sustainability, long-term storage, and accessibility. Hardware and software may become obsolete, data may be corrupted or lost, funding for maintaining and storing data may cease, and non-standardised methods of collecting data may render data incomparable for analysis (Richards-Rissetto & Von Schwerin 2017). The destructive nature of archaeology promotes a work-culture of rigorous documentation and reflexivity which allows for excavated sites to be revisited and the data to be reused. Future-proofing this data is no easy feat as documentational and data formatting standards vary on many levels, country to country, institution to institution, and company to company. The intention for documentation by the different agents/agencies also plays a role. Storing vast amounts of data requires curation which, much like the initial documentation itself, is a highly subjective action. Once stored however, digital data may just gather proverbial dust if it is not available for reuse. Different organisations are handling the issue of long-term storage and reuse in different ways, there are vast discrepancies between organisations in terms of what data has been made publicly available and their future goals in terms of accessibility (Bellis 2020). Transparency is important in all scientific disciplines and is closely tied to the accessibility of data. Making data transparent and available for (re)use and scrutiny will foster diverse interpretations and continuous interaction in and between disciplines. Open archives increases the longevity and relevance of projects (Lukas, Engel & Mazzucato 2018). Solutions to the issue of storage and reusability may lie in a fundamental restructuring of archaeological knowledge production, research practice, developing new theories, and pragmatical approaches for sharing information in a global digital infrastructure (Dallas 2015). The data collected for this thesis is currently stored in an external hard drive connected to my personal desktop computer, copies exist on a Google Drive folder linked to my student credentials. These storage methods are hardly the most future proof, neither do they serve in the interest of transparency as they are only accessible to others at my discretion. Discipline specific data repositories do exist in case of publication, some in exchange for fees (Scientific Data 2021).

For the purpose of contributing to an increasingly globalised research field, making all the data (both raw and processed) publicly available via the aforementioned Google Drive folder or a public data repository would be ideal, but it is not without issue. Data gatekeeping and responsibility is simply transferred. Reliance on third-party data hosting services, accredited or not, ties into a greater issue of ownership within archaeology.

'Who owns cultural heritage?' is a question which has long been discussed and continues to be discussed due to the sensitive nature of culture in regard to a sense of community, and both personal and national identity (Kobyliniski 2013). Digitisation of archaeological remains adds another layer of complexity to this issue. Ancient artefacts are not protected by copyright, but visual mediums such as photographs and 3D-models of artefacts are a different case (Resta *et al* 2002; Bell & Turin 2013; Boserup 2016). Precedents set in US legal courts have drawn the line at *originality*. Once a reproduction of an artefact or cultural heritage site is altered, as is the case for virtual reconstruction, then the model may be copyrighted (Thompson 2017). With this precedent in mind, sharing both the raw data (photographs) and the models (DPCs and textured models) comes with risk of conflicting claims of ownership. Sharing finalised 3D-data (most commonly as textured models) can be achieved through web applications such as *3DHop* or *Sketchfab*, though the finalised models of the Huseby Klev, Gamla Skogsby, and Falsterbo specimens are hampered by poor quality textures. An alternative solution would be the web application *Potree*, in which point clouds instead of textured models are uploaded. The web applications allow for simple measurements to be taken, as such they offer a simple way of sharing the 3D-data in a transparent manner. The material used for this thesis comes from different institutions. These institutions have a vested interest in how they wish to share their material and any accompanying data, yet I am the one who created the models and added my own originality into the material. It would be inappropriate to publish the 3D-data (models and DPCs) without explicit consent from all parties, as such only the meta- and osteometric data have been shared.

## 1.2. Aims, Purpose, Research Questions, and Limitation

The aims of this thesis are to contribute to current research of 3D-applications on osteoarchaeological material and to contribute to the development of a methodology for digitally recording, identifying, and distinguishing taphonomic markers on said osteological material. A further aim is to discuss the efficacy of digital 3D-recording and analytical methods

plus the resultant visualisations for osteological research purposes. The following research questions will be used to help steer this thesis:

- How can morphological changes due to taphonomy best be digitised and visualised, which tool(s) is best suited for documentation of microscopic markers?
- How can cut marks made by metal and stone tools be identified and distinguished using digital tools?
- How can digital 3D-visualisations be made a viable complement and/or substitute for the original material for research purposes? More specifically how can digital models be constructed to be usable for both qualitative and quantitative studies?

Bones may suffer many different pathological and taphonomic modifications throughout their history, many of these modifications are subtle and hard to detect. For the purposes of this thesis only modification made by human agents will be studied. Several butchering marks rendered onto fresh bones using lithic and metal tools will be used in comparison to archaeological material. A specific goal is to create high quality 3D-models by applying microphotogrammetry on specific/targeted areas which are to be used for both qualitative and quantitative analysis. By replicating and verifying previous researchers' experimental methods, it is my hope to present a thorough and transparent methodology with which to create 3D-models using microphotogrammetry, as well as to expand upon the discussion surrounding potential methods of presentation for these models, both in terms of mediation and research collaboration. This type of discussion has been missing in the previous research, which will be presented under *1.4. Research History*, most likely due to page and format restrictions of the publishing medium.

### 1.3. Theoretical Framework and Perspective

Digital tools and methods have altered our perception of archaeological material and continues to influence our interaction with said material. This alteration has at times been subtle and without much reflection. Digital archaeology is in need of a theoretical framework and requires reflexivity incorporated into the workflow when producing archaeological knowledge. Each step in the process means a subjective filtering of data – though it should be noted subjectivity has always been a problem within archaeology. The implications of our actions as osteologist and archaeologists when conducting research and producing

knowledge needs to be understood at a fundamental level. How archaeological research and praxis is conducted has been irrevocably altered due to digital tools. As such, self-reflection and transparency in research utilising digital tools and methods is important (Reilly 1991; Edgeworth 2014; Garstki 2017; Huvila & Huggett 2018; Perry & Taylor 2018; Caraher 2019).

Digital 3D-modelling has gained popularity as visualisation technologies have continued to advance and grown in sophistication. The process of creating such models is argued by Garstki (2016) to be a new fundamental pillar in the way archaeologists record, analyse, and mediate data. The importance of 3D-visualisation may rival that of traditional photography. A 2D-photograph is by its very nature limited to a single perspective. Another advantage of 3D-renderings of material is that the potential risk of damaging the material is removed. Garstki (2016) continues by writing that such a shift has huge ramifications for the field and forces us to reflect upon the subjective nature of the recording process. Simply put: *what is captured in the frame and what is left out?* For this thesis, capturing and modelling specific sections of the material instead of the entire specimen was chosen. This choice was made in part due to previous research, specifically Placinte Robedizo (2016) who highlighted the need to capture areas of interest in high resolution. Furthermore, the use of modern material in place of archaeological material means that producing a 3D-model or rendering would be superfluous when developing specific methodology as there is no valuable information to gain on the areas of the bone which have not been subject to cutting. This may not be true for archaeological material in which pathologies or taphonomic factors may have left their mark on areas outside those specified for the experimental part of this thesis. The need for producing 3D-models of archaeological material would thus have to be assessed in a case-by-case basis.

It is important to remember that a digital model of an object (in the case of this thesis: bones) is only an approximation of the real object and will never be a true representation of its real-life counterpart. The production of a 3D-model/replica results in an analytical focus shift: the replica undergoes analysis instead of the original specimen. Furthermore, the replica is a representation of the object at a very specific point in space and time (Younan & Treadaway 2015; Seguchi *et al* 2019). The authenticity of replicas and how they may be perceived and experienced by the observer is an ongoing discussion, and digital/3D-printed replicas represent another facet in this discussion (Jones 2010; Wilson *et al* 2018; see also Di

Giuseppantonio Di Franco, Galeazzi & Vassallo 2018). A critical understanding of the tools used in the creation of digital replicas allows for greater analytical potential, which is why Placiente Robedizo (2016) argues for dual expertise when digitising osteological material so that important features such as taphonomic markers and pathologies are accurately recorded and visualised with a high level of identifiability.

#### 1.4. Research History

In the interest of clarity, the following section has been divided into two categories: analogue and digital research histories. The majority of case studies presented in the digital research section do however intersect with the traditional case studies of taphonomic markers as they share similar aims and purposes. In the section regarding digital research history, several different case studies will be presented in order to highlight the potential of 3D-imaging technology.

##### 1.4.1. Experimental Archaeology and Butchering Patterns

The study of butchering marks and patterns provide insight to the development and usage of different tools and techniques. This allows for a more complete representation of past societies and their economies, in addition to their pre-, peri- and post-mortem treatment of animals (Larje 1992). Ethnographic accounts tell of Navajo (Native American people) butchering practices of sheep for consumption. The accounts reveal that the process is relatively homogenous among the Navajo population with little deviations. Butchering takes place locally with minimal to no destruction of bones. Loss of metapodials and phalanges may occur if the skin is sent to a tanner (Binford & Bertram 1977). Unique taphonomic processes do not always leave unique markers on osteological material. Bones which have been discarded but were not interred may be subject to trampling by both humans and animals. Rocks, pebbles, sand, and other sedimentary materials abrade the bones and leave behind striations which are almost indistinguishable to certain types of cut marks without proper observational tools. Obfuscation of cut marks is more likely when trampling has occurred, rather than when abrasive particles have been driven by wind or water (Behrensmeyer, Gordon & Yanagi 1986). Weathering and fragmentation also conceal the true frequency of butchery marks. Taphonomic agents such as dogs (*Canis lupus familiaris*) indulge in osteophagia which results in further loss of skeletal elements at a site. The aforementioned case study by Binford and Bertram (1977) also tells of dogs at Navajo sites who had access to

complete skeletons whilst dogs at Nunamiut (inuit people of Alaska) sites are tethered and only receive select pieces of caribou. However, both Navajo and Nunamiut dogs feast upon bones which were previously processed by human agents. Gnaw marks may thus obscure and/or destroy cut marks. Given the long history of dogs in Scandinavia ([Arnesson-Westerdahl 1984](#); [Larsson 1988](#); [Iregren & Jennbert 2014, 2015](#)), similar scenarios are more than likely to have occurred in numerous (pre)historic Scandinavian sites as well. Taphonomic factors such as osteophagia, trampling, and weathering complicates the study of butchering patterns and technique by way of bone assemblages, regardless of whether analog or digital methods are employed.

The collective wealth of osteological information has allowed for relatively complete mapping of cut marks, butchered species, and their anatomical distribution with regards to different cultures ([Fig. 1](#)). Mesolithic Scanian sites have revealed that butchering methods are relatively consistent with few variations. The Mesolithic culture-groups in Scandinavia frequently hunted wild boar for their meat, marrow, fat, and hides. Boar remains are found in almost all Mesolithic sites in southern Scandinavia, ritual use of bones and teeth are not uncommon. Cut marks are observed in roughly one sixth of the Mesolithic wild boar material from Scanian sites ([Magnell 2005: 9](#)). Marks on mandibles indicate two methods of skinning, and disarticulation occurred at every extremital joint. The site of Ageröd I:HC exhibit lower usage of metapodials and proximal phalanges. Sites in modern day Denmark, particularly Kongemose and Præstelyngen, suggest roasting of large partitions with few disarticulating cuts. Examples from Tågerup indicate infrequent exposure to fire suggesting, meat was predominantly removed from the bones before cooking ([Magnell 2005: 51f](#)). As was alluded to earlier, the anatomical distribution of cut marks is directly related to the purpose of butchery. Butchery patterns vary between cultures, geographical regions and time periods, yet the most common sequence of actions when processing a carcass are: 1) *skinning* – marks are frequently seen in the extremities and the cranium. 2) *disarticulating* – cut marks are visible around the various (key) joints of the body. 3) *defleshing* – filleting marks are seen transverse across the bones. Anatomically complex bones require, and thus display, more cuts. 4) *marrowing* – splintering of bones either with a heavy stone/tool or with bipolar percussion using hammer and anvil (stones) ([Larje 1992](#)). Historical sites offer researchers the advantage of complementing osteological material with contemporary documents and



iconography. This is exemplified in the case study of Kastelholm and Raseborg castles from the 14-16<sup>th</sup> century (modern day Åland and Finland) by [Kivikero \(2019\)](#). Cut marks and historical documents reveals the existence of uniform butchering methods. Cut- and chop marks were observed in roughly one fourth of the remains from Raseborg and Kastelholm, distributed amongst almost all anatomical elements. The majority of cut marks were located on the costae, vertebrae, and coxae. [Kivikero \(2019\)](#) concludes that utilisation of an animal's whole carcass was a common occurrence. Few, if any, parts were unfit for human consumption, even parts which yielded miniscule amounts of meat.

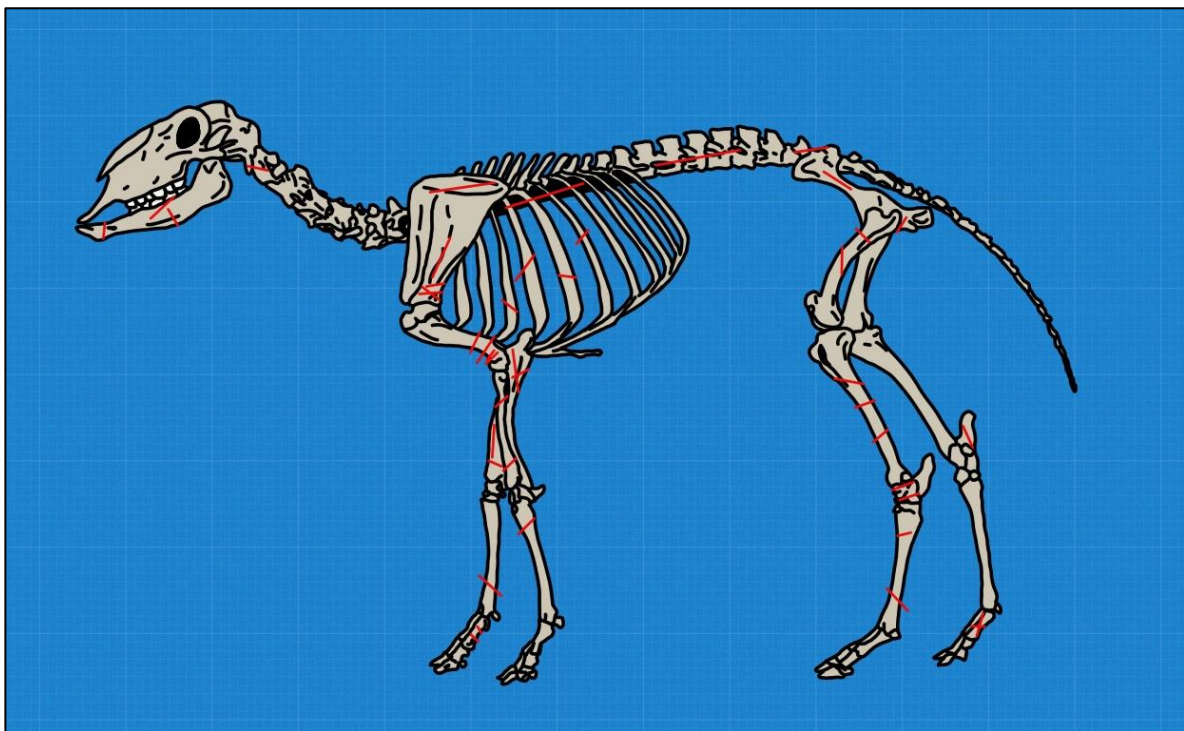


**Figure 1. Anatomical distribution of cut marks commonly found on sheep (*Ovis aries*) from archaeological contexts. Based on the works of [Larje \(1992\)](#) and [Kivikero \(2019\)](#).**

Cutting instruments made from steel or other metals and alloys offer advantages over many stone tools as they can hold their edge longer than lithic tools and are thus generally sharper. Lithic tools are also discarded in greater frequency than metal tools ([Greenfield 1998](#); [Hellgren 2017](#)). The material of choice and relative sharpness of the cutting instrument plays a role in the (micro)morphology of the cut marks ([Larje 1992](#)). Cut marks are of course visible to the naked eye, and temporal contexts can give an indication of which type of cutting instrument was utilised as well as to imply the material composition of the suspected instrument. However, microscopic analysis is preferable in order to accurately identify the

material of the cutting instrument, either through qualitative or quantitative methods. Microscopic examination is important when analysing bones that are dated to periods characterised by material transition, such as the Neolithic and the Bronze Age.

Microscopic analysis may be augmented by experimental cut marks which serve as a basis for comparison. An experimental study by [Walker and Long \(1977\)](#) used steel, flint and obsidian cutting tools applied on fresh bone in order to examine the micromorphological differences. Metapodials from domesticated bovine cattle (*Bos taurus*) were cut perpendicular to the length of the bones, through the periosteal tissue. Cut mark cross-sections were made from transparent polyvinyl and subjected to microscopic examination. The results demonstrate that steel and unretouched obsidian tools leave V-shaped cross-sections which were relatively uniform in their morphology ([Fig. 2](#)). Bifacial lithic tools left concave side profiles and interconnected grooves but no distinct apex. The mode of cutting also affects the morphology of cut marks. Sawing motions created parallel grooves on one side when steel was used, whilst biface flakes deformed both sides of the primary groove. For all tools, depth was lesser than width. [Greenfield \(1998\)](#) corroborated [Walker and Long's \(1977\)](#) results. The cut marks in Greenfield's study were however made on a pine wood, the argument for using this medium instead of bone was that wood would leave a more accurate imprint when slicing. [Greenfield \(1998\)](#) employed a variety of stone tools and modern steel tools with varied levels of sharpness. Silicon moulds of the resulting grooves were analysed using a scanning electron microscope (SEM). Observational angle of the cut mark was important for identification, an overhead view of 90° degrees is ill-suited as shape and depth is lost, 75-90° was a good parameter for identifiability.

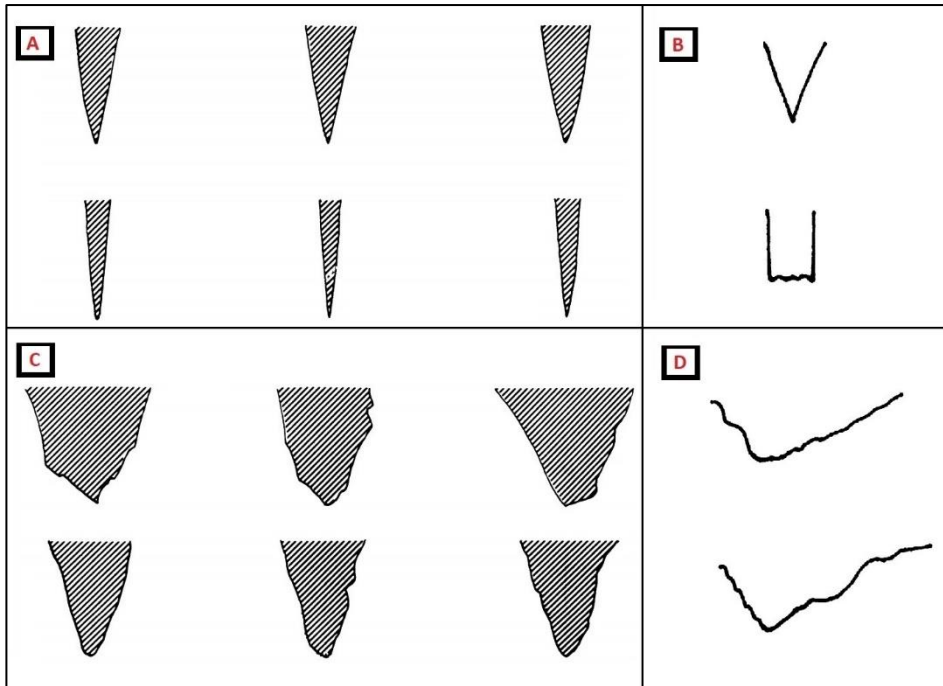


**Figure 2. Cross-sectional view of cut mark grooves. A & B) Metal tools, C & D) Lithic tools. Image sources: Walker & Long (1977) and Greenfield (1998).**

Osteometry and subsequent statistical analysis is a less intrusive method which do not require the application of any casting material directly on the bones. [Hellgren's \(2017\)](#) thesis is an example of a relatively non-intrusive investigation into the usage of lithic and metal cutting tools in south Scandinavian sites. The study was less intrusive than casting physical moulds, though directly measuring on the bones still occurred. The time period examined in the study ranges from the Late Bronze Age to Pre-Roman Iron Age. By categorising the animals and the placement of the cut marks, [Hellgren \(2017\)](#) aimed to shed light on how tools and techniques for butchering animals developed with the proliferation of metal and subsequent replacement of lithic tools. Measurements taken at various points around the cut grooves provided a basis for statistical analysis which was used to understand the variability seen in the cut marks. The results indicate that stone tools left grooves which were on average wider and longer than grooves made with metal tools. This further supported the results of [Walker and Long \(1977\)](#) and [Greenfield \(1998\)](#). [Hellgren's \(2017\)](#) results also showed that an even use of stone and bronze tools occurred during the Bronze Age with metal tools gradually becoming the instrument of choice as time progressed, concluding that the anatomical placement of cut marks during the investigated time period demonstrated the adoption and development of novel butchering methods.

#### 1.4.2. Osteological 3D-modelling

Pathologies and taphonomy remodel bones on the macro and micro scale, but osteometric analysis is difficult to conduct accurately using traditional methods when the scale approaches microscopic levels. Qualitatively and quantitatively assessing these types of remodelling require novel technological approaches. Previous methods of microscopic analysis are often qualitative in their approach, micro-photogrammetry provides researchers with the possibility of assessing cut marks both qualitatively and quantitatively (Bello & Soligo 2008).

Placiente Robedizo's (2016) thesis employed human osteological material and focused on how pathological (cribra orbitalia and callus formations) and taphonomic traits (root impressions) may be replicated in the digital space using three different methods of creating and visualising the 3D-models: laser scan-based model, image-based model, and a combined model of laser scanned geometry with image-based texture. The conclusion reached was that cribra orbitalia is difficult to capture and identify, the delicate capillary features are either lost or distorted in the 3D-models. Placiente Robedizo (2016) thus suggests focusing data acquisition on a particular area or trait of interest and creating models of a targeted area instead of the complete bone. Creating digital models of a limited area has been conducted in several case studies, though some of whom opted for creating models of entire specimens (Bello & Soligo 2008; Bello, Parfitt & Stringer 2009; Bello 2011; Bello *et al* 2011; Maté-González *et al* 2015; 2016; Otárola-Castillo *et al* 2017; Courtenay *et al* 2018). An overview of these case studies will provide insight into the potentials of computer vision and 3D-technology has in areas of study where knowledge gaps exist.

Bello and Soligo (2008) laid the groundwork on which several of the abovementioned case studies were built upon. They used experimental archaeology and targeted digital 3D-modelling with the purpose to differentiate between metal and stone tools. Cut marks made with a modern steel knife and an unretouched flint flake on fresh bones from a domestic pig (*Sus scrofa domesticus*). Measurements for performing quantitative analysis were taken on seven cross-sections using six parameters. Their results indicate that statistical differentiation is possible by using the parameters either individually or in conjunction with each other. The parameters set by Bello and Soligo (2008) were used, refined, and expanded upon in subsequent case studies by Bello, Parfitt & Stringer (2009), Bello (2011), Bello *et al* (2011),

Bello, De Groote and Delbarre's (2013). Maté-González *et al* (2015; 2016) and Courtenay *et al* (2018) performed their own experiments employing the refined parameters (Fig. 3). Their results were compared against archaeological material, further substantiating the usefulness of the parameters.

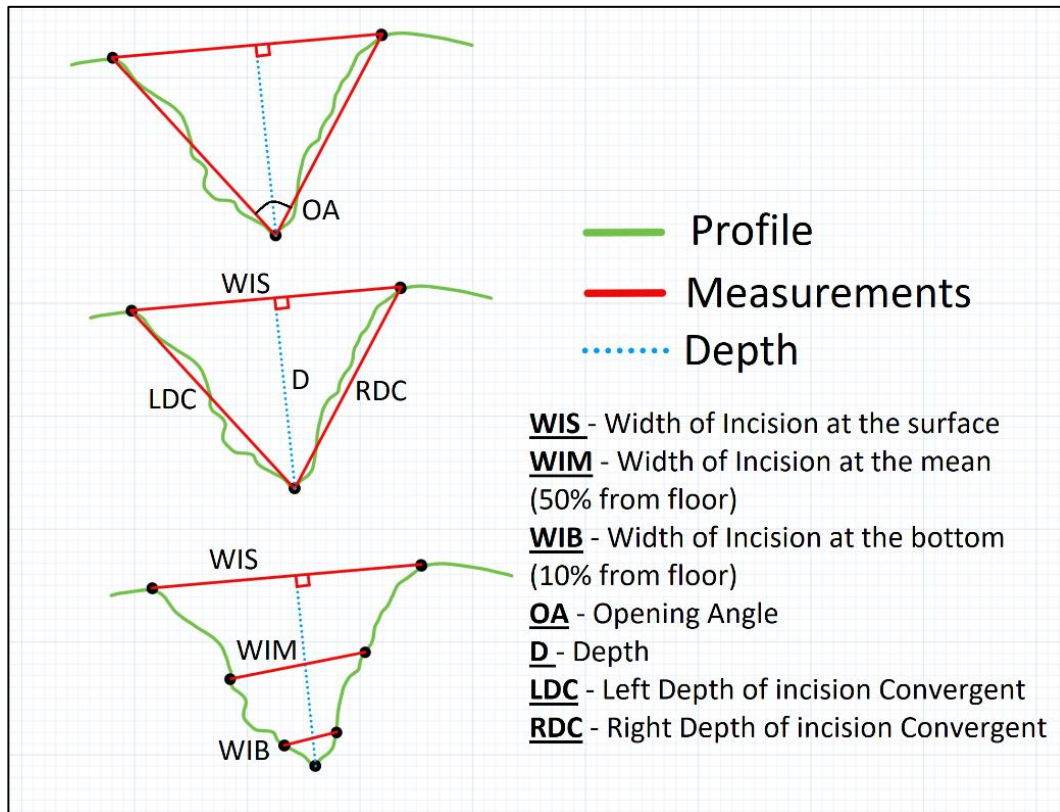


**Figure 3. Profile landmarks used for statistical analysis, these are the parameters set by Bello and Soligo (2008) but further refined and expanded. Image based on Maté-González *et al* (2016).**

Despite the successful research projects presented above, photogrammetry is not without issues. Bello *et al* (2011) encountered issues during their investigation of dental material from Gough's Cave. The optical qualities of the enamel, such as translucency and reflectivity, impaired accurate acquisition of the tooth's surface. The resulting images had areas of unusable black pixels. Higher magnification alleviated the problem but did not eliminate it entirely. Mathys *et al* (2018) present an alternative solution in the form of spectral imaging (capturing images at different wave lengths). This may be used instead of applying a possibly harmful matt coating on highly reflective but fragile material such as ancient tooth enamel and bones. Maté-González *et al* (2015) experiment and analysis utilised, among other recording tools, microphotogrammetry via digital camera and macro lens. Image capturing was performed using parallel photography as well as oblique and convergent photography

capture. Oblique overlapping photography worked best and provided models which were useful for analysis. Building on previous experience, [Maté-González et al \(2016\)](#) used metal, quartzite, and flint tools as experimental cutting instruments. Quantitative differentiation was achieved via principal component analysis (PCA). The analysis indicated clear distinction between the materials. [Maté-González et al \(2016\)](#) observed that metal tools produce a relatively clean and deep V-shaped groove with little micro-striations on the profile wall. Flint tools had a wider upper section in relation to the depth and quartzite was relatively wide and shallow in profile. The profile characteristics are in accordance with the results of [Walker and Long \(1977\)](#) and [Greenfield \(1998\)](#), this further validates the use of microphotogrammetry for cut mark analysis.

Regardless of method or material, a number of variables will always have a role to play in osteological research, among these variables is taphonomy. [Bello, Parfitt & Stringer \(2009\)](#) performed comparative studies between experimental cut marks on modern material and paleolithic fossil finds from Boxgrove, modern day England. The finds have been attributed to *Homo heidelbergensis*. Conditions at Boxgrove are ideal for the preservation of osteological material, few macro-level taphonomic modification have been reported. Yet osteometric discrepancies do exist between fossil and modern materials. [Bello, Parfitt & Stringer](#) hypothesize that taphonomy and/or repeat use of the same instrument (thus blunting) may be the culprit. Further research into micromorphological alteration due to taphonomy as well as into the effects of dulling due to repeat use of flint tools is recommended, this sentiment is echoed by [Bello \(2011\)](#). Human and hominid agency, and consequent actions, are variables which are difficult to account for. Experimental cut marks have been made at different angles (45° and 90°) relative to the surface of the bone in order to simulate possible angles of attack at which defleshing may have occurred ([Bello and Soligo 2008](#); [Otárola-Castillo et al 2017](#); [Courtenay et al 2018](#)). [Otárola-Castillo et al \(2017\)](#) and [Courtenay et al's \(2018\)](#) case studies employed statistical classification which were demonstrated to be highly accurate at differentiating angled cut marks. [Otárola-Castillo et al \(2017\)](#) observed that the angle differed depending on butchers' posture, wrist action, and fine motor skills. Extrapolating this observation implies that topographically complex bones will have cut marks with distinct micromorphology due to variations in dexterity and hand coordination when cutting. Another variable rooted in agency and action is the amount of force which is applied when cutting.

Comparative studies by [Bello, Parfitt & Stringer \(2009\)](#) and [Bello \(2011\)](#) of cut marks made by *H. heidelbergensis* and modern humans (*Homo sapiens*) highlighted discrepancies regarding depth of the groove and floor radii. The greater depth in the *H. heidelbergensis* material is hypothesised to be due to their robustness and strength, whilst wider floor radii is credited to instrument blunting from repeated use without retouching. Cut marks do not exclusively entail butchering marks, as exemplified in [Bello, De Groote and Delbarre's \(2013\)](#) study of artistic carvings Upper Palaeolithic reindeer antlers and horse metatarsal. 3D-microscopic analysis revealed that the carvings were made using multiple incisions: preparatory/contouring incisions prior to more detailed engraving. Micrometric properties of the incisions on the antler differ to those on the metatarsal. Explanations may be the strength and skill of the carver, the typology of tool and technique that was utilised, as well differences in hardness of bone and antler. [Bello, De Groote and Delbarre \(2013\)](#) conclude that 3D-microimaging technologies may allow for tracking of individual artists in prehistory.

The type of analysis employed by previous researchers ([Bello & Soligo 2008](#); [Bello, Parfitt & Stringer 2009](#); [Bello 2011](#); [Bello et al 2011](#); [Maté-González et al 2015: 2016](#)) has however been criticised as being unfulfilling. [Otárola-Castillo et al \(2017\)](#) state that 3D-analysis have not reached their full potential. They further state that 3D-resources are underutilised, data is wasted, and argue that 2D cross-sections of profiles are misused as analogous to the whole cut mark. They employed statistical analysis and superimposition of 3D-models to successfully differentiate between cut marks made with various tools and techniques. However, they did not perform a direct comparison between the accuracy of 2D-methods to those of 3D-techniques. [Courtenay et al \(2018\)](#) note that juxtaposing different methodologies is frequently missing when arguments are made for the analytical superiority of either method. In light of this, they performed their own set of experimental cut marks, 3D-recorded the data, and compared the different analytical methods. Their results showed that both types of analysis provide differentiation and classification of cuts marks with an accuracy of above 95%, concluding that 2D cross-sectional analysis of 3D-models are not inferior to strictly 3D-methods and should thus not be dismissed, especially when considering that both methods have a high-on equal success rate for identification and classification of cut marks.

## 2. Material and Method

The experimental part of this thesis as well as the data collection for producing the 3D-models was performed at the Department of Archaeology and Ancient History at Lund University. All recording tools were provided by the institution. The experimental cutting tools were from my own personal collection, more information in the coming subsection. Like the previous section, the following section is divided into separate analogue and digital modules.

### 2.1. Experimental Material and Method

Based upon previous research and experiments, it was decided that a single type of motion was to be used: a unidirectional cutting stroke. [Otárola-Castillo \*et al\* \(2018\)](#) made a distinction between “cuts” and “slices”, defining cuts as the striations made with the tool held perpendicular relative to bones’ surface, and slices as striations made with the tool held at an oblique angle relative to the bones’ surface. For the purpose of this thesis, only cuts were made.

Four instruments were used for cutting the bones. An all-purpose steel knife, and three flint blades made from south Scandinavian Senonian and Danian flint. These tools were chosen due to their edge characteristics and qualities ([Table 1](#)). The flint was gathered during fieldwalking in Norra Fälåden, Lund, and from the shallow waters of Ribersborg beach, Malmö. The flint tools were knapped and retouched with direct percussion and pressure flaking using a combination of hard hammerstones and soft hammers ([Fig. 4](#)). The typology of the cutting instrument was deemed to be irrelevant considering only the edge would make contact with the bones, though it should be noted that archaeological cutting tools are categorised in part according to their edge characteristics. The cutting edge is on the side of the ruler in [fig. 5](#).





**Figure 4.** Soft and hard hammers used for knapping experimental flint tools. Left to right: antlers from roe deer (*Capreolus capreolus*) and red deer (*Cervus elaphus*), hard hammer stone and abrader.

**Table 1.** Description of cutting instruments.

Instrument	Material	Edge characteristics	Uni/Biface	Comment
All-purpose knife	Steel	Plain edge	-	Freshly sharpened
Heavy Point/Flake	Flint	Non-retouched	-	
Blade	Flint	Retouched	Uniface	
Drill/awl	Flint	Retouched	Biface	



**Figure 5.** Cutting instruments used in thesis experiment. A) All-purpose steel knife, B) unretouched heavy point/flake, C) uniface blade, D) biface drill/awl.

The modern osteological material was purchased from N. Holmgrens Charkuterifabrik in Lund. The material consists of radii and ribs from a single lamb (*Ovis aries*) (Fig. 6). The bones were procured, stored in a frozen state, and left to thaw overnight in room temperature before cutting. Transverse cut-marks were rendered on the bones, with a nearly perpendicular angle relative to the bone's surface (Fig. 7). After performing the cuts, the bones were submerged in simmering water, soft tissues such as the periosteum and sinews were carefully removed by hand so as to not cause any interfering or overlapping striations. The bones were degreased in water using household dish detergent. As mentioned in the research history section, reflective material such as enamel causes issues when acquiring photographs (Bello *et al* 2011). No teeth were part of this thesis' material, but modern osteological material lack any of the low-reflective patina found on archaeological material. Removal of reflective and glossy material such as fat was important, as was ensuring proper white-balancing before acquiring the photographs. Hence, degreasing was performed to remove any fat from the cut groove and because the shiny and reflective quality of fatty material could negatively impact the photography by rendering blank areas on the images. After degreasing, the bones were left to dry in room temperature before acquiring the photographs necessary to build the image-based 3D-model.



**Figure 6. Fresh lamb radii and ribs on the day of procurement.**

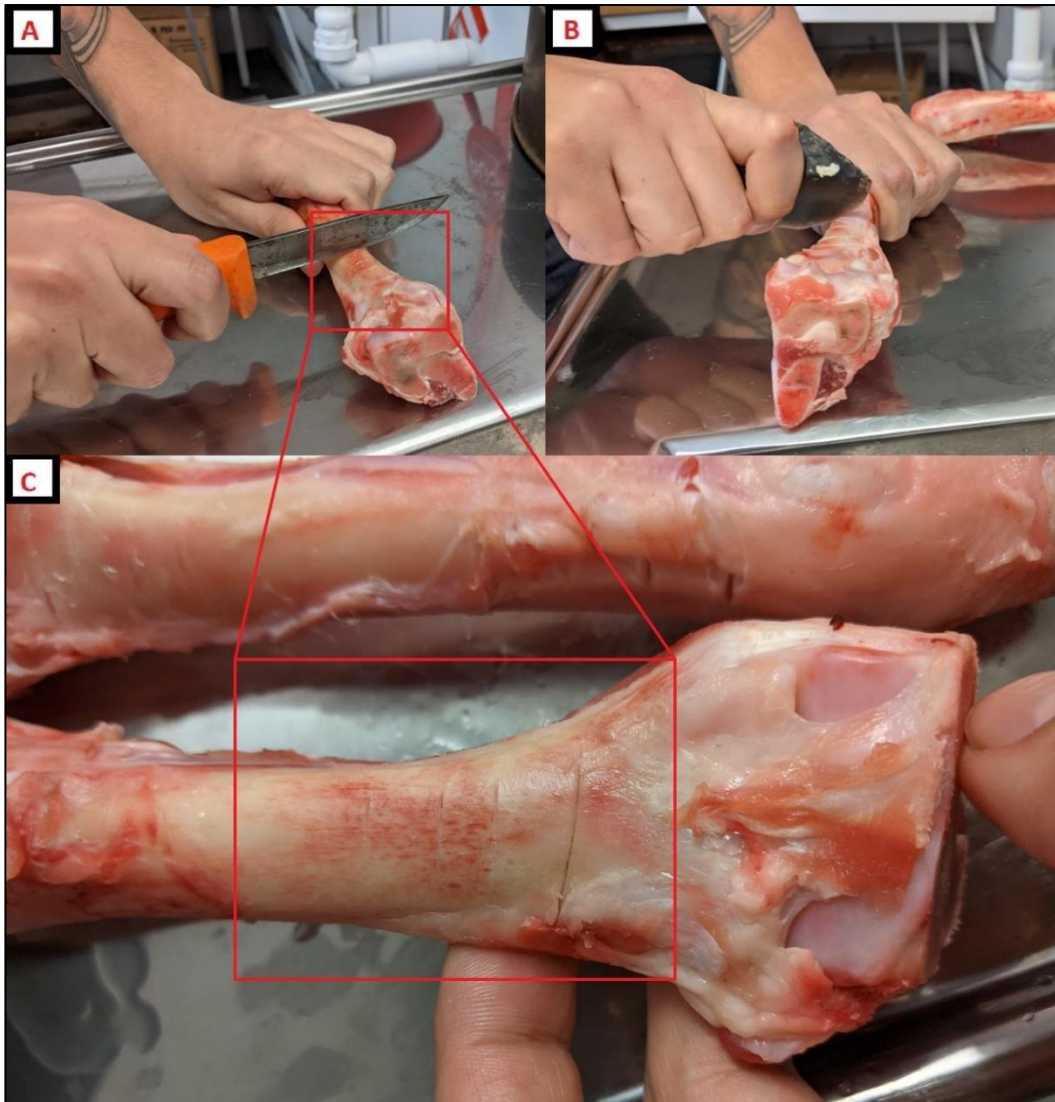


**Figure 7. A and B) Cuts made transverse across the surface of the bone using steel and unretouched flint respectively, C) overhead view of cut marks. Photograph: Daniel Forsberg (A and B) and Gianni Bello Cifuentes (C plus editing).**

#### 2.1.1. Archaeological material

Osteoarchaeological material from the Swedish sites of Huseby Klev (Bohuslän), Gamla Skogsby (Öland) and Falsterbo (Skåne) which exhibit the relevant taphonomic markers (Fig. 8) were used as a basis for comparison. The material was sourced from the reference collection at the institution as well as from excavated material from Bohusläns museum and Kalmar läns museum. The Mesolithic site of Huseby Klev was excavated between 1992 and 1994 (Nordqvist 2005). The material used was a single intermediate phalange from a brown bear (*Ursos arctos*). The site of Gamla Skogsby has been typologically dated to the late Roman and early Germanic Iron Age, around 500 CE (Papmehl-Dufay 2020). The unidentified bone

fragment was excavated in the autumn of 2020 and is, alongside other fragments, currently under analyses (Reinhold 2021/report pending). Excavations in Falsterbo has yielded material that are dated to the medieval period, the bovine cattle rib fragment was stored in a box labelled “Falsterbo 1908”, but any contextual information is missing (Ersgård 1978). The temporal differences between Huseby Klev, Gamla Skogsby, and Falsterbo ensures that there is no overlap regarding the material composition of the cutting instruments.

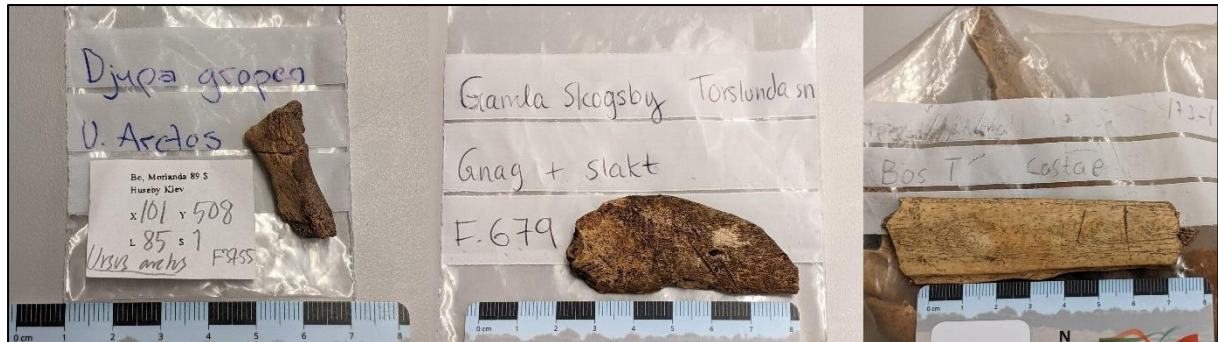


**Figure 8. Archaeological bone material used as a basis for comparison, left to right: bear phalange from Huseby Klev, a hitherto unidentified long bone fragment from Gamla Skogsby, and bovine cattle rib from Falsterbo.**

## 2.2. Digital Material and Method

A passive sensor in the form of a digital camera with appropriate accessories was employed for acquiring the photographs necessary to create the 3D-models. The digital camera utilised was a Canon EOS 6D Mark II, with a 1:1 90-mm macro lens attached to it. The camera was mounted on a tripod to ensure stability and to allow for oblique data capturing at different horizontal angles. The vertical angle used was approximately 75° relative to the surface of the bone. The bones were placed inside a lightbox which provided optimal light condition and equal dispersed light exposure across the entire surface which removed any unwanted shadows on the areas of interest (Fig. 9). Given the nature of macrophotography, the camera was set to only focus on a small section of the whole cut mark. This meant that the entirety of the cut mark was not in focus at all times. The purpose behind this was to take the measurements at the focal point. As will be explained in further detail under the following section 2.2.1. *Quantifying Cut Mark Morphology*, only the profiles of the cut marks will be utilized instead of the entirety of the cut mark. Another quirk of macrophotography is high sensitivity to minute movements, even to delicate movements and touches such as pressing

the capture button. In light of this, the camera's interval timer was activated and set to capture pictures every three seconds. This granted enough time to adjust and rotate the stand to different horizontal angles in-between each picture (Fig. 10). The interval timer was set to capture 45 pictures, however, not all images were used. Blurry and out of focus images were manually culled, and occasionally additional pictures were acquired when it was deemed necessary. The total number of images used for each model is presented in table 2. None of the modern cut marks presented in the table were made into proper textured models as that was both beyond the scope of this thesis and irrelevant due to the fact that no insightful information is gained.



**Figure 9. Photograph acquisition set up: digital camera, lightbox, tripod, and improvised stand (lid from a boardgame on top of a book) to provide optimal distance between lens and object. Pictured is the Huseby Klev bear phalange. It was balanced on top of a piece of rubber eraser to provide better acquisition angle. A millimetre-scale (10x10mm) was placed on top of the bone, next to the cut mark.**

**Table 2. Technical data of photographs used for point cloud and model creation.**

<b>Material</b>	<b>N° of images</b>	<b>Focal length</b>	<b>Aperture</b>	<b>ISO</b>	<b>Shutter speed</b>	<b>Textured model</b>
Huseby Klev	28	90 mm	F/8	160	1/13	✓
Gamla Skogsby	16	90 mm	F/8	160	1/13	✓
Falsterbo	26	90 mm	F/8	160	1/15	✓
Steel #4	18	90 mm	F/8	160	1/15	-
Steel #6	41	90 mm	F/8	160	1/15	-
Steel #8	44	90 mm	F/8	160	1/15	-
Unretouched #3	21	90 mm	F/8	160	1/15	-
Unretouched #4	45	90 mm	F/8	160	1/15	-
Unretouched #5	39	90 mm	F/8	160	1/15	-
Uniface #2	24	90 mm	F/8	160	1/15	-
Uniface #12	19	90 mm	F/8	160	1/15	-
Uniface #19	31	90 mm	F/8	160	1/15	-
Biface #1	36	90 mm	F/8	160	1/15	-
Biface #5	16	90 mm	F/8	160	1/15	-
Biface #17	26	90 mm	F/8	160	1/15	-

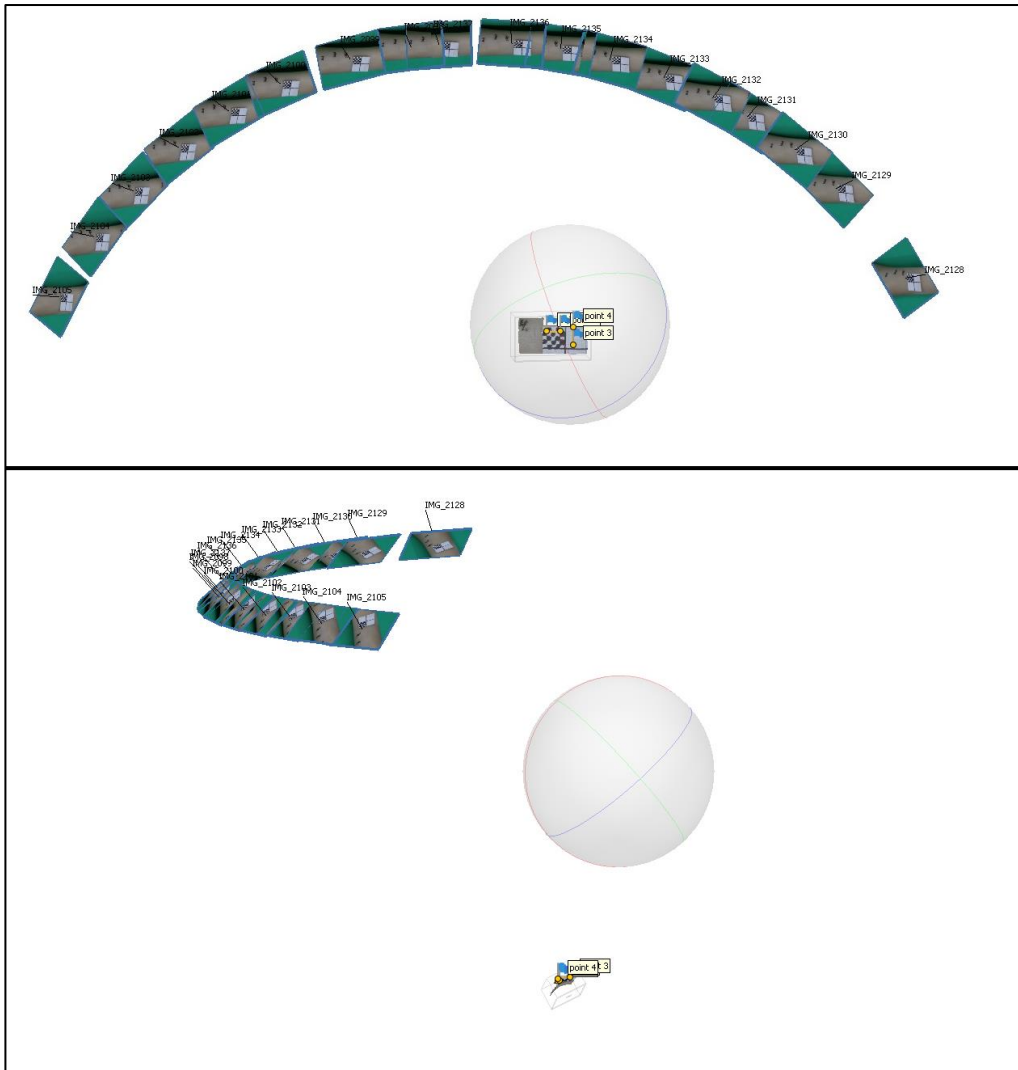


**Figure 10. Screenshots from Metashape showing the relative positioning of the camera during acquisition. Pictured is the cropped dense cloud of cut mark Steel #4.**

Computer hardware employed was a CPU Intel Core i5-6600K clocked at 3.50GHz with an AMD Radeon R9 Fury Series GPU with 4GB VRAM, and 16 GB of RAM. Software employed for the creation and visualisation of the photogrammetric 3D-models was Agisoft Metashape™. Metashape allows for the automatic creation of a metadata report, which includes among other things camera location, settings, and processing parameters. The report for each textured model is attached as [Appendix IV](#). The workflow for creating each model is seen in [fig. 11](#). The Cloud Compare™ software was used for taking the measurements required for the statistical analysis, this was performed after the models had been scaled within Metashape. More information regarding the measurements taken is found in the following section.

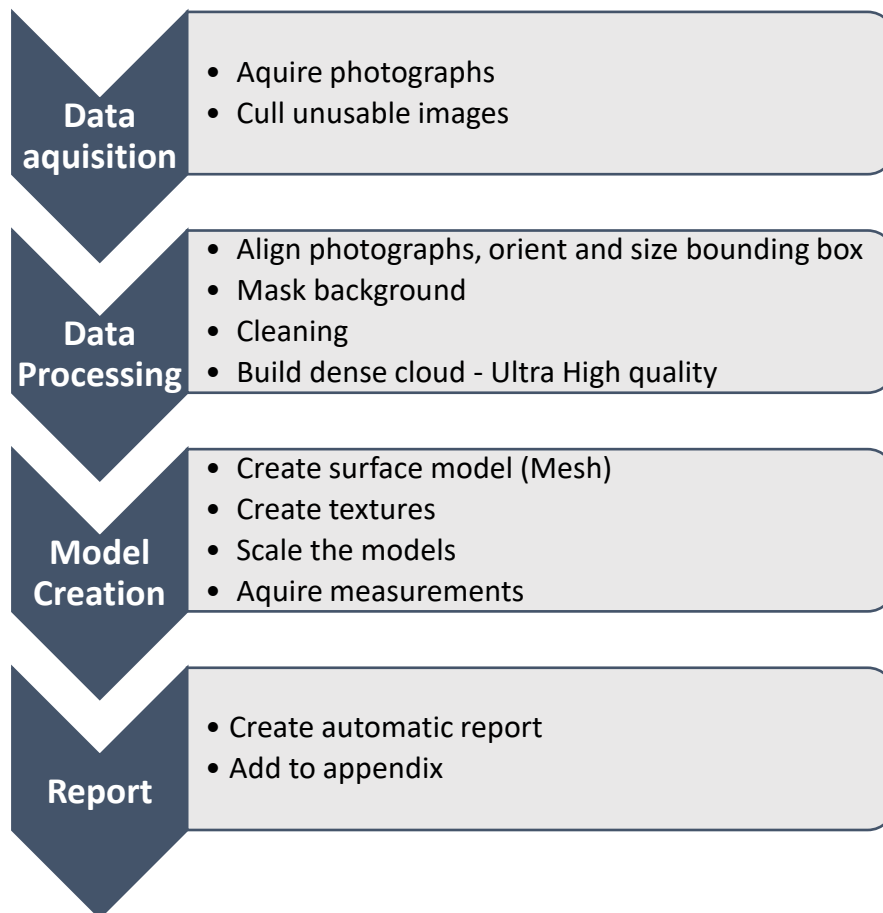


**Figure 11. Workflow for creating photogrammetric models.**

### 2.3. Quantifying Cut Mark Morphology

The multiple variance statistical analysis in this thesis follows the methodology developed by previous researchers presented under *1.4.2. Osteological 3D-modelling*. Seven characteristics of the cut mark profile have previously been used for conducting the principal component analysis (PCA). [Bello, De Groote and Delbarre \(2013\)](#) noted that *opening angle* (OA) impacted the variances explanation significantly, [Courteney et al \(2018\)](#) tested and verified this statement by performing two sets of PCAs: one which included OA and one which excluded it. Their findings indicate that excluding the OA in the calculations gives clearer results. As such, OA has been omitted from this thesis' PCA.

The dense point cloud (DPC) of the different models were imported to Cloud Compare in order to accurately take the necessary measurement for the PCA. Cloud Compare allows for the creation of *envelope lines* of a given cross-section. The envelope line was used as a guide



when selecting three points with the *point picker*-tool. These three points (Fig. 12) represent the *Width of the Incision at the Surface* and the deepest point of the groove (Fig. 3).

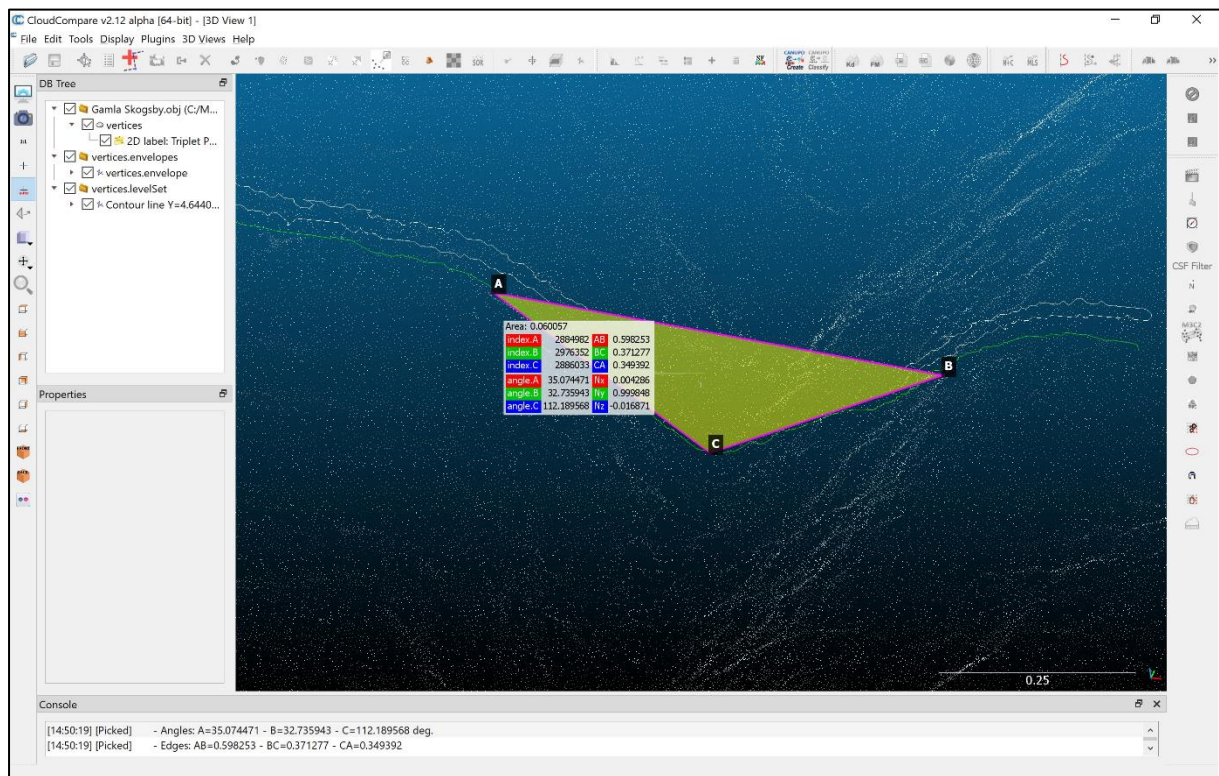


**Figure 12. Screenshot of Cloud Compare where the upper envelope-line (green line) of the Gamla Skogsby cut mark's profile has been drawn and upon which three points of measurements have been selected. The data visible in this screenshot was not used as this was a trial run to acquaint myself with the program. The final data that was used is provided in appendix II.**

Maté-González *et al* (2016) wrote that the two points used for measuring the *Width of the Incision at the Bottom* (WIB) were placed at “/.../ approximately at 10% of the end of the mark”, whereas Courtenay *et al* (2018) were more precise and wrote “At 10% of end of the mark /.../” (emphases by me), this applies to *Width of the Incision at the Mean* (WIM) as well. Yet they both fail to mention exactly how these points were selected, only stating that the measurements were taken with no further indication of whether it was an estimation or with the use of precision tools within their preferred software. As previously seen in the cut mark profiles (Fig. 2) by Walker and Long (1977) and Greenfield (1998) the jagged walls of the groove may shift direction at irregular intervals. To my knowledge, Cloud Compare lacks the option to add additional points to an already drawn line, contour, or figure. The placement of new points on the contour would thus be arbitrary at best, as such I was not able to fully replicate the method presented in previous research. Cloud Compare automatically provides

the area of the triangle created by the three measurements points – two surface points which supply the *WIS* measurement and one point at the deepest part of the profile which is used for calculating the *Depth*-measurement. Basic trigonometry is employed for calculating the *Depth*-measurement (Fig. 13). The calculation was performed automatically within Excel when *WIS*- and *area*-data were recorded, the *area*-data was not used for any other purpose. All measurements are available in [Appendix II](#).

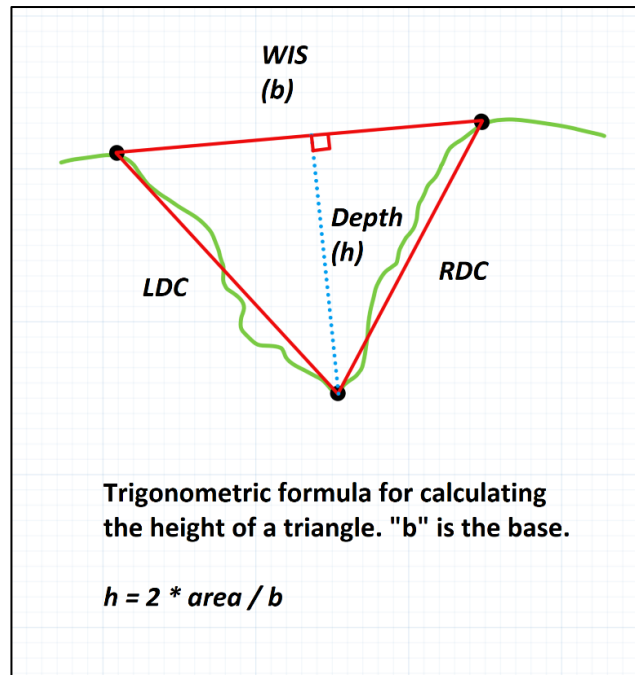


**Figure 13. Trigonometry used for calculating the depth of the incisions. Area is automatically given when placing the three measurements points in Cloud Compare.**

Measurements were taken at 10 different cross-sections of each cutmark's DPC, though still within the small area which was in focus during the data acquisition. There are three main reasons for taking measurements at the 10 different cross-sections: 1) is to acquire an average sample of the profile measurements, 2) the measurements will serve as an approximation or analogy to other specimens, 3) employing these 10 cross-sections will be a more thorough of utilise the 3D-data which has been obtained – less of the available data is wasted and discarded so to speak. Previous researchers have taken measurements from a single cross-section, uniformity across the entire length of the cutting instruments, and thus cut marks, is never guaranteed. With this in mind, averaging the measurements as well as using them as stand-ins for other cut marks is warranted. The expected results from using the 10 cross-sections of each specimen as an analogy for other specimens is a clear clustering in the PCA scatter plots. This will serve as a proof-of-concept that the employed method is viable.

The measurements *Left Depth of the incision Convergent* (LDC) and *Left Depth of the incision Convergent* (RDC) are a function of the placement of the *WIS*-points and the *depth*-point, as such they are not primary information regarding the cut mark profile. In the interest of streamlining the methodology, two sets of PCAs will be conducted (in addition to the PCA using the average data). One will include the *LDC*- and *RDC*-measurements, and one will exclude them. This is to test whether the inclusion of these measurements contribute to any significant clustering of points and thus to the interpretation of the cut marks. The PCAs were conducted using the SPSS™ software, the input/output logs are attached as [Appendix III](#).

### 3. Results

#### 3.1. Preliminary Ocular Assessment on the Macro Scale

The cut marks on the Huseby Klev, Gamla Skogsby, and Falsterbo material are relatively uniform and clean, as previously seen in [fig. 8](#). They are however wider and deeper than the modern cut marks. Their width and depth may be due to taphonomy breaking down the profile walls, another possibility is that they are the results of a different type of butchery action. The grooves may be due to high impact chopping instead of cutting or slicing. This will become clearer in the statistical analysis. Comparison between the modern cut marks reveals little difference between the steel knife and the unretouched flint point. The cut marks made from these two types of tools appear uniform and clean ([Fig. 14](#)).

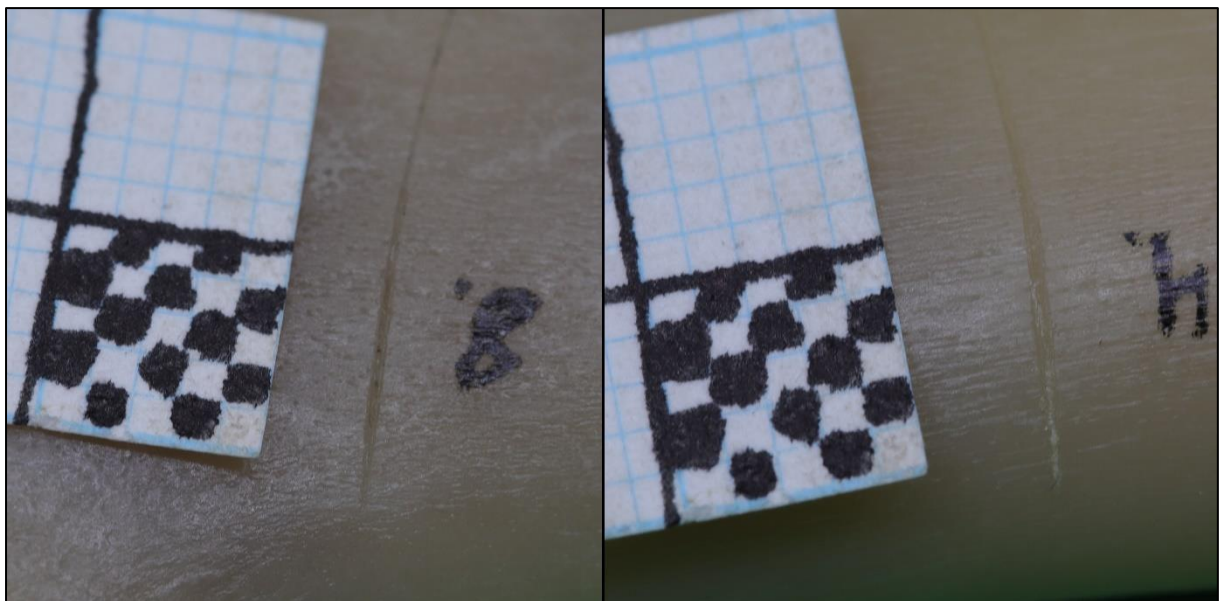


**Figure 14. Comparison between modern cut marks: steel cut mark #8 (left) and unretouched flint cut mark #4 (right).**

The retouched instruments left cut marks characterised by an uneven and slightly rough surface, frequently accompanied by parallel grooves. This is a result of how the serrations are (mis)aligned along the cutting edge. The serrations made contact with the bone in close proximity either as an individual tooth or in group(s). A comparison of the uniface and the biface instruments have left markers that appear relatively distinct from one another. Upon further scrutiny, the grooves made from the biface instruments do appear to be less uniform and with rougher texture than the uniface grooves (Fig. 15).



**Figure 15. Example of cut marks with parallel grooves made by retouched flint tools. Uniface cutmark #2 on the left and biface cut marks #5 on the right.**

Producing a bifacial blade is achieved by alternating sides when pressure flaking, which creates a zigzag-patterned cutting edge. This in turn results in irregular groove shapes when cutting. These results were expected as they have been documented by previous researchers (Walker & Long 1977; Greenfield 1998) who accredited the origin of such features to the uneven lateral surfaces of the cutting edge. The uneven surface of the blades caused striations and micro-fragmentation of the bones along the length of the grooves as well as microscopic *ridges* or *shoulders* on the surface. It should be noted that instruments with more uniform lateral sides, such as the steel knife used for this thesis' experiment, also create this *shoulder*-feature (Fig. 16).

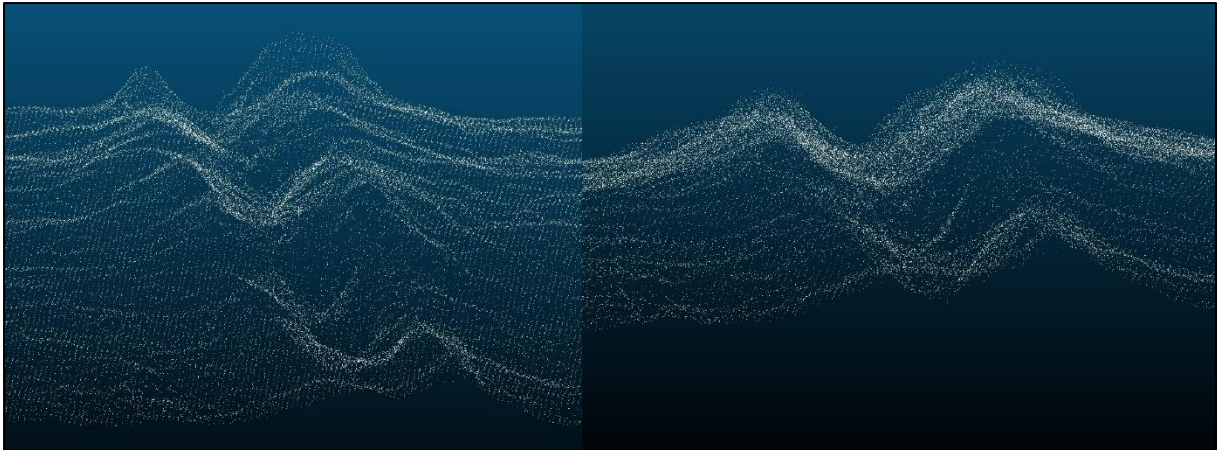


**Figure 16. Screenshots from Cloud Compare, two different angles of cut mark Steel #4's dense point cloud which has prominent ridges/shoulders on both sides of the groove.**

### 3.2. Assessment of the Digital Models

Due to limited access to the camera equipment, it was not possible to capture data or create models of all the experimental cut marks. The models that were created underwent further cropping to remove unnecessary data. Thus, the models vary in the number of vertices and faces. As previously mentioned under 2.2.1. *Quantifying Cut Mark Morphology*, only the profile of the cut marks was used for acquiring biometric data instead of the whole length of the cut marks, hence the reason for why the whole bone was not captured and modelled in its entirety. Cropping of the models was performed in Metashape and in Cloud Compare. The cropping performed in Cloud Compare did not permanently remove data, instead it created a separate entity which eased the task of extracting measurements.

Problems with the data acquisition meant that not all photographed cut marks had suitable images that could be used to render models with sufficient level of details for taking measurements. The DPCs of cut marks *Unretouched #3, #4 and #5, Uniface #19 and Biface #17* exhibited little to no difference in elevation between the groove and the rest of the bone, they were too shallow to be of any use. Whereas the DPC of *Uniface #2* had significant gaps of data points in the area of interest. The cut marks *Biface #1 and Biface #5* also had problems with their depth data. Instead of the groove being too shallow to be registered and rendered as a morphological depression, it was rendered as an elevation on top of the bones (Fig. 17). The data points gathered from the Huseby Klev, Gamla Skogsby, and Falsterbo material provided excellent DPCs that had clear and distinct grooves. This is due to greater width and

depth which makes it easier for the camera and Metashape to accurately register differences in elevation. As mentioned in the previous subsection, there is a possibility that the cut marks are a result of chopping action instead of a cutting or slicing action. The consequences of operating under the assumption that they are a result from cutting or slicing instead of chopping will be discussed in section 4.1. *Discussion of Methodology and Results*.

**Table 3. Summarised assessment of specimen Dense Point Clouds.**

<b>Material</b>	<b>Utilized</b>	<b>Comment</b>
Huseby Klev	Yes	Clear and distinct groove
Gamla Skogsby	Yes	Clear and distinct groove
Falsterbo	Yes	Clear and distinct groove
Steel #4	Yes	Clear and distinct groove
Steel #6	Yes	Somewhat distinct groove
Steel #8	Yes	Somewhat distinct groove
Unretouched #3	No	Little/no relative depth data
Unretouched #4	No	Very shallow, contains data gaps
Unretouched #5	No	Little/no relative depth data
Uniface #2	No	Insufficient data points
Uniface #12	No	Somewhat distinct groove, contains data gaps
Uniface #19	No	Little/no relative depth data
Biface #1	No	Groove rendered as elevation
Biface #5	No	Groove rendered as elevation
Biface #17	No	Little/no relative depth data

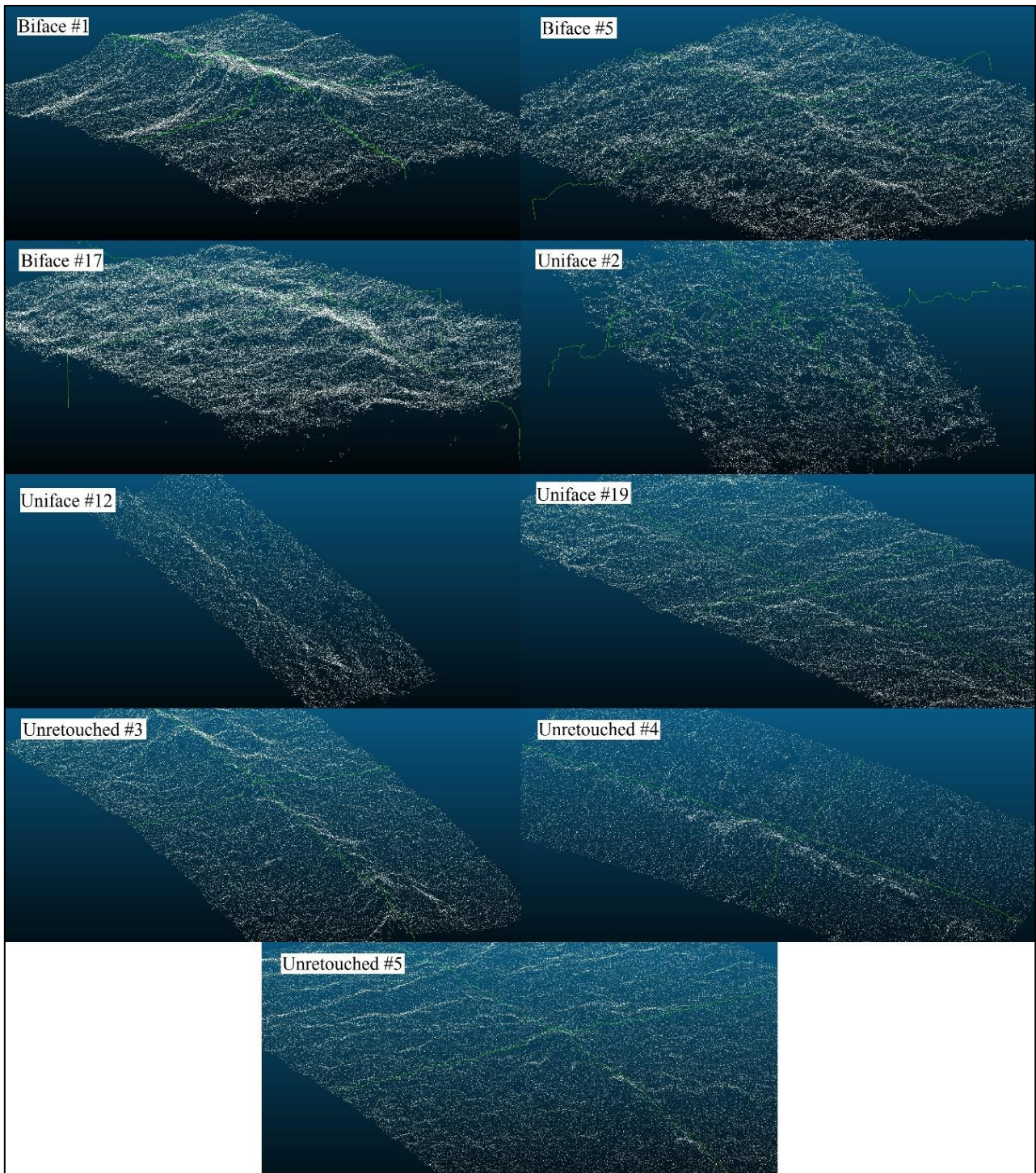


**Figure 17. Screenshot collage from Cloud Compare of the unusable Data Point Clouds of the experimental cut marks. Upper envelope-lines have been rendered on both the X- and Y-axis of the cut mark for easier visualisation of the problems encountered regarding depth.**

The textured models of the archaeological specimens had an underlying DPCs which allowed for depth to be clearly visible. However, the actual textures were not of the highest quality. Particularly noticeable is the Falsterbo cut mark whose textures are distorted and blurry (Fig. 18). Conducting a qualitative comparison using these textured models is possible but less than

ideal. A quantitative analysis will fare better as it does not rely on the quality of the texture, instead relying on the quality of the underlying geometry. The textured models were not used for any formal analysis in this thesis, instead they were created as a proof-of-concept point for mediation and research collaboration – web applications such 3DHop and Sketchfab rely on textured modelled.

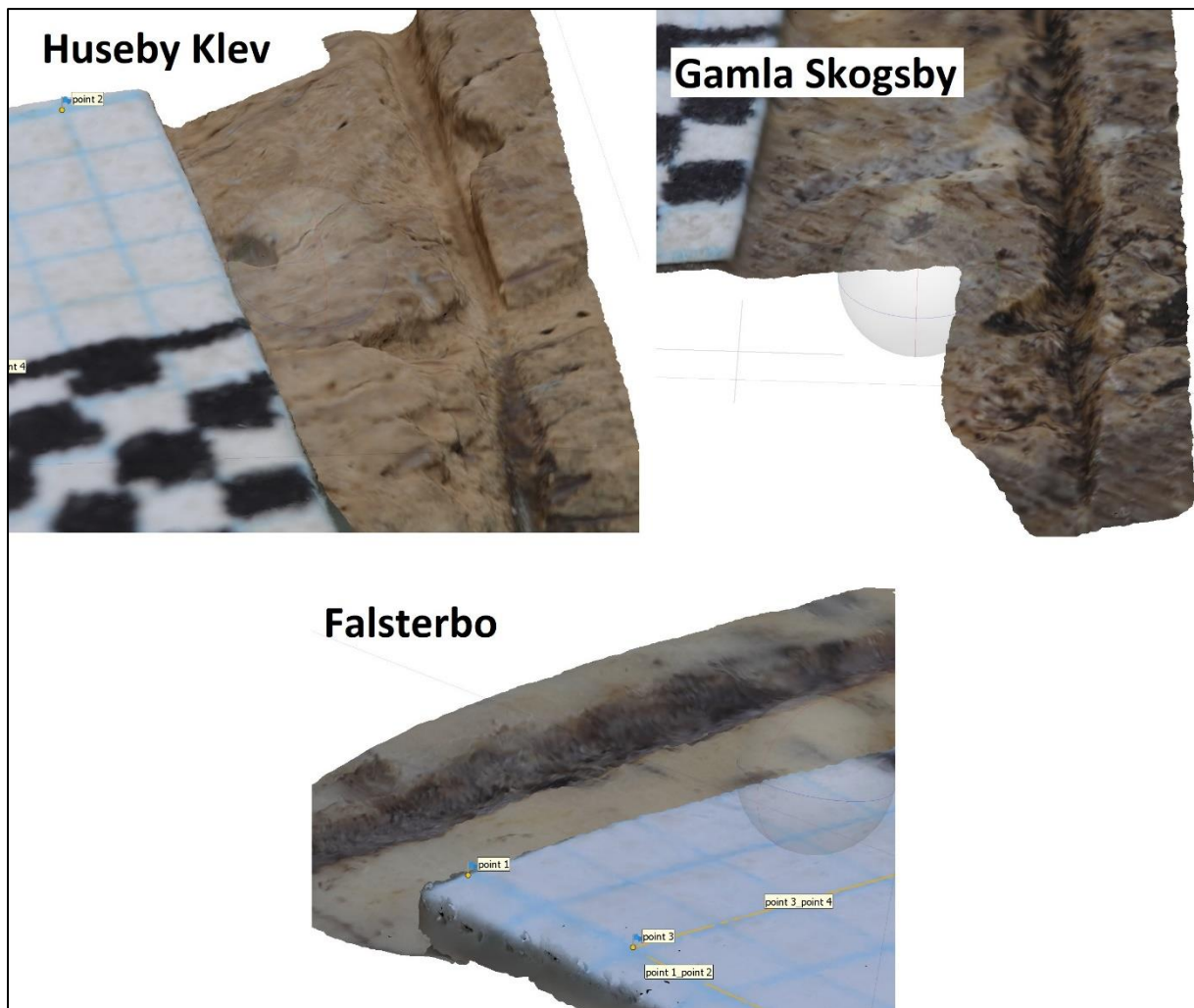


**Figure 18. Comparison of the textured models.**

### 3.3. Qualitative Comparisons of Dense Point Clouds

The three archaeological specimens exhibit different shapes on their profile (Fig. 19). The left profile wall of the Huseby Klev specimen is almost perpendicular to the grooves floor, the right wall is rough, irregular, and has a steep inclination relative to the floor. The bottom does not have a distinct apex, instead it has a relatively flat surface. This is probably a result from a dull cutting instrument. The specimen from Gamla Skogsby, on the other hand, has a clear



apex and the transitional angles between surface and groove are not as extreme when compared to those of Huseby Klev. The profile walls are also more uniform in comparison, this uniformity is expected of cut marks made from metal instruments. Falsterbo, even on the macro scale, was distinct from the other archaeological cut mark. The distinction is even more clear on the micro scale. The profile walls transition relatively smoothly, there is no steep drop as the Huseby Klev specimen nor is it as angled as the Gamla Skogsby specimen. An apex is somewhat visible though not as sharp and distinct as the one found in the Gamla Skogsby specimen. This may be due to the use of a dull instrument.

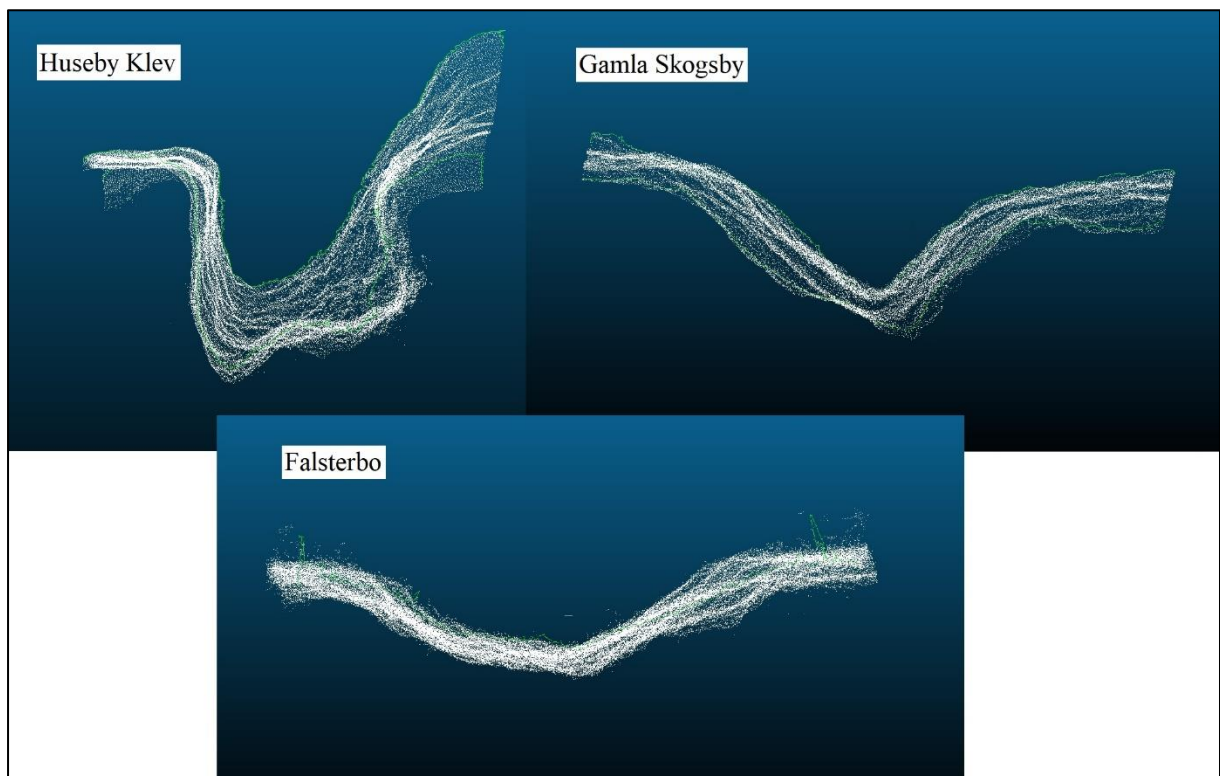


**Figure 19. Comparison of the three archaeological cut marks profile. Same portion where the 10 cross-sections were measured for the statistical analysis.**

### 3.4. Quantitative Results – Principal Component Analysis

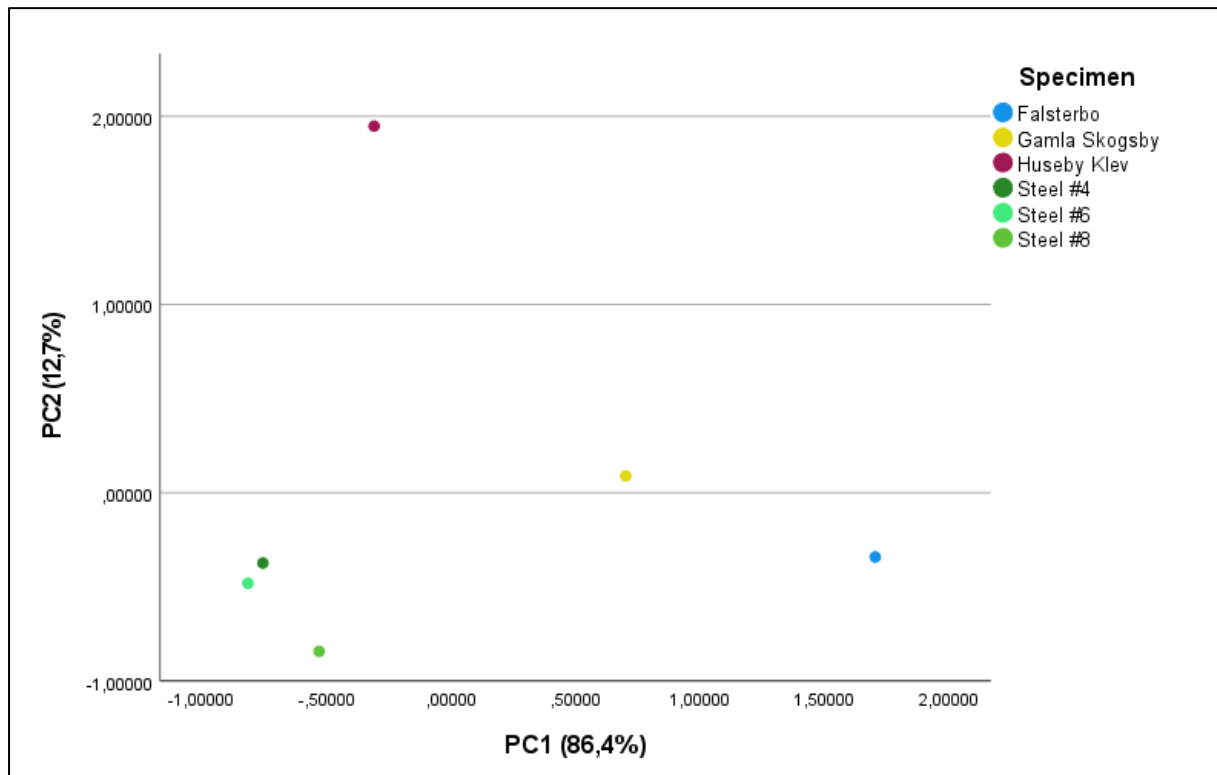


**Figure 20. PCA scatter plot based on the average values from the 10 cross-sections on each specimen, using 4 components.**

The average value PCA scatter plot (Fig. 20) has the points from each specimen dispersed across almost the entire graph. The archaeological material is significantly separated from each other and from the modern material. Falsterbo and Gamla Skogsby are fairly close to one another. However, since the osteological material and therefore the 3D-data consisted of only six usable specimens in total, it means that any type clustering is non-existent except in regard to the modern cut marks made from steel. The modern cut marks were, according to the osteometric data, shallower and narrower than their archaeological counterparts which is why they occupy the lower left corner of the graph.

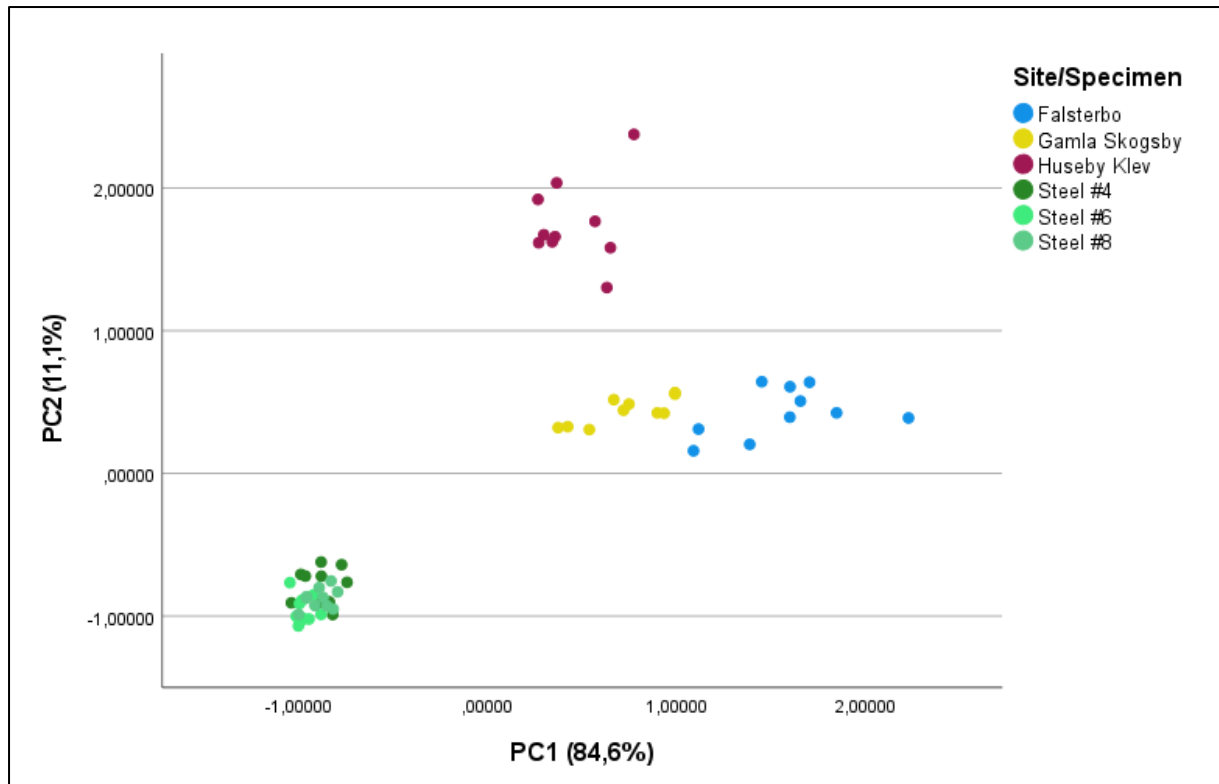


**Figure 21. PCA scatter plot using 10 cross-sections and four components.**

The three archaeological specimens are clearly distinguished, and their points are closely clustered to one another in the scatter plot (Fig. 21) where the four components (i.e. measurements) have undergone dimensional reduction. The points from the bear phalange from Huseby Klev are separate from those of Falsterbo and Gamla Skogsby who are adjacent to one another. The close adjacency of the Falsterbo and Gamla Skogsby specimens/clusters was expected as their temporal contexts dictates that metal instruments were the cause of the cut marks. Another expected result was the clustering of points representing the modern cut marks case *Steel #4, #6 and #8*.

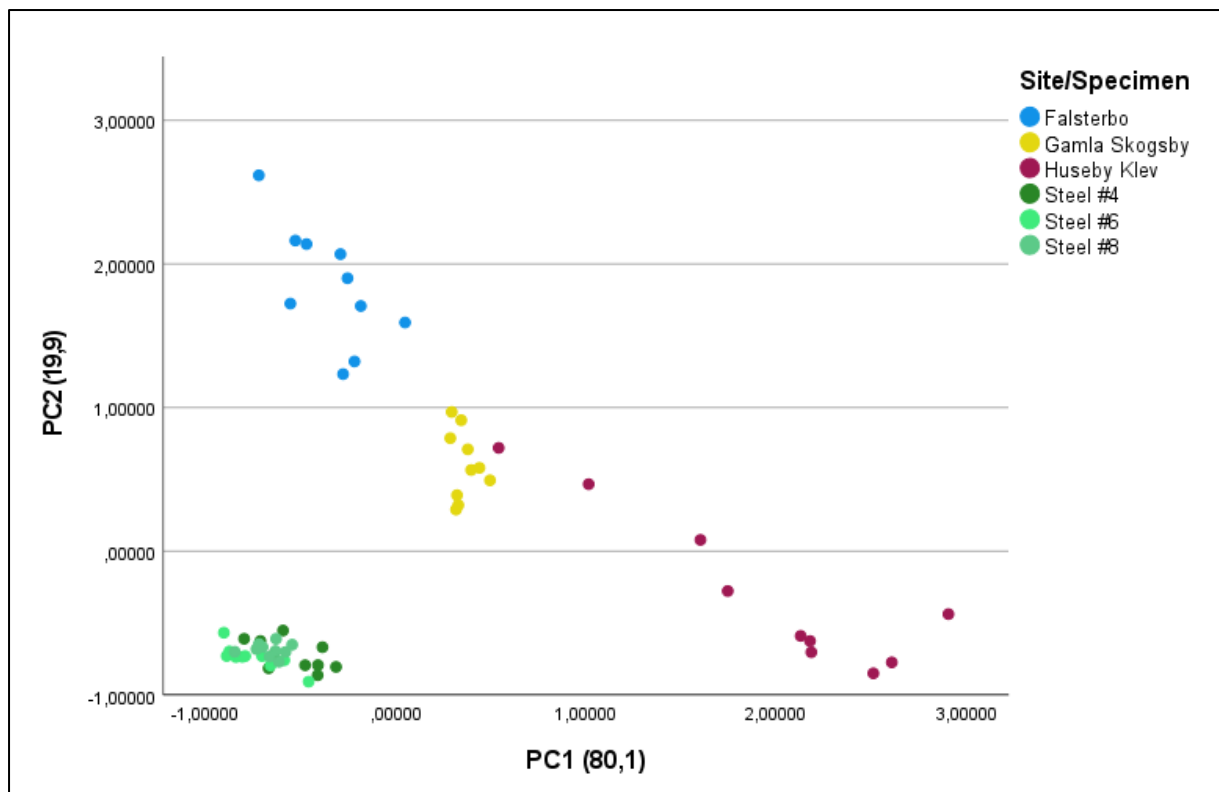


**Figure 22. PCA scatter plot using 10 cross-sections but only two components.**

By omitting the *LDC- and RDC*-measurements, and only using two components for the PCA and subsequent graph (Fig. 22), the points from the archaeological specimens do not cluster together as tightly as seen in the previous graph. They are still fairly separated but individual points from the Huseby Klev specimen trend towards the Gamla Skogsby cluster. Of note is the inverse placement of the archaeological points, particularly Falsterbo and Huseby Klev which occupy top-left and bottom-right part of the graph. The Gamla Skogsby points remain relatively unchanged on both the X- and Y-axis. The modern cut marks remain distinct and separate from the archaeological cut marks.

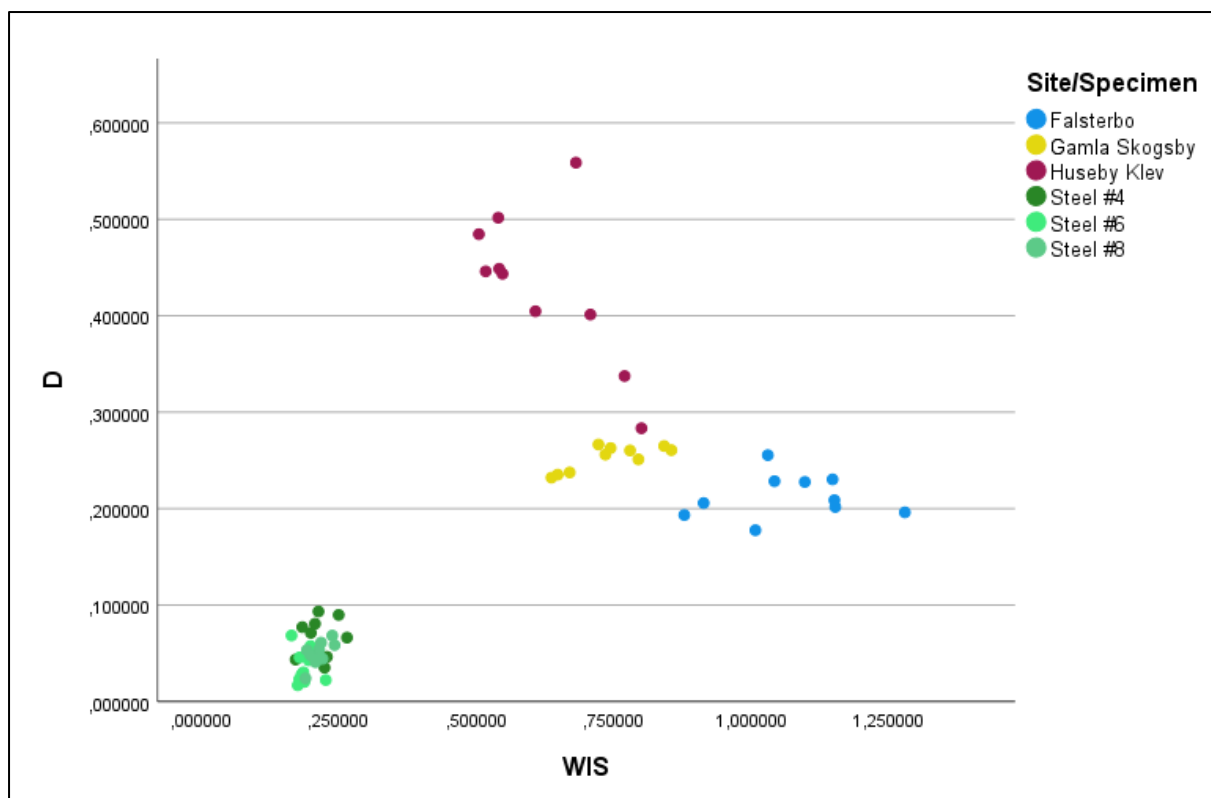


**Figure 23. Non-PCA scatter plot using the WIS and Depth measurements.**

Using only the *WIS*- and *Depth*-measurement, a non-PCA scatter plot (Fig. 23) was created. The clustering resembles those seen in fig. 21. Despite no points overlapping, and the clustering not being as tight as in the previous graph, the different specimens are still clearly distinguished on the scatter plot. The outlier being the points from Huseby Klev which have not clustered together as tightly. Similar to the previous graph, individual points from Huseby Klev can be seen trending towards the Gamla Skogsby cluster. Modern cut marks are, once again, separate to the archaeological cut marks.

## 4. Discussion

This section will comprise of two subsections which will discuss 1) the methods and results, and 2) sources of errors and possible future remedies as well as possible future research projects.

### 4.1. Discussion of Methodology and Results

Cut and slice mark analysis using microscopes is always an option when direct handling of osteological material is possible, whilst remote work and analysis is only possible if the 3D-model is of sufficient quality to accurately portray the taphonomic and pathological

modifications in a manner which is identifiable for would be observers. Time and budget may not always be allocated for a thorough investigation of certain material, but digitisation makes the material available for a global network of interested researchers. Digital 3D-modelling is a faster analytical method than producing a polyvinyl, rubber, or silicon mould, which, as stated in [Walker and Long's \(1977\)](#) paper, can take several days. Performing the data acquisition on a single cut mark required approximately two/three minutes between the first and the final photograph (according to the metadata from the images of several specimens) and an additional few minutes to find proper camera setup, angle, and placement. Processing the images and creating the dense clouds for a single model as well as textures was achieved in under an hour. Obtaining the measurements in Cloud Compare was also a swift affair, requiring approximately ten to fifteen minutes per model. This includes locating and cropping the area of interest, creating the *envelope*-lines, and taking the necessary measurements from each cross-section.

The results presented in the previous section demonstrate that the utilised method is valid for distinguishing butchering marks, however, a larger sample size is warranted for drawing definitive conclusions. The Huseby Klev cut mark was qualitatively assessed as having distinct profile in comparison to both the Gamla Skogsby and Falsterbo cut marks which were more uniform regarding the profile walls. The almost perpendicular left wall and steep right wall on the Huseby Klev cut mark is likely the result of a dull instrument, possibly serrated/retouched on one side. As previously mentioned, the modern grooves made with retouched edges are irregular as a result of the serrations making contact with the bone either individually or in groups. Causing lateral striation along the entirety of the cut mark. The nearly perpendicular (i.e. lacking lateral striation) left wall and the irregularly shaped steep (i.e. having lateral striation) right wall of the Huseby Klev suggests an angled use of a uniface lithic instruments. The Gamla Skogsby and Falsterbo specimen exhibit little to no discrepancies between their left and right walls ([Fig. 19](#)), suggesting perpendicular use of cutting instrument. The qualitative assessment is complemented by quantitative values: the first two PCA scatter plots ([Fig. 20](#) & [Fig. 21](#)) demonstrate the similarities between the Gamla Skogsby and Falsterbo cut marks. The first principal component (X-axis) has a significance rating of around 85%, meaning that proximity between points on the X-axis are more substantial than proximity on the Y-axis. On the third PCA scatter plot ([Fig. 22](#)), which omitted the *LDC*- and

RDC-measurements, Falsterbo and Huseby Klev swapped their relative positions and the Huseby Klev points trailed from the Gamla Skogsby cluster to the lower right part of the graph. The irregular micromorphology of the lithic cutting instrument in comparison to metal instruments has been observed by previous researchers ([Walker & Long 1977](#); [Greenfield 1998](#); [Bello & Soligo 2008](#); [Bello, Parfitt & Stringer 2009](#); [Bello 2011](#); [Bello et al 2011](#)). This is the likely reason for why the Huseby Klev points are less clustered. The modern steel cut marks clustered together and were separated from the archaeological marks as was expected. The observed separation is due to narrower breadth and shallower depth in comparison to the archaeological cut marks. According to previous research, force utilised is determined by intent, anatomical position (for example disarticulation contra defleshing of different elements), the robustness and strength of the butcher, the size of the butchered individual, and whether or not the butchered individual was intended consumption or inhumation. Striations with relatively broader grooves are likely a result of greater use of force. Butchery marks made during disarticulating are demonstrated to be broader, deeper, and with a more acute angle than marks produced by filleting ([Bello, Parfitt & Stringer 2009](#); [Bello 2011](#)). The Huseby Klev specimen is both from a large animal (brown bear) and an anatomical element which tends to be disarticulated, in this case a phalange, during skinning ([Larje 1992](#)). Unfortunately, the steel cut marks were also the only modern cut marks from which osteometric data was retrieved. Cut mark *Unretouched #4* was the best candidate for a possible comparison but due to datapoint gaps on the floor/bottom of the groove it would be negligent to try and extract measurements from it. Having measurements from the retouched cut marks is needed to compare against the Huseby Klev cut mark, specifically measurements from the uniface cut marks. Having measurements from cut marks made with the instrument used at an angle is also necessary. As it stands, the notion that the Huseby Klev striation is the result of a uniface tool cutting at an angle, thus a slice per [Otárola-Castillo et al's \(2018\)](#) definition, remains just a hypothesis.

As previously mentioned, the analysis has been performed under the assumption that the archaeological cut marks are a consequence of cutting or slicing action. Preliminary assessment of the striations noted the greater width and depth in comparison to the modern cut marks. The results from the 3D-data confirm differences with the modern material but offer no insight regarding the relative differences between steel and flint. Having results from

any of the flint tools would allow for a relative comparison of the differences between steel and flint. As such, the quantitative comparison of modern and archaeological material is hampered by a lack of data. Cutting or slicing action may apply less force to the surface of the bone but this is dependent on the size of the butchered animal, purpose for butchering, anatomical element, and typology of the tool (e.g. small knife or heavy axe) (Binford & Bertram 1977; Larje 1992; Bello, Parfitt & Stringer 2009; Bello 2011; Kivikero 2019). Archaeological butchery marks due to cutting and slicing actions would be expected to cluster closer to modern slicing cut marks. This has not been observed in this thesis' results. The most likely explanation is that the archaeological butchery marks are resultant of chopping actions. Despite a flawed premise regarding the nature of the striations, the method inadvertently demonstrates its viability for distinguishing chop marks from each other and from slice marks, though more data would allow for drawing more concrete conclusions.

One goal of this thesis was to streamline the methodology utilised for quantifying the butchery mark profiles. The goal was to be met by testing the number of components needed to create a PCA scatter plot that would allow for the clear separation of cut marks made by different instruments, different in regard to material composition and edge characteristics. This goal has not been met in full due to the fact that an exact replication of the method used in previous research was not possible. Two components, the *WIM*- and the *WIB*-measurements, were not obtained and thus not utilised when performing the PCA. The results presented previously do indicate that clear and distinct clustering of datapoints can be achieved using the four attained measurements. Additionally, this inadvertently demonstrates that a streamlined methodology in which superfluous measurements have been culled is a viable tactic. The results are however not entirely conclusive since they are not based on all measurements which previous research suggests. As such, further testing in which the PCA is performed with and without the *WIM*- and *WIB*-measurements is required to draw more definitive conclusions. Regardless, comparing the 10 cross-sectional PCA plots using four components (Fig. 21) and two components (Fig. 22) reveal that using two components lead to less defined clustering. This is due to the nature of how PCA works. The *LDC*- and *RDC*-measurements act as stabilisers, for lack of a better word, when the data is subjected to the PCA algorithm. Exchanging these measurements/stabilisers with *WIM* and *WIB* is recommended as they represent primary information of the striations profile.



The quality of the DPCs that were created and used in this thesis demonstrate that microphotogrammetry is a viable option for non-intrusive analysis of cut-marks. It is my opinion that further refinement of the camera settings (aperture, ISO, shutter speed) and positioning will allow for greater contrast between the cut marks and the rest of bone surface, thus yielding better DPCs. Using a stronger detergent for degreasing will also help in this regard. Applying a matt coating is standard practice when documenting highly reflective materials though [Mathys et al \(2018\)](#) point out it may damage fragile material, they recommend the use of spectral imaging instead. Aside from improving the acquisition method, modifying the parameters for performing the experimental cut marks will also allow for the creation of usable DPCs and models of cut marks made by unretouched and retouched flint tools. The DPCs used for the PCA in this thesis have enough data points to take almost all the necessary measurements. What was lacking were the proper tools with which to do so. To accurately retrieve the *WIM*- and *WIB*-measurements a measuring tool which snaps to the contour of the cross-section is needed.

#### 4.2. Sources of Error and Future Research

Digital taphonomy, for lack of better words, occurs at almost every step of creating a 3D-model. The resolution, DPI and level of zoom at which data is recorded is dependent on the limitations of the camera and lens employed. The total number of pictures taken is not always the same number that are used for creating the model. Pictures that may be blurry and out of focus are discarded before importing to Metashape or other photogrammetry programs but ensuring perfection in each photograph is impossible. Even after quality assurance there is no guarantee that all pictures will be used. There will always be a trade-off between taking plentiful photographs that contain the necessary data for creating an accurate model whilst also limiting the number of pictures that are used in order to achieve reasonable rendering times and thus a competitive strategy for recording archaeological data. Culling unnecessary and/or unwanted datapoints is an integral step in the process of creating a digital 3D-model. The removal of these points is performed both manually and automatically, though with the automatic point cleaning there is an inherent risk that datapoints are removed from the area of interest. Consequently, the created geometry and texture are not true representations of the specimen at hand. However, the subjective nature of data collection, interpretation, and hypothesization has always been prevalent in archaeology. Issues regarding accurate

representation and perceived objectivity permeates all aspects of archaeology and is not limited to digital methods and tools (Reilly 1991; Garstki 2017; Richards-Rissetto & Von Schwerin 2017).

Recreating the experimental butchering that has been demonstrated in this thesis should be performed using skeletal elements that are large enough to grip properly. A problem which was encountered when cutting the lamb ribs was insufficient grip and stability. The ribs were attached to each other via soft tissues but disjointed from the spine which would otherwise serve as an anchor point allowing proper force to be applied. Less force was applied on the ribs than on the radii despite having no intention to do so. The typology of tools also comes into play here, blades attached to a handle are easier to wield and leverage than unattached blades, as was the case for the lithic tools used for this thesis. It is my hypothesis that insufficient force is partially the reason for why depth was not properly captured. The grooves were simply not deep enough to be registered. Differences in elevation were not distinguished by the camera and software. Additional refinement and testing of optimal camera settings would also help in capturing data on relatively shallow cut marks. Furthermore, the modern lamb material had already been defleshed, stripped to the bone, by the butcher prior to procurement. Processing a whole animal, preferably with the hide and meat intact, is favourable as it would be easier to apply force on small bones. The force applied will fluctuate depending on the body part and amount of soft tissue. It would also be a more true to life recreation of (pre)historic butchering scenarios and conditions. The intended use of the method presented in this thesis is to identify material composition of cutting instruments indirectly via analysis of the bone surface modification. Blunting of these instruments has been mentioned as a variable which impacts the research aim but studying tool blunting could just as easily be a primary aim. Conducting use-wear analysis at different stages of butchering and documenting how repeated use of the same cutting instrument affects the micromorphology of both the cutting edges and the cut marks is recommended. The experimental butchering in this thesis was performed under ideal and controlled conditions for the explicit purpose of creating cut marks on the bones. Instruments become dull with usage and a skilled butcher will avoid hitting bone at the best of times as it would blunt their instruments more rapidly. Skin, meat, sinews, and whether or not elements are still attached to one and other have an effect on the processing of a carcass. The required

force and angle of attack for defleshing changes with the anatomical element. The topography of a bone also effects the way in which meat is deboned. The density of the bone is another variable which may impact the micromorphology of a groove. Scenarios such as butchering in the field after a successful hunt have their own set variables that can influence butchering patterns. Cold temperatures, for example, impacts the fine motor skills of butchers regardless of expertise, this may cause overlapping cut marks and a destruction of the micromorphology crucial for discriminating between lithic and metal tools. The controlled experimental approach is however useful for creating an initial basis for reference.

As previously presented under *1.4.1. Experimental Archaeology and Butchering Patterns*, [Binford & Bertram's \(1977\)](#) ethnographical studies of faunal remains indicate that the level of preservation of bone assemblages differ depending on butchering practices and cultural tradition. The presence of non-human taphonomic agents such as dogs also affects preservation. This means that the method presented in this thesis may not be universally applicable. However, the case study by [Bello, De Groot and Delbarre \(2013\)](#) offers hope in this regard, demonstrating that it is possible to distinguish multiple levels of taphonomic markers using 3D-modelling. Seeing as how they utilised a different recording method, it is warranted to explore the efficacy of microphotogrammetric recording methods on overlapping taphonomic markers. Another suggestion is to use this methodology to determine or estimate the size of dogs via morphology of the gnaw marks. The logic being that the bigger the tooth mark, the bigger the dog. Finding individual tooth marks that are relatively clean and distinguishable from one another may prove to be a difficult task due to the fact that dogs are not known for their table manners.

## 5. Conclusion

The aims of this thesis were to replicate and validate the methodology of previous research into cut mark morphology, as well as to make the methodology more transparent for replication and to contribute to the growing discourse surrounding the online sharing of 3D-data. The aims were guided by three questions:

- How can morphological changes due to taphonomy best be digitised and visualised, which tool(s) is best suited for documentation of microscopic markers?

- How can cut marks made by metal and stone tools be identified and distinguished using digital tools?
- How can digital 3D-visualisations be made a viable complement and/or substitute for the original material for research purposes? More specifically how can digital models be constructed to be usable for both qualitative and quantitative studies?

Microphotogrammetry has been demonstrated to be a viable non-intrusive option for the study of cut marks in archaeological material, both via qualitative and quantitative approaches. A digital camera equipped with a macro lens can capture microscopic details with enough clarity to produce usable 3D-data via Metashape. The Cloud Compare software is good for performing a qualitative analysis and adequate for performing a quantitative analysis. There are however several actions that can be taken to further refine the methodology. These actions entail optimising the camera settings (aperture, ISO, shutter speed) to better contrast and capture the cut mark features as well as using a more reliable and non-arbitrary software tool for gathering measurements. For building a comparative database of modern cut marks, it is suggested to use more force when cutting to ensure a proper impression of the tool on the bone regardless of whether a metal or lithic tool is used. Increasing the sample size used in the PCA and increasing sample variance is imperative to draw more robust conclusions. This includes variances such as chopping action, different angles of attack and varying degrees of pressure when cutting or slicing. Further testing to streamline the quantitative approach by only using primary osteometric information of the cut marks profile is also needed.

Conclusions regarding butchering tools may be drawn by studying the morphology of cut marks. This is true even in circumstances and at sites where there is an absence of the suspected artefacts or material. The method and results which has been presented demonstrates that microphotogrammetry can be viable method for the purpose of identifying and distinguishing cut marks either qualitatively or quantitatively, but more research and comparative data is needed.

## 6. REFERENCES

### PUBLISHED SOURCES

- ARNESSON-WESTERDAHL, A, 1984. Hunden från Ytterbergs udde – ett mesolitiskt hundfynd av stor betydelse för landets fauna- och domesticeringshistoria. In: *Västergötlands fornminnesförenings tidskrift* 1983–1984. S. 211–216.
- BELL, J. A., CHRISTEN, K. & TURIN, M. 2013. After the Return. *Museum Worlds*, 1, 195-203.
- BELLIS, O. 2020. *Overview of the State of Long-Term Preservation in terms of Reuse, Visualization, and Distribution of 3D Data in Archaeology*. Master Thesis, Department and Archaeology and Ancient History. Lund: Lund University. 10.13140/RG.2.2.20552.75523.
- BELLO, S. M. 2011. New Results from the Examination of Cut-Marks Using Three-Dimensional Imaging. *Developments in Quaternary Sciences*, 249–262. <https://doi.org/10.1016/B978-0-444-53597-9.00013-3>
- BELLO, S. & PARFITT, S. & STRINGER, C. 2009. Quantitative micromorphological analyses of cut marks produced by ancient and modern handaxes. *Journal of Archaeological Science*. 36. 1869-1880. 10.1016/j.jas.2009.04.014.
- BELLO, S. M., & SOLIGO, C. 2008. A new method for the quantitative analysis of cutmark micromorphology. *Journal of Archaeological Science*, 35(6), 1542–1552. <https://doi.org/10.1016/J.JAS.2007.10.018>
- BELLO, S.M., VERVENIOTOU, E., CORNISH, L. & PARFITT, S.A. 2011. 3-dimensional microscope analysis of bone and tooth surface modifications: comparisons of fossil specimens and replicas. *Scanning*, 33: 316-324. <https://doi.org/10.1002/sca.20248>
- BELLO S.M, DE GROOTE I, DELBARRE G. 2013. Application of 3-dimensional microscopy and micro-CT scanning to the analysis of Magdalenian portable art on bone and antler. *Journal of Archaeological Science* 40(5):2464–2476 DOI 10.1016/j.jas.2012.12.016.
- BEHRENSMEYER, A. 1978. Taphonomic and ecologic information from bone weathering. *Paleobiology*, 4(2), 150-162. doi:10.1017/S0094837300005820
- BEHRENSMEYER, A., GORDON, K. & YANAGI, G. 1986. Trampling as a cause of bone surface damage and pseudo-cutmarks. *Nature* 319, 768–771 (1986). <https://doi.org/10.1038/319768a0>
- BINFORD, L. & BERTRAM, J. 1977. Bone Frequencies – and Attritional Processes. In Binford, L.R. (red.) (1977). *For theory building in archaeology: essays on faunal remains*,

- aquatic resources, spatial analysis, and systemic modeling. New York: Academic P.
- BOETHIUS A, KJÄLLQUIST M, MAGNELL O, APEL J. 2020. Human encroachment, climate change and the loss of our archaeological organic cultural heritage: Accelerated bone deterioration at Ageröd, a revisited Scandinavian Mesolithic key-site in despair. *PLoS ONE* 15(7): e0236105. <https://doi.org/10.1371/journal.pone.0236105>
- BOSERUP, I. 2016. The Manuscript and the Internet: digital repatriation of cultural heritage. *IFLA Journal*, 31, 169-173.
- BUIKSTRA, J. E. & DEWITTE, S. 2019. A Brief History and 21st Century Challenges. *Ortner's Identification of Pathological Conditions in Human Skeletal Remains*.
- CARAHER, W. 2019. Slow Archaeology, Punk Archaeology, and the 'Archaeology of Care'. *European Journal of Archaeology*, 22, 372-385.
- COSTANZA, R., GRAUMLICH, L., STEFFEN, W., ET AL. (2007). Sustainability or collapse: What can we learn from integrating the history of humans and the rest of nature? *Ambio* 36(7), 522–527. (6 pp)
- COURTENAY LA, MATÉ-GONZÁLEZ MÁ, ARAMENDI J, YRAVEDRA J, GONZÁLEZ-AGUILERA D, DOMÍNGUEZ-RODRIGO M. 2018. Testing accuracy in 2D and 3D geometric morphometric methods for cut mark identification and classification. *PeerJ*. 2018 Jul 5;6:e5133. doi: 10.7717/peerj.5133. PMID: 30002969; PMCID: PMC6035860.
- DALLAS, C. 2015. Curating Archaeological Knowledge in the Digital Continuum: from Practice to Infrastructure. *Open Archaeology*, 1.
- DELL'UNTO, N. 2018. "3D Models and Knowledge Production." Included in: *Archaeology and Archaeological Information in the Digital Society* (2018). Huvila, I. (ed.). Oxon: Routledge. pp. 54-69. (15 p.)
- DELL'UNTO, N., LANDESCHI, G., APEL, J. & POGGI, G. 2017. 4D recording at the trowel's edge: Using three-dimensional simulation platforms to support field interpretation. *Journal of Archaeological Science: Reports*, 12, 632-645.
- DERUDAS, P, SGARELLA, MC & CALLIERI, M. 2018, A 3D Digital Approach for the Study and Presentation of the Bisarcio Site. in M Matsumoto & E Uleberg (eds), *CAA2016: Oceans of Data. Proceedings of the 44th Conference on Computer Applications and Quantitative Methods in Archaeology*. Archaeopress, Oxford, pp. 389-398.
- DI GIUSEPPANTONIO DI FRANCO, P., GALEAZZI, F., & VASSALLO, V. 2018. Authenticity and cultural heritage in the age of 3D digital reproductions. McDonald Institute for Archaeological Research, Cambridge, UK. ISBN 978-1-902937-85-4.

<https://doi.org/10.17863/CAM.27029>

- DRAKE, A. G., COQUERELLE, M., KOSINTSEV, P. A., BACHURA, O. P., SABLIN, M., GUSEV, A. V., FLEMING, L. S. & LOSEY, R. J. 2017. Three-Dimensional Geometric Morphometric Analysis of Fossil Canid Mandibles and Skulls. *Sci Rep*, 7, 9508.
- EDGEWORTH, M. 2014. "From Spade-Work to Screen-Work: New Forms of Archaeological Discovery in Digital Space." Included in: *Visualisation in the Age of Computerization* (2014). Carusi, A., Sissel Hoel, A., Webmoor, T. & Woolgar, S. (eds)., London: Routledge. pp. 40-58. (18 p.)
- ERSGÅRD, L. 1978. *Det medeltida Falsterbo – aktuella problem och undersökningar*. ALE, no. 4, pp. 1-22.
- FORTE, M, DELL'UNTO, N, JONSSON, K & LERCARI, N. 2015. Interpretation Process at Çatalhöyük using 3D. in I Hodder & A Marciniak (eds), *Assembling Çatalhöyük*. vol. 1, *Themes in Contemporary Archaeology*, vol. 1, Maney, Leeds.
- GALEAZZI, F. & RICHARDS-RISSETTO, H. 2018. Editorial Introduction: Web-based Archaeology and Collaborative Research. *Journal of Field Archaeology*, 43, S1-S8.
- GARSTKI, K. 2016. Virtual Representation: the Production of 3D Digital Artifacts. *Journal of Archaeological Method and Theory*, 24, 726-750.
- GIACOMINI, G., SCARAVELLI, D., HERREL, A., VENEZIANO, A., RUSSO, D., BROWN, R. P. & MELORO, C. 2019. 3D Photogrammetry of Bat Skulls: Perspectives for Macro-evolutionary Analyses. *Evolutionary Biology*, 46, 249-259.
- GREENFIELD, H, J. 1998. The origins of metallurgy: Distinguishing stone from metal cutmarks on bones from archaeological sites. *Journal of archaeological science* 26(7). (797-808)
- HANOT, P., GUINTARD, C., LEPETZ, S. & CORNETTE, R. 2017. Identifying domestic horses, donkeys and hybrids from archaeological deposits: A 3D morphological investigation on skeletons. *Journal of Archaeological Science*, 78, 88-98.
- HELLGREN, F. 2017. *Hård rock eller Heavy metall? En jämförande studie mellan skärspår gjorda av sten- kontra metallredskap i övergångsperioden yngre bronsålder och förromersk järnålder*. Master Thesis, Department and Archaeology and Ancient History. Lund: Lund University. <https://lup.lub.lu.se/student-papers/search/publication/8910735>
- HUDSON, M. J., AOYAMA, M., HOOVER, K. C., & UCHIYAMA, J. 2012. Prospects and challenges for an archaeology of global climate change. *Wiley Interdisciplinary Reviews: Climate Change* 3, 313–328. (16 pp)

- HUGGETT, J. 2015. A Manifesto for an Introspective Digital Archaeology. *Open Archaeology*, 1.
- HUVILA, I. & HUGGETT, J. 2018. Archaeological Practices, Knowledge Work and Digitalisation. *Journal of Computer Applications in Archaeology*, 1, 88-100.
- IREGREN, E. & JENNBERT, K. 2014. Hunden under forntiden: nära kompanjoner i livet och döden. *Hundsport: Svenska kennelklubbens tidskrift*, (12), p. 59-64
- IREGREN, E. & JENNBERT, K. 2015. Människan och hunden under yngre stenålder: ett förändrat liv.... *Hundsport: Svenska kennelklubbens tidskrift*, (7-8), p. 53-58.
- JONES, S. (2010). "Negotiating Authentic Objects and Authentic Selves. Beyond the Deconstruction of Authenticity." Included in: *Journal of Material Culture* 15, pp. 181-203. (23 p.)
- KIVIKERO, H. 2019. Tracing Dead Meat. Butchering animals in the Castles of Kastelholm and Raseborg in the 14th to 16th Centuries.
- KOBYLINSKI, Z. 2013. Cultural heritage: values and ownership. In Bergerbrant, S & Sabatini, S (red.) (2013). *Counterpoint: essays in archaeology and heritage studies in honour of professor Kristian Kristiansen*. Oxford: Archaeopress
- LARJE, R. 1992. Osteological evidence of change in butchering technique. *Laborativ arkeologi* 6. (23-29)
- LARSSON, L. 1988. The Skateholm Project. Late Mesolithic Settlement at a South Swedish Lagoon. I Larsson, L. (red.) *The Skateholm Project I – Man and Environment*. Stockholm: Almqvist & Wiksell International, pp. 9–19.
- LUKAS, D., ENGEL, C. & MAZZUCATO, C. 2018. Towards a Living Archive: Making Multi Layered Research Data and Knowledge Generation Transparent. *Journal of Field Archaeology*, 43, S19-S30.
- MACĀNE, A. 2012. *Fusing osteology with virtual reality - Three dimensional morphological differences between harp seal (Pagophilus groenlandicus) and ringed seal (Phoca hispida)*. Master Thesis, Department and Archaeology and Ancient History. Lund: Lund University. <http://lup.lub.lu.se/student-papers/record/2545039>
- MACHERIDIS, S. 2015. Image-Based 3D Modeling as a Documentation Method for Zooarchaeological Remains in Waste-Related Contexts. *Ethnobiology Letters*, 6, 242-248.



- MAGNELL, O. 2005. *Tracking wild boar and hunters: osteology of wild boar in Mesolithic South Scandinavia*. Diss. (sammanfattning) Lund: Lunds universitet, 2005
- MANZANO, B. L., MEANS, B. K., BEGLEY, C. T. & ZECHINI, M. 2015. Using Digital 3D Scanning to Create "Artifictions" of the Passenger Pigeon and Harelip Sucker, Two Extinct Species in Eastern North America: The Future Examines the Past. *Ethnobiology Letters*, 6, 232-241.
- MATÉ-GONZÁLEZ, M.A., YRAVEDRA, J., GONZÁLEZ-AGUILERA, D., PALOMEQUE-GONZÁLEZ, J.F., DOMÍNGUEZ-RODRIGO, M. 2015. Microphotogrammetric characterization of cut marks on bones. *Journal of Archaeological Science*, 62 (2015), pp. 128-142, 10.1016/j.jas.2015.08.006
- MATÉ-GONZÁLEZ, M.A., YRAVEDRA, J., GONZÁLEZ-AGUILERA, D., PALOMEQUE-GONZÁLEZ, J.F., DOMÍNGUEZ-RODRIGO, M. 2016. Micro-photogrammetric and morphometric differentiation of cut marks on bones using metal knives, quartzite, and flint flakes. *Archaeological and Anthropological Sciences*, 62 (2016), pp. 128-142, 10.1007/s12520-016-0401-5
- MATHYS, A., SEMAL, P., BRECKO, J. & VAN DEN SPIEGEL, D. 2019. Improving 3D photogrammetry models through spectral imaging: Tooth enamel as a case study. *PLoS One*, 14, e0220949.
- MEANS, B. K. 2017. Promoting a More Interactive Public Archaeology. *Advances in Archaeological Practice*, 3, 235-248.
- MICCICHE, R., CAROTENUTO, G. & SINEO, L. 2018. The utility of 3D medical imaging techniques for obtaining a reliable differential diagnosis of metastatic cancer in an Iron Age skull. *Int J Paleopathol*, 21, 41-46.
- NORDQVIST, B. 2005. *Huseby klev. En kustboplats med bevarat organiskt material från äldsta mesolitikum till järnålder. Bohuslän, Morlanda socken, Huseby 2:4 och 3:13, RAÄ 89 och 485: arkeologisk förundersökning och undersökning*. Mölndal: Riksantikvarieämbetet, UB Väst, Avdelningen för arkeologiska undersökningar. <http://samla.raa.se/xmlui/handle/raa/4087>
- OHNO, K. & KAWAKUBO, Y. 2019. Three-dimensional investigations of fragile archaeological human remains. *3D Data Acquisition for Bioarchaeology, Forensic Anthropology, and Archaeology*.
- OSTROWSKI, W. & HANUS, K. 2016. Budget UAV Systems for the Prospection of Small- and Medium-Scale Archaeological Sites. *ISPRS - International Archives of the Photogrammetry, Remote Sensing and Spatial Information Sciences*, XLI-B1, 971-977.

- OTÁROLA-CASTILLO E, TORQUATO M, HAWKINS HC, JAMES E, HARRIS J, MAREAN C, MCPHERNON S, THOMPSON J. 2018. Differentiating between cutting actions on bone using 3D geometric morphometrics and Bayesian analyses with implications to human evolution. *Journal of Archaeological Science* 89:56–67 DOI 10.1016/j.jas.2017.10.004.
- PAPMEHL-DUFAY, L. 2020. *I hövdingens kök? Arkeologisk undersökning i Gamla Skogsby oktober 2019*. Kalmar: Kalmar Studies in Archaeology XVII. Kalmar Växjö: Linnéuniversitetet.
- PELLETIER, M., KOTIAHO, A., NIINIMAKI, S. & SALMI, A. K. 2020. Identifying early stages of reindeer domestication in the archaeological record: a 3D morphological investigation on forelimb bones of modern populations from Fennoscandia. *Archaeol Anthropol Sci*, 12, 169.
- PERRY, S. & TAYLOR, J.S. 2018. "Theorising the Digital: A Call to Action for the Archaeological Community." Included in: *Oceans of Data: Proceedings of the 44th Conference on Computer Applications and Quantitative Methods in Archaeology*. Matsumoto, M. & Uleberg, E. (eds). Oxford: Archaeopress. pp. 11-22. (11 p.)
- PLACIENTE ROBEDIZO, B. 2016. The Identifiability of Osteological Traits on 3D Models of Human Skeletal Remains. Master Thesis, Department and Archaeology and Ancient History. Lund: Lund University. <http://lup.lub.lu.se/student-papers/record/8893957>
- POLIG, M. 2017. 3D GIS for building archeology – Combining old and new data in a three-dimensional information system in the case study of Lund Cathedral. *Studies in Digital Heritage*, 1, 225-238.
- RAMSTHALER, F., KETTNER, M., GEHL, A. & VERHOFF, M. A. 2010. Digital forensic osteology: morphological sexing of skeletal remains using volume-rendered cranial CT scans. *Forensic Sci Int*, 195, 148-52.
- RESTA, P., ROY, L., DE MONTANO, M. K. & CRISTAL, M. 2002. Digital repatriation: virtual museum partnerships with indigenous peoples. *International Conference on Computers in Education, 2002. Proceedings*.
- RICHARDS-RISSETTO, H. & VON SCHWERIN, J. 2017. A catch 22 of 3D data sustainability: Lessons in 3D archaeological data management & accessibility. *Digital Applications in Archaeology and Cultural Heritage*, 6, 38-48.
- REILLY, P. 1991. Towards a virtual archaeology. CAA90. *Computer Applications and Quantitative Methods in Archaeology 1990* (BAR International Series 565). Tempus Reparatum, Oxford, Pp. 132-139
- RYAN, K., BETTS, M. W., OLIVER-LLOYD, V., CLEMENT, N., SCHLADER, R., YOUNG, J. &

- GARDINER, M. 2014. Identification of a Pre-Contact Polar Bear Victim at Native Point, Southampton Island, Nunavut, Using 3D Technology and a Virtual Zooarchaeology Collection. *Arctic*, 67.
- SEGUCHI, N., DUDZIK, B., MURPHY, M.-M. & PRENTISS, A. M. 2019. Introduction. *3D Data Acquisition for Bioarchaeology, Forensic Anthropology, and Archaeology*.
- THOMPSON, E. L. 2017. Legal and ethical considerations for digital recreations of cultural heritage. *Chapman Law Review*, 20(1), 153-176
- ULGUIM, P., 2018a. Digital Remains Made Public: Sharing the dead online and our future digital mortuary landscape. *AP: Online Journal in Public Archaeology* 8, 153. doi:10.23914/ap.v8i2.162
- ULGUIM, P. 2018b. Models and Metadata: The Ethics of Sharing Bioarchaeological 3D Models Online. *Archaeologies*, 14, 189-228.
- VERHOEVEN, G. 2011. Taking computer vision aloft - archaeological three-dimensional reconstructions from aerial photographs with photostan. *Archaeological Prospection*, 18, 67-73.
- VILLA, C., FROHLICH, B. & LYNNERUP, N. 2019. The Role of Imaging in Paleopathology. *Ortner's Identification of Pathological Conditions in Human Skeletal Remains*.
- WALKER, P., & LONG, J. 1977. An Experimental Study of the Morphological Characteristics of Tool Marks. *American Antiquity*, 42(4), 605-616. doi:10.2307/278934
- WILHELMSON, H. & DELL'UNTO, N. 2015. Virtual taphonomy: A new method integrating excavation and postprocessing in an archaeological context. *Am J Phys Anthropol*, 157, 305-21.
- WILSON, P. F., STOTT, J., WARNETT, J. M., ATTRIDGE, A., SMITH, M. P. & WILLIAMS, M. A. 2017. Evaluation of Touchable 3D-Printed Replicas in Museums. *Curator: The Museum Journal*, 60, 445-465.
- YOUNAN S., & TREADAWAY C. 2015. Digital 3D models of heritage artefacts: Towards a digital dream space. *Digital Applications in Archaeology and Cultural heritage* 2(4):240–7.

UNPUBLISHED/PENDING SOURCE

REINHOLD, L.K. 2021. *Osteologisk rapport för utgrävning i Gamla Skogsby, hösten 2020.*  
[Title may be subject to change]

ONLINE RESOURCE

3DHOP. 2021. *3D Heritage Online Presenter.* <https://3dhop.net/> [Accessed 2021-06-28]

SCIENTIFIC DATA. 2021. *Recommended Data Repositories.*  
<https://www.nature.com/sdata/policies/repositories> [Accessed 2021-05-20]

SKETCHFAB. 2021. <https://sketchfab.com/> [Accessed 2021-06-28]

POTREE. 2021. <https://potree.github.io/> [Accessed 2021-06-28]

## 7. APPENDICES

### Appendix I - HUSEBY KLEV DATABASE

Excerpt from the Huseby Klev database, transposed to fit this document.

Löp-nr	553	5024	2020	2018
Helhets kontext	Djupa gropen	Djupa gropen	Tältet	Tältet
Lager	85	46	51	20
Djurgrupp	Mammalia	Mammalia	Mammalia	Mammalia
Djurtyp	Pälsvilt	Pälsvilt	Pälsvilt	Pälsvilt
Fynd-nr	3755	622	280	3216
Art	U.Arctos	V.Vulpes	C.Lupus	V.Vulpes
Element	Phalang 2	Humerus	Kranium	Kranium
Del	Hel	Distal	Frontale	Occipitale
Sida	-	Dex	Dex	-
Antal	1	1	1	1
Mått	-	-	-	SD: 8 BT: 16,1 Bd:18,4
Vikt	1,9	0,7	2	0,4
Kön	-	-	-	-
Ålder	> 2 år	-	-	-
Wheatering	-	-	2	1
Trampling	-	-	1	-
Gnag	-	-	-	-
Slakt	Skärmärke	Skärmärken	Skärmärken	Skärmärken
Bränd	-	-	-	-
Patologi	-	-	-	-
Fluvial påverkan	Vatten och stenslitning	Vatten och stenslitning	-	-
Beartbetat	-	-	-	-
Kommentar	Märke under proximal del	Märken syns på diverse ställen över hela ytan	-	-

## Appendix II - CUT MARK MEASUREMENTS

Average data of the 10 slices of each specimen. Measurements in mm.

Specimens	WIS	D	LDC	RDC
Huseby Klev	0,621927	0,431085	0,683954	0,458994
Gamla Skogsby	0,742577	0,252801	0,391440	0,512010
Falsterbo	1,069234	0,212598	0,548419	0,605981
Steel #4	0,215640	0,119559	0,119559	0,136145
Steel #6	0,188301	0,099962	0,099962	0,104333
Steel #8	0,214733	0,049888	0,108165	0,130062

Table of all data collected from each specimen.

Specimen	Cross-section	WIS	D	LDC	RDC	Area
Huseby Klev	A	0,800163	0,283430	0,883715	0,285817	0,113395
Huseby Klev	B	0,769545	0,337561	0,887520	0,341432	0,129884
Huseby Klev	C	0,707510	0,401337	0,800755	0,401602	0,141975
Huseby Klev	D	0,607789	0,404752	0,704325	0,405967	0,123002
Huseby Klev	E	0,548071	0,443578	0,580885	0,476128	0,121556
Huseby Klev	F	0,541958	0,448799	0,527216	0,521350	0,121615
Huseby Klev	G	0,517527	0,446129	0,528448	0,503908	0,115442
Huseby Klev	H	0,505139	0,484686	0,603326	0,506159	0,122417
Huseby Klev	I	0,540297	0,501743	0,630542	0,526154	0,135545
Huseby Klev	J	0,681274	0,558838	0,692812	0,621422	0,190361
Gamla Skogsby	A	0,636882	0,232225	0,372424	0,416480	0,073950
Gamla Skogsby	B	0,648250	0,235317	0,366879	0,435775	0,076272
Gamla Skogsby	C	0,669934	0,237620	0,344330	0,483200	0,079595
Gamla Skogsby	D	0,734715	0,256124	0,383282	0,517414	0,094089
Gamla Skogsby	E	0,854478	0,260714	0,468020	0,533798	0,111387
Gamla Skogsby	F	0,794550	0,251176	0,391479	0,554433	0,099786
Gamla Skogsby	G	0,722134	0,266574	0,399628	0,501182	0,096251
Gamla Skogsby	H	0,841246	0,265000	0,443223	0,553527	0,111465
Gamla Skogsby	I	0,744181	0,262874	0,391604	0,524544	0,097813
Gamla Skogsby	J	0,779404	0,260384	0,353527	0,599751	0,101472
Falsterbo	A	1,146872	0,230415	0,647098	0,589115	0,132128
Falsterbo	B	1,151852	0,201766	0,724000	0,499132	0,116202
Falsterbo	C	1,278077	0,196204	0,587863	0,750040	0,125382
Falsterbo	D	1,096574	0,227755	0,556134	0,631676	0,124875
Falsterbo	E	1,150215	0,208803	0,561342	0,675459	0,120084
Falsterbo	F	0,912971	0,205886	0,477858	0,523893	0,093984
Falsterbo	G	1,029445	0,255538	0,554646	0,594856	0,131531
Falsterbo	H	1,006888	0,177686	0,502619	0,565373	0,089455
Falsterbo	I	1,041533	0,228504	0,466115	0,675117	0,118997
Falsterbo	J	0,877913	0,193427	0,406514	0,555153	0,084906
Steel #4	A	0,172653	0,043556	0,107414	0,086272	0,003760
Steel #4	B	0,184776	0,077185	0,134612	0,107270	0,007131

Steel #4	C	0,207827	0,080721	0,114206	0,150512	0,008388
Steel #4	D	0,250819	0,089834	0,144783	0,164057	0,011266
Steel #4	E	0,225152	0,035185	0,078557	0,158862	0,003961
Steel #4	F	0,205393	0,051462	0,081508	0,151215	0,005285
Steel #4	G	0,229532	0,046390	0,105164	0,142892	0,005324
Steel #4	H	0,214089	0,093372	0,142661	0,141436	0,009995
Steel #4	I	0,200284	0,071279	0,148076	0,100245	0,007138
Steel #4	J	0,265872	0,066333	0,138609	0,158692	0,008818
Steel #6	A	0,176511	0,016871	0,080576	0,099166	0,001489
Steel #6	B	0,183345	0,027936	0,082527	0,109320	0,002561
Steel #6	C	0,186809	0,030341	0,070104	0,127283	0,002834
Steel #6	D	0,179380	0,023224	0,081112	0,104281	0,002083
Steel #6	E	0,188417	0,020317	0,119081	0,073929	0,001914
Steel #6	F	0,165253	0,068513	0,121543	0,094346	0,005661
Steel #6	G	0,179834	0,045798	0,095534	0,106356	0,004118
Steel #6	H	0,227362	0,022343	0,123959	0,107776	0,002540
Steel #6	I	0,199771	0,057646	0,100211	0,131144	0,005758
Steel #6	J	0,196330	0,042744	0,124974	0,089732	0,004196
Steel #8	A	0,215426	0,054162	0,099765	0,142346	0,005834
Steel #8	B	0,193122	0,053272	0,106124	0,114485	0,005144
Steel #8	C	0,216849	0,045977	0,083921	0,153677	0,004985
Steel #8	D	0,208850	0,040833	0,104726	0,119601	0,004264
Steel #8	E	0,239162	0,068431	0,136508	0,139047	0,008183
Steel #8	F	0,221712	0,044274	0,074588	0,167633	0,004908
Steel #8	G	0,190598	0,024114	0,116386	0,080439	0,002298
Steel #8	H	0,218874	0,061168	0,126740	0,124007	0,006694
Steel #8	I	0,243305	0,058585	0,115093	0,155686	0,007127
Steel #8	J	0,199434	0,048066	0,117803	0,103695	0,004793

## Appendix III - SPSS PCA OUTPUT LOG

```

FACTOR
/VARIABLES WIS D LDC RDC
/MISSING LISTWISE
/ANALYSIS WIS D LDC RDC
/PRINT INITIAL DET KMO EXTRACTION ROTATION
/PLOT EIGEN
/CRITERIA FACTORS(2) ITERATE(25)
/EXTRACTION PC
/CRITERIA ITERATE(25)
/ROTATION VARIMAX
/SAVE REG(ALL)
/METHOD=CORRELATION.
    
```

----- F A C T O R   A N A L Y S I S -----

### Factor Analysis - Averages of the 10 cross-sections on each specimen

Notes		
Output Created		06-MAY-2021 13:55:48
Comments		
Input	Active Dataset	DataSet0
	Filter	<none>
	Weight	<none>
	Split File	<none>
	N of Rows in Working Data File	6
Missing Value Handling	Definition of Missing	MISSING=EXCLUDE: User-defined missing values are treated as missing.
	Cases Used	LISTWISE: Statistics are based on cases with no missing values for any variable used.



Syntax	<p>FACTOR</p> <p>/VARIABLES WIS D LDC RDC</p> <p>/MISSING LISTWISE</p> <p>/ANALYSIS WIS D LDC RDC</p> <p>/PRINT INITIAL DET KMO EXTRACTION ROTATION</p> <p>/PLOT EIGEN</p> <p>/CRITERIA FACTORS(2) ITERATE(25)</p> <p>/EXTRACTION PC</p> <p>/CRITERIA ITERATE(25)</p> <p>/ROTATION VARIMAX</p> <p>/SAVE REG(ALL)</p> <p>/METHOD=CORRELATION.</p>	
Resources	Processor Time	00:00:01,16
	Elapsed Time	00:00:00,82
	Maximum Memory Required	3264 (3,188K) bytes
Variables Created	FAC1_1	Component score 1
	FAC2_1	Component score 2

### Correlation Matrix<sup>a</sup>

a. Determinant = ,000

### KMO and Bartlett's Test

Kaiser-Meyer-Olkin Measure of Sampling Adequacy.		,502
Bartlett's Test of Sphericity	Approx. Chi-Square	24,534
	df	6
	Sig.	,000

### Communalities

	Initial	Extraction
WIS	1,000	,998
D	1,000	,994
LDC	1,000	,981
RDC	1,000	,992

Extraction Method: Principal  
Component Analysis.

### Total Variance Explained

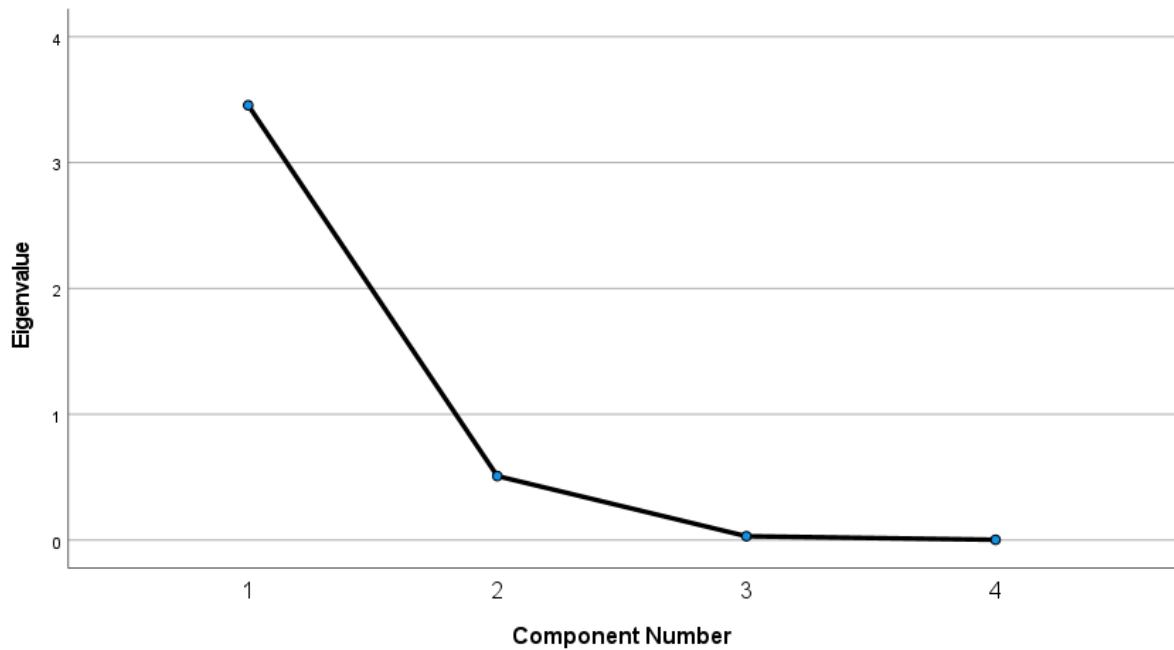
Component	Total	Initial Eigenvalues		Extraction Sums of Squared Loadings	
		% of Variance	Cumulative %	Total	% of Variance
1	3,456	86,403	86,403	3,456	86,403
2	,509	12,734	99,137	,509	12,734
3	,031	,784	99,921		
4	,003	,079	100,000		

### Total Variance Explained

Component	Extraction Sums of Squared Loadings		Rotation Sums of Squared Loadings		
	Cumulative %	Total	Total	% of Variance	Cumulative %
1	86,403	2,138	53,440		53,440
2	99,137	1,828	45,697		99,137
3					
4					

Extraction Method: Principal Component Analysis.

### Scree Plot



### Component Matrix<sup>a</sup>

	Component	
	1	2
WIS	,913	-,405
D	,860	,504
LDC	,975	,178
RDC	,965	-,245

Extraction Method: Principal

Component Analysis.<sup>a</sup>

a. 2 components extracted.

### Rotated Component Matrix<sup>a</sup>

	Component	
	1	2
WIS	,950	,310
D	,303	,950
LDC	,605	,784
RDC	,881	,464

Extraction Method: Principal

Component Analysis.

Rotation Method: Varimax with  
Kaiser Normalization.<sup>a</sup>

a. Rotation converged in 3  
iterations.

### Component Transformation Matrix

Component	1	2
1	,743	,669
2	-,669	,743

Extraction Method: Principal Component  
Analysis.

Rotation Method: Varimax with Kaiser  
Normalization.

```

* Chart Builder.
GGRAPH
  /GRAPHDATASET NAME="graphdataset" VARIABLES=PC1 PC2 Specimen MISSING=LISTWISE
REPORTMISSING=NO
  /GRAPHSPEC SOURCE=INLINE
  /FITLINE TOTAL=NO SUBGROUP=NO.
BEGIN GPL
  SOURCE: s=userSource(id("graphdataset"))
  DATA: PC1=col(source(s), name("PC1"))
  DATA: PC2=col(source(s), name("PC2"))
  DATA: Specimen=col(source(s), name("Specimen"), unit.category())
  GUIDE: axis(dim(1), label("PC1 (86,4%)"))
  GUIDE: axis(dim(2), label("PC2 (12,7%)"))
  GUIDE: legend(aesthetic(aesthetic.color.interior), label("Specimen"))
  GUIDE: text.title(label("Scatter Plot of PC2 (12,7%) by PC1 (86,4%) by
Specimen"))
  ELEMENT: point(position(PC1*PC2), color.interior(Specimen))
END GPL.

```

### GGraph - Scatter plot of averages

		Notes
Output Created		06-MAY-2021 13:58:06
Comments		
Input	Active Dataset	DataSet0
	Filter	<none>
	Weight	<none>
	Split File	<none>
	N of Rows in Working Data	6
File		

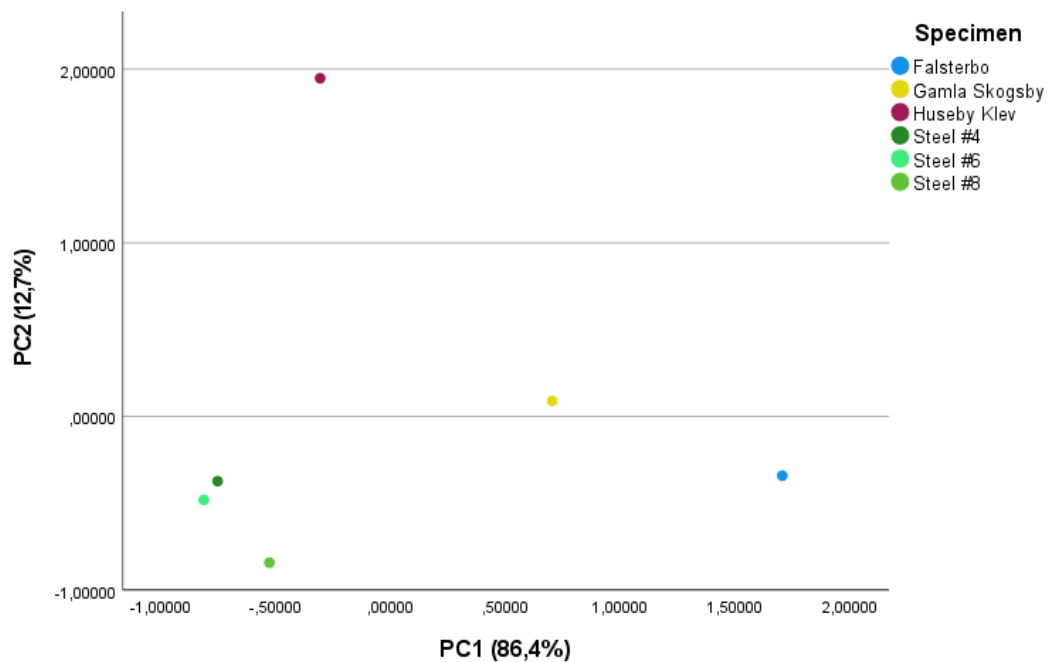
Syntax

```

GGGRAPH
  /GRAPHDATASET NAME="graphdataset" VARIABLES=PC1
PC2 Specimen MISSING=LISTWISE REPORTMISSING=NO
  /GRAPHSPEC SOURCE=INLINE
  /FITLINE TOTAL=NO SUBGROUP=NO.
BEGIN GPL
  SOURCE: s=userSource(id("graphdataset"))
  DATA: PC1=col(source(s), name("PC1"))
  DATA: PC2=col(source(s), name("PC2"))
  DATA: Specimen=col(source(s), name("Specimen"),
unit.category())
  GUIDE: axis(dim(1), label("PC1 (86,4%)"))
  GUIDE: axis(dim(2), label("PC2 (12,7%)"))
  GUIDE: legend(aesthetic(aesthetic.color.interior),
label("Specimen"))
  GUIDE: text.title(label("Scatter Plot of PC2 (12,7%) by PC1
(86,4%) by Specimen"))
  ELEMENT: point(position(PC1*PC2), color.interior(Specimen))
END GPL.

```

Resources	Processor Time	00:00:01,02
	Elapsed Time	00:00:00,51



```

FACTOR
  /VARIABLES WIS D LDC RDC

```

```

/MISSING LISTWISE
/ANALYSIS WIS D LDC RDC
/PRINT UNIVARIATE INITIAL DET KMO EXTRACTION ROTATION
/PLOT EIGEN ROTATION
/CRITERIA FACTORS(2) ITERATE(25)
/EXTRACTION PC
/CRITERIA ITERATE(25)
/ROTATION VARIMAX
/SAVE REG(ALL)
/METHOD=CORRELATION.

```

### Factor Analysis - 4 variables, analogous/simulation 10 cross-sections of each specimen

#### Notes

Output Created		04-MAY-2021 14:43:42
Comments		
Input	Data	C:\Users\Gianni Bello\OneDrive\Dokument\Skola\Masters programme\4 - Spring 2021, Masters thesis\PCA-spss.sav
	Active Dataset	DataSet1
	Filter	<none>
	Weight	<none>
	Split File	<none>
	N of Rows in Working Data File	60
Missing Value Handling	Definition of Missing	MISSING=EXCLUDE: User-defined missing values are treated as missing.
	Cases Used	LISTWISE: Statistics are based on cases with no missing values for any variable used.
Syntax	<p>FACTOR</p> <pre> /VARIABLES WIS D LDC RDC /MISSING LISTWISE /ANALYSIS WIS D LDC RDC /PRINT UNIVARIATE INITIAL DET KMO EXTRACTION ROTATION /PLOT EIGEN ROTATION /CRITERIA FACTORS(2) ITERATE(25) /EXTRACTION PC /CRITERIA ITERATE(25) /ROTATION VARIMAX /SAVE REG(ALL) /METHOD=CORRELATION. </pre>	
Resources	Processor Time	00:00:00,41

	Elapsed Time	00:00:00,31
	Maximum Memory Required	3264 (3,188K) bytes
Variables Created	FAC1_1	Component score 1
	FAC2_1	Component score 2

### Descriptive Statistics

	Mean	Std. Deviation	Analysis N
WIS	,50873547	,341238814	60
D	,17457962	,146846104	60
LDC	,32524990	,243475479	60
RDC	,32458765	,215070700	60

### Correlation Matrix<sup>a</sup>

a. Determinant = ,000

### KMO and Bartlett's Test

Kaiser-Meyer-Olkin Measure of Sampling Adequacy.		,401
Bartlett's Test of Sphericity	Approx. Chi-Square	442,008
	df	6
	Sig.	,000

### Communalities

	Initial	Extraction
WIS	1,000	,993
D	1,000	,980
LDC	1,000	,914
RDC	1,000	,944

Extraction Method: Principal

Component Analysis.

### Total Variance Explained

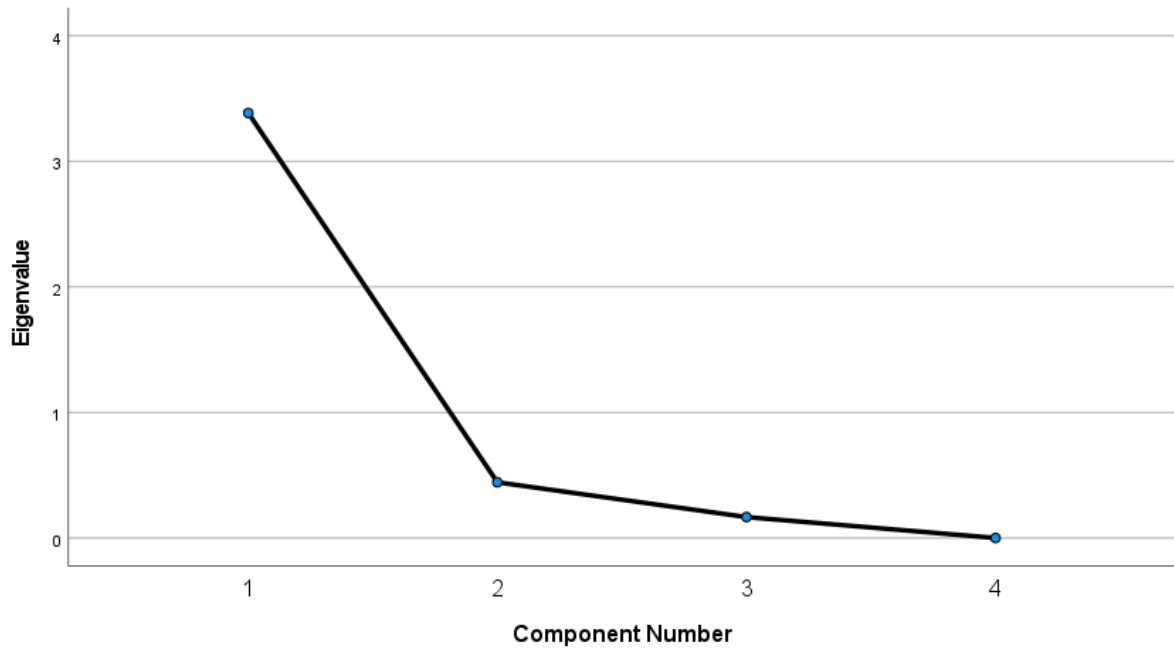
Component	Initial Eigenvalues			Extraction Sums of Squared Loadings	
	Total	% of Variance	Cumulative %	Total	% of Variance
1	3,386	84,638	84,638	3,386	84,638
2	,445	11,121	95,759	,445	11,121
3	,168	4,199	99,959		
4	,002	,041	100,000		

### Total Variance Explained

Component	Extraction Sums of Squared Loadings		Rotation Sums of Squared Loadings		
	Cumulative %	Total	% of Variance	Cumulative %	Total
1	84,638	2,022	50,561	50,561	
2	95,759	1,808	45,199	95,759	
3					
4					

Extraction Method: Principal Component Analysis.

Scree Plot



### Component Matrix<sup>a</sup>

	Component	
	1	2
WIS	,912	-,401



D	,875	,464
LDC	,942	,164
RDC	,950	-,205

Extraction Method: Principal

Component Analysis.<sup>a</sup>

a. 2 components extracted.

### Rotated Component Matrix<sup>a</sup>

	Component	
	1	2
WIS	,941	,327
D	,325	,935
LDC	,578	,761
RDC	,835	,497

Extraction Method: Principal

Component Analysis.

Rotation Method: Varimax with  
Kaiser Normalization.<sup>a</sup>

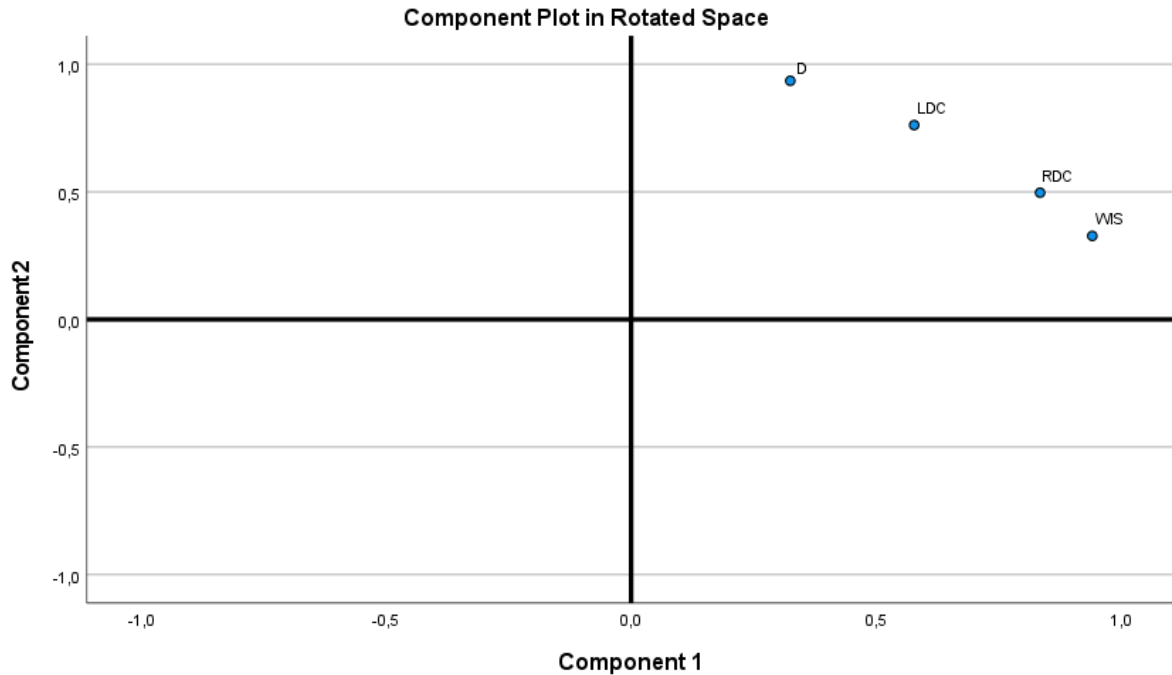
a. Rotation converged in 3  
iterations.

### Component Transformation Matrix

Component	1	2
1	,732	,681
2	-,681	,732

Extraction Method: Principal Component  
Analysis.

Rotation Method: Varimax with Kaiser  
Normalization.



\* Chart Builder.

GGRAPH

/GRAPHDATASET NAME="graphdataset" VARIABLES=PC1 PC2 CrossSection MISSING=LISTWISE  
REPORTMISSING=NO

/GRAPHSPEC SOURCE=INLINE

/FITLINE TOTAL=NO SUBGROUP=NO.

BEGIN GPL

SOURCE: s=userSource(id("graphdataset"))

DATA: PC1=col(source(s), name("PC1"))

DATA: PC2=col(source(s), name("PC2"))

DATA: CrossSection=col(source(s), name("CrossSection"), unit.category())

GUIDE: axis(dim(1), label("PC1 (84,6%)"))

GUIDE: axis(dim(2), label("PC2 (11,1%)"))

GUIDE: legend(aesthetic(aesthetic.color.interior), label("CrossSection"))

GUIDE: text.title(label("Scatter Plot of PC2 (11,1%) by PC1 (84,6%) by

CrossSection"))

ELEMENT: point(position(PC1\*PC2), color.interior(CrossSection))

END GPL.

\* Chart Builder.

GGRAPH

/GRAPHDATASET NAME="graphdataset" VARIABLES=PC1 PC2 Specimen MISSING=LISTWISE  
REPORTMISSING=NO

/GRAPHSPEC SOURCE=INLINE

/FITLINE TOTAL=NO SUBGROUP=NO.

BEGIN GPL

SOURCE: s=userSource(id("graphdataset"))

DATA: PC1=col(source(s), name("PC1"))

DATA: PC2=col(source(s), name("PC2"))

DATA: Specimen=col(source(s), name("Specimen"), unit.category())

GUIDE: axis(dim(1), label("PC1 (84,6%)"))

GUIDE: axis(dim(2), label("PC2 (11,1%)"))

GUIDE: legend(aesthetic(aesthetic.color.interior), label("Site/Specimen"))

GUIDE: text.title(label("Scatter Plot of PC2 (11,1%) by PC1 (84,6%) by  
Site/Specimen"))

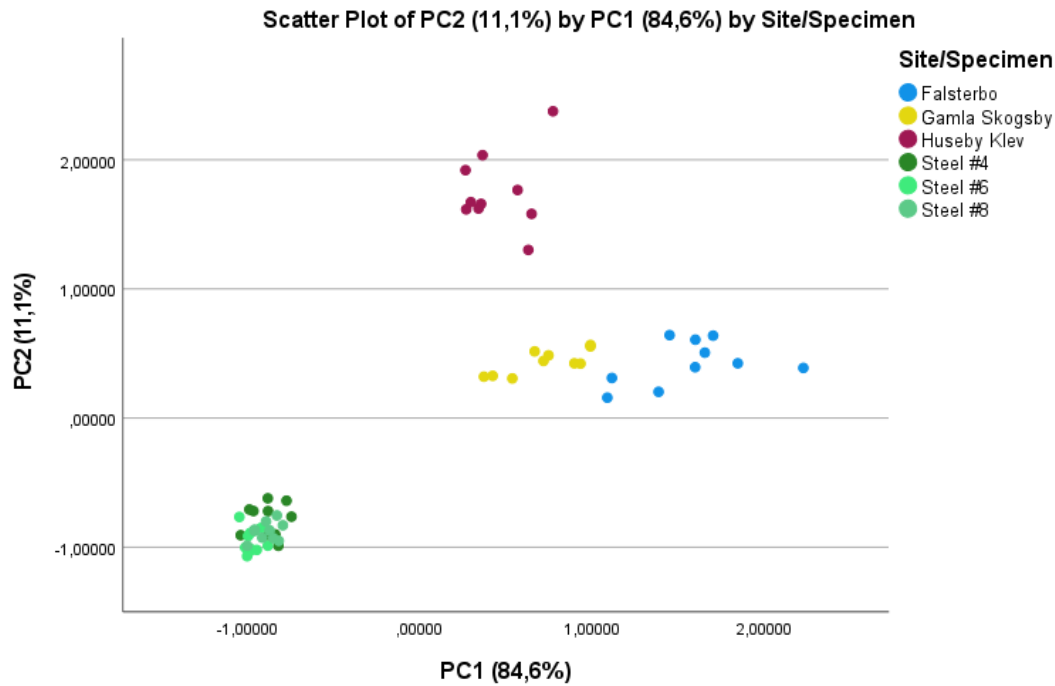
ELEMENT: point(position(PC1\*PC2), color.interior(Specimen))

END GPL.

## GGraph

### Notes

Output Created		04-MAY-2021 14:52:56
Comments		
Input	Data	C:\Users\Gianni Bello\OneDrive\Dokument\Skola\Masters programme\4 - Spring 2021, Masters thesis\PCA-spss.sav
	Active Dataset	DataSet1
	Filter	<none>
	Weight	<none>
	Split File	<none>
	N of Rows in Working Data File	60
	Syntax	<pre> GGRAPH   /GRAPHDATASET NAME="graphdataset" VARIABLES=PC1 PC2 Specimen   MISSING=LISTWISE REPORTMISSING=NO   /GRAPHSPEC SOURCE=INLINE   /FITLINE TOTAL=NO SUBGROUP=NO. BEGIN GPL   SOURCE: s=userSource(id("graphdataset"))   DATA: PC1=col(source(s), name("PC1"))   DATA: PC2=col(source(s), name("PC2"))   DATA: Specimen=col(source(s), name("Specimen"), unit.category())   GUIDE: axis(dim(1), label("PC1 (84,6%)"))   GUIDE: axis(dim(2), label("PC2 (11,1%)"))   GUIDE: legend(aesthetic(aesthetic.color.interior), label("Site/Specimen"))   GUIDE: text.title(label("Scatter Plot of PC2 (11,1%) by PC1 (84,6%) by   Site/Specimen"))   ELEMENT: point(position(PC1*PC2), color.interior(Specimen)) END GPL. </pre>
Resources	Processor Time	00:00:00,28
	Elapsed Time	00:00:00,22



DATASET ACTIVATE DataSet1.

SAVE OUTFILE='C:\Users\Gianni Bello\OneDrive\Dokument\Skola\Masters programme\4 - Spring 2021, '+  
'Masters thesis\PCA-spss.sav'  
/COMPRESSED.

FACTOR  
/VARIABLES WIS D  
/MISSING LISTWISE  
/ANALYSIS WIS D  
/PRINT UNIVARIATE INITIAL DET KMO EXTRACTION ROTATION  
/PLOT EIGEN ROTATION  
/CRITERIA FACTORS(2) ITERATE(25)  
/EXTRACTION PC  
/CRITERIA ITERATE(25)  
/ROTATION VARIMAX  
/SAVE REG(ALL)  
/METHOD=CORRELATION.

**Factor Analysis - 2 variables, analagous/simulation 10 cross-sections of each specimen**

### Notes

Output Created	04-MAY-2021 15:47:16
Comments	

Input	Data	C:\Users\Gianni Bello\OneDrive\Dokument\Skola\Masters programme\4 - Spring 2021, Masters thesis\PCA- spss.sav
	Active Dataset	DataSet1
	Filter	<none>
	Weight	<none>
	Split File	<none>
	N of Rows in Working Data File	60
	Missing Value Handling	Definition of Missing
Cases Used		LISTWISE: Statistics are based on cases with no missing values for any variable used.
Syntax	<p>FACTOR</p> <p>/VARIABLES WIS D</p> <p>/MISSING LISTWISE</p> <p>/ANALYSIS WIS D</p> <p>/PRINT UNIVARIATE INITIAL DET KMO</p> <p>EXTRACTION ROTATION</p> <p>/PLOT EIGEN ROTATION</p> <p>/CRITERIA FACTORS(2) ITERATE(25)</p> <p>/EXTRACTION PC</p> <p>/CRITERIA ITERATE(25)</p> <p>/ROTATION VARIMAX</p> <p>/SAVE REG(ALL)</p> <p>/METHOD=CORRELATION.</p>	
Resources	Processor Time	00:00:00,45
	Elapsed Time	00:00:00,59
	Maximum Memory Required	1336 (1,305K) bytes
Variables Created	FAC1_2	Component score 1
	FAC2_2	Component score 2

### Descriptive Statistics

	Mean	Std. Deviation	Analysis N
WIS	,50873547	,341238814	60
D	,17457962	,146846104	60

### Correlation Matrix<sup>a</sup>

a. Determinant = ,638

### KMO and Bartlett's Test

Kaiser-Meyer-Olkin Measure of Sampling Adequacy.		,500
Bartlett's Test of Sphericity	Approx. Chi-Square	25,799
	df	1
	Sig.	,000

### Communalities

	Initial	Extraction
WIS	1,000	1,000
D	1,000	1,000

Extraction Method: Principal Component Analysis.

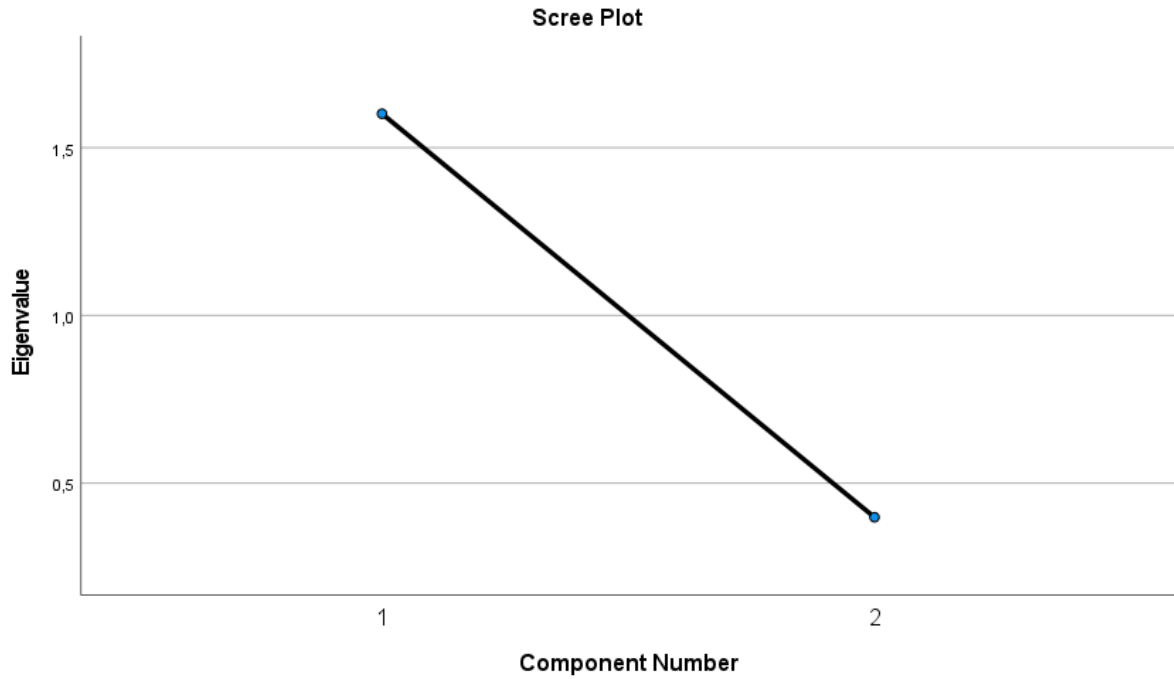
### Total Variance Explained

Component	Total	Initial Eigenvalues		Extraction Sums of Squared Loadings	
		% of Variance	Cumulative %	Total	% of Variance
1	1,601	80,064	80,064	1,601	80,064
2	,399	19,936	100,000	,399	19,936

### Total Variance Explained

Component	Extraction Sums of Squared Loadings		Rotation Sums of Squared Loadings		
	Total	% of Variance	Total	% of Variance	Cumulative %
1	1,000	50,000	1,000	50,000	50,000
2	1,000	50,000	1,000	50,000	100,000

Extraction Method: Principal Component Analysis.



### Component Matrix<sup>a</sup>

	Component	
	1	2
WIS	,895	,447
D	,895	-,447

Extraction Method: Principal

Component Analysis.<sup>a</sup>

a. 2 components extracted.

### Rotated Component Matrix<sup>a</sup>

	Component	
	1	2
WIS	,317	,948
D	,948	,317

Extraction Method: Principal

Component Analysis.

Rotation Method: Varimax with

Kaiser Normalization.<sup>a</sup>

a. Rotation converged in 3 iterations.

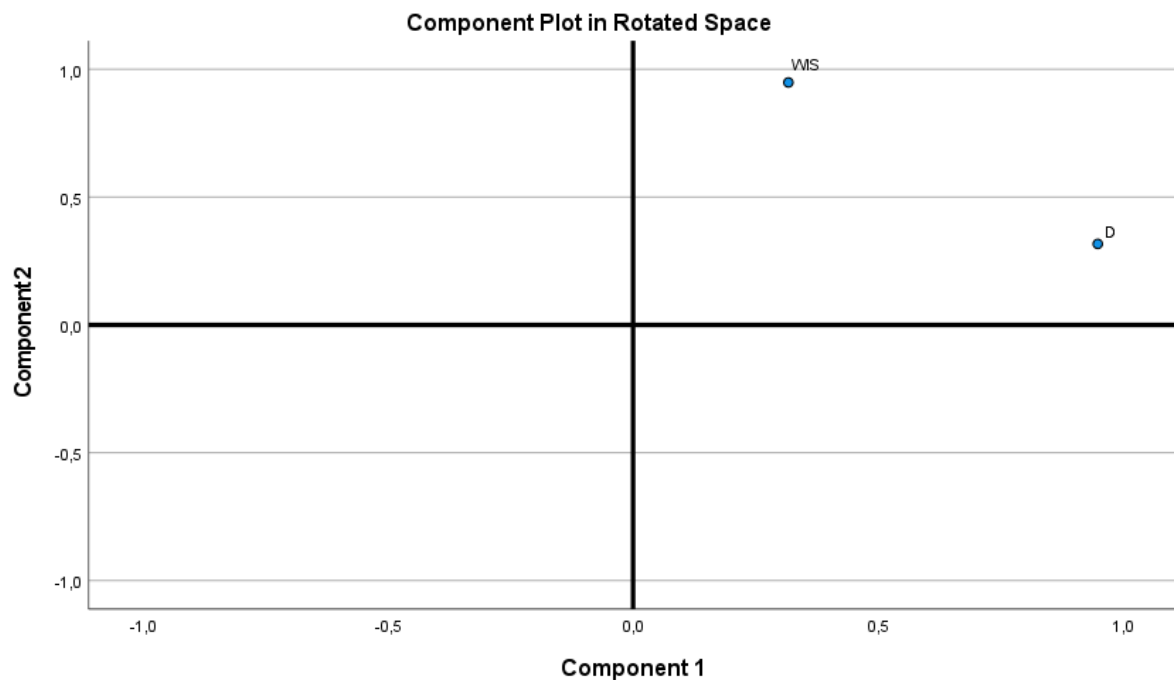
### Component Transformation Matrix

Component	1	2
1	,707	,707
2	-,707	,707

Extraction Method: Principal Component Analysis.

Rotation Method: Varimax with Kaiser

Normalization.



\* Chart Builder.

GGRAPH

/GRAPHDATASET NAME="graphdataset" VARIABLES=PC1wisdSim PC2wisdSim Specimen

MISSING=LISTWISE

REPORTMISSING=NO

/GRAPHSPEC SOURCE=INLINE

/FITLINE TOTAL=NO SUBGROUP=NO.

BEGIN GPL

SOURCE: s=userSource(id("graphdataset"))

DATA: PC1wisdSim=col(source(s), name("PC1wisdSim"))

DATA: PC2wisdSim=col(source(s), name("PC2wisdSim"))

DATA: Specimen=col(source(s), name("Specimen"), unit.category())

GUIDE: axis(dim(1), label("PC1 (80,1)"))

GUIDE: axis(dim(2), label("PC2 (19,9)"))



```

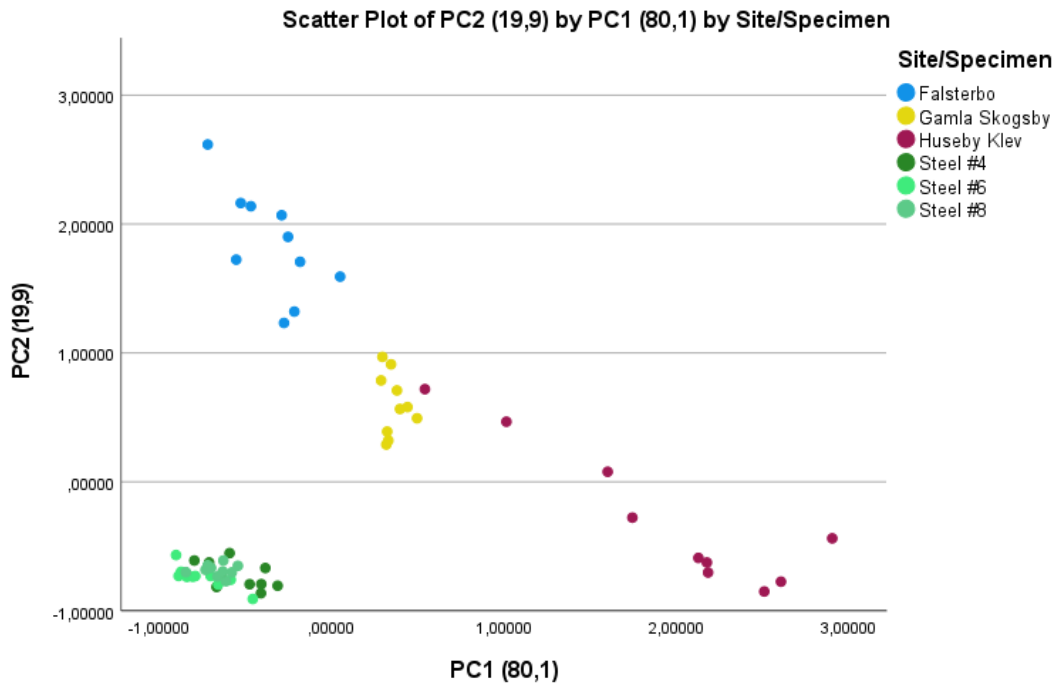
GUIDE: legend(aesthetic(aesthetic.color.interior), label("Site/Specimen"))
GUIDE: text.title(label("Scatter Plot of PC2 (19,9) by PC1 (80,1) by
Site/Specimen"))
ELEMENT: point(position(PC1wisdSim*PC2wisdSim), color.interior(Specimen))
END GPL.

```

## GGraph

### Notes

Output Created		04-MAY-2021 15:51:16
Comments		
Input	Data	C:\Users\Gianni Bello\OneDrive\Dokument\Skola\Masters programme\4 - Spring 2021, Masters thesis\PCA-spss.sav
	Active Dataset	DataSet1
	Filter	<none>
	Weight	<none>
	Split File	<none>
	N of Rows in Working Data File	60
Syntax	<pre> GGRAPH   /GRAPHDATASET NAME="graphdataset" VARIABLES=PC1wisdSim PC2wisdSim Specimen MISSING=LISTWISE   REPORTMISSING=NO   /GRAPHSPEC SOURCE=INLINE   /FITLINE TOTAL=NO SUBGROUP=NO. BEGIN GPL   SOURCE: s=userSource(id("graphdataset"))   DATA: PC1wisdSim=col(source(s), name("PC1wisdSim"))   DATA: PC2wisdSim=col(source(s), name("PC2wisdSim"))   DATA: Specimen=col(source(s), name("Specimen"), unit.category())   GUIDE: axis(dim(1), label("PC1 (80,1)"))   GUIDE: axis(dim(2), label("PC2 (19,9)"))   GUIDE: legend(aesthetic(aesthetic.color.interior), label("Site/Specimen"))   GUIDE: text.title(label("Scatter Plot of PC2 (19,9) by PC1 (80,1) by Site/Specimen"))   ELEMENT: point(position(PC1wisdSim*PC2wisdSim), color.interior(Specimen)) END GPL. </pre>	
Resources	Processor Time	00:00:00,17
	Elapsed Time	00:00:00,20



\* Chart Builder.

GGRAPH

/GRAPHDATASET NAME="graphdataset" VARIABLES=WIS D Specimen MISSING=LISTWISE  
REPORTMISSING=NO

/GRAPHSPEC SOURCE=INLINE

/FITLINE TOTAL=NO SUBGROUP=NO.

BEGIN GPL

SOURCE: s=userSource(id("graphdataset"))

DATA: WIS=col(source(s), name("WIS"))

DATA: D=col(source(s), name("D"))

DATA: Specimen=col(source(s), name("Specimen"), unit.category())

GUIDE: axis(dim(1), label("WIS"))

GUIDE: axis(dim(2), label("D"))

GUIDE: legend(aesthetic(aesthetic.color.interior), label("Site/Specimen"))

GUIDE: text.title(label("Scatter Plot of D by WIS by Site/Specimen"))

ELEMENT: point(position(WIS\*D), color.interior(Specimen))

END GPL.

## GGraph - not PCA, scatter plot using WIS and D

### Notes

Output Created		04-MAY-2021 15:58:34
Comments		
Input	Data	C:\Users\Gianni Bello\OneDrive\Dokument\Skola\Masters programme\4 - Spring 2021, Masters thesis\PCA-spss.sav
	Active Dataset	DataSet1
	Filter	<none>
	Weight	<none>
	Split File	<none>

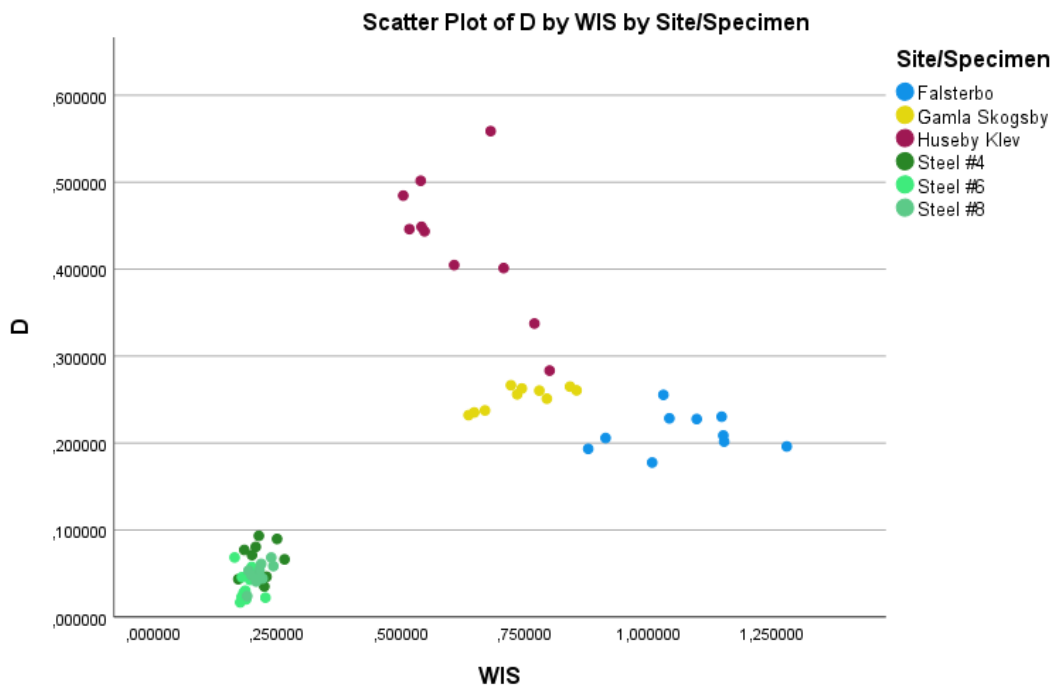
Syntax

```
GGRAPH
/GRAPHDATASET NAME="graphdataset" VARIABLES=WIS D Specimen
MISSING=LISTWISE REPORTMISSING=NO
/GRAPHSPEC SOURCE=INLINE
/FITLINE TOTAL=NO SUBGROUP=NO.
BEGIN GPL
SOURCE: s=userSource(id("graphdataset"))
DATA: WIS=col(source(s), name("WIS"))
DATA: D=col(source(s), name("D"))
DATA: Specimen=col(source(s), name("Specimen"), unit.category())
GUIDE: axis(dim(1), label("WIS"))
GUIDE: axis(dim(2), label("D"))
GUIDE: legend(aesthetic(aesthetic.color.interior), label("Site/Specimen"))
GUIDE: text.title(label("Scatter Plot of D by WIS by Site/Specimen"))
ELEMENT: point(position(WIS*D), color.interior(Specimen))
END GPL.
```

Resources

Processor Time  
Elapsed Time

00:00:00,17  
00:00:00,19



DATASET ACTIVATE DataSet1.

SAVE OUTFILE='C:\Users\Gianni Bello\OneDrive\Dokument\Skola\Masters programme\4 - Spring 2021, '+  
'Masters thesis\PCA-spss.sav'  
/COMPRESSED.

# Huseby Klev

**Huseby Klev model report**

**20 April 2021**



# Survey Data

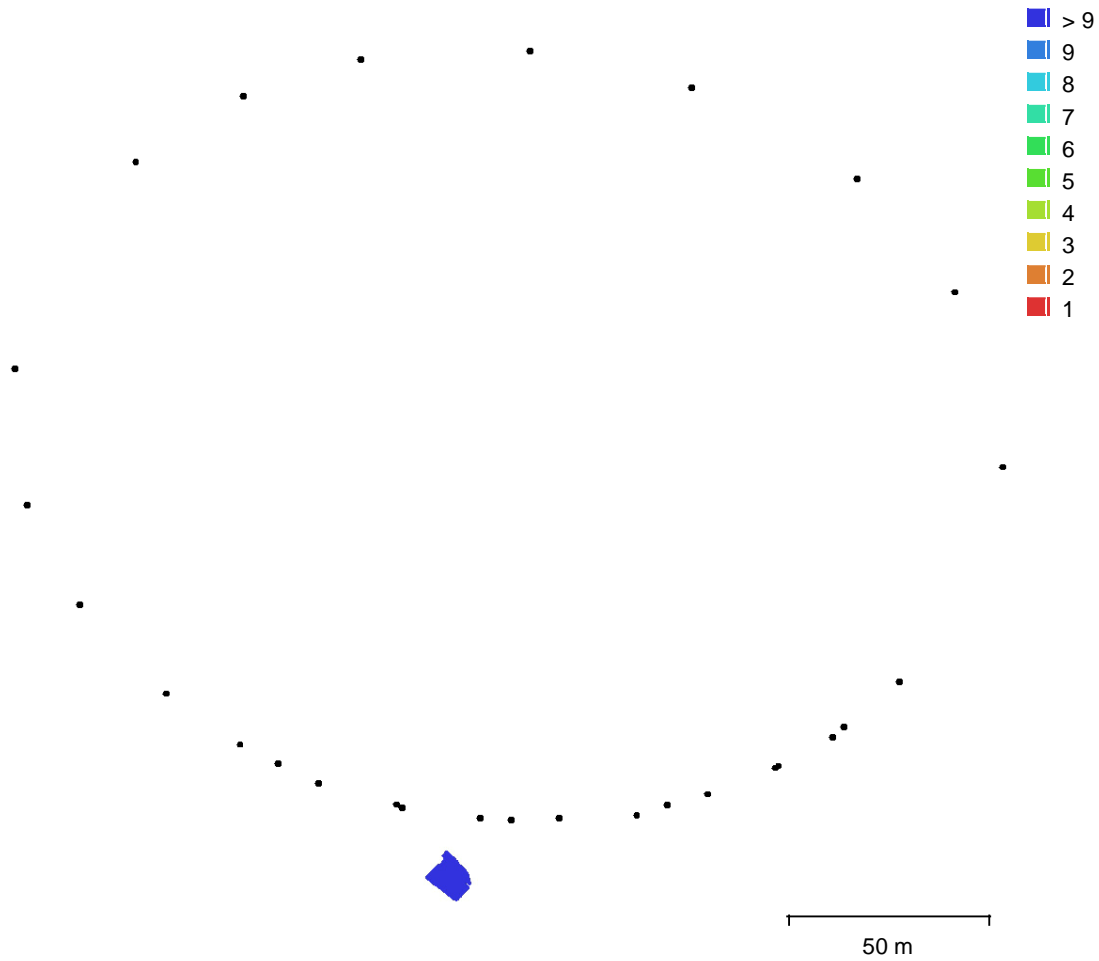


Fig. 1. Camera locations and image overlap.

Number of images:	28	Camera stations:	28
Flying altitude:	210 m	Tie points:	4,826
Ground resolution:	5.7 mm/pix	Projections:	22,017
Coverage area:	79.3 m <sup>2</sup>	Reprojection error:	1.33 pix

	Resolution	Focal Length	Pixel Size
II, TAMRON SP 90mm F/2.8 Di VC USD MACRO1:1 F017 (90mm)	6240 x 4160	90 mm	3.79 x 3.79

Table 1. Cameras.

# Camera Calibration

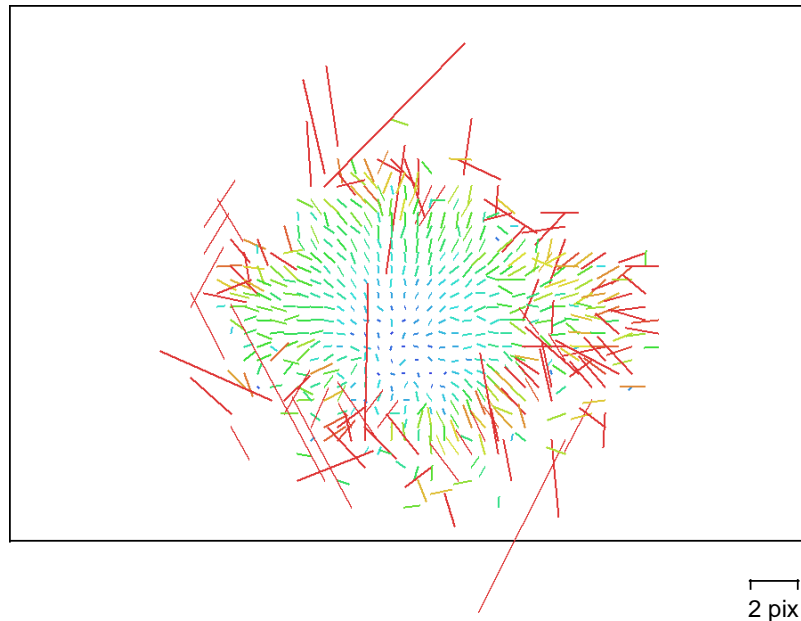


Fig. 2. Image residuals for Canon EOS 6D Mark II, TAMRON SP 90mm F/2.8 Di VC USD MACRO1:1 F017 (90mm).

## Canon EOS 6D Mark II, TAMRON SP 90mm F/2.8 Di VC USD MACRO1:1 F017 (90mm)

28 images

Type	Resolution	Focal Length	Pixel Size
<b>Frame</b>	<b>6240 x 4160</b>	<b>90 mm</b>	<b>3.79 x 3.79 <math>\mu\text{m}</math></b>

	Value	Error	F	Cx	Cy	K1	K2	K3	P1	P2
<b>F</b>	<b>36843.2</b>	4.5e+02	1.00	-0.32	-0.44	-0.21	0.15	-0.10	-0.28	-0.05
<b>Cx</b>	<b>28.5307</b>	33		1.00	0.74	0.06	-0.23	0.24	0.55	0.60
<b>Cy</b>	<b>-244.208</b>	3.7e+02			1.00	0.03	-0.29	0.30	0.64	0.85
<b>K1</b>	<b>0.489947</b>	0.29				1.00	-0.84	0.70	0.00	-0.18
<b>K2</b>	<b>-84.0504</b>	2.1e+02					1.00	-0.96	-0.15	-0.20
<b>K3</b>	<b>15189.4</b>	5.6e+04						1.00	0.13	0.24
<b>P1</b>	<b>0.00658874</b>	0.00092							1.00	0.56
<b>P2</b>	<b>-0.0648067</b>	0.0065								1.00

Table 2. Calibration coefficients and correlation matrix.

# Scale Bars

<b>Label</b>	<b>Distance (m)</b>	<b>Error (m)</b>
point 1_point 2	3.96622	-0.0337776
point 3_point 4	5.02754	0.0275377
<b>Total</b>		<b>0.030816</b>

Table 3. Control scale bars.

# Digital Elevation Model

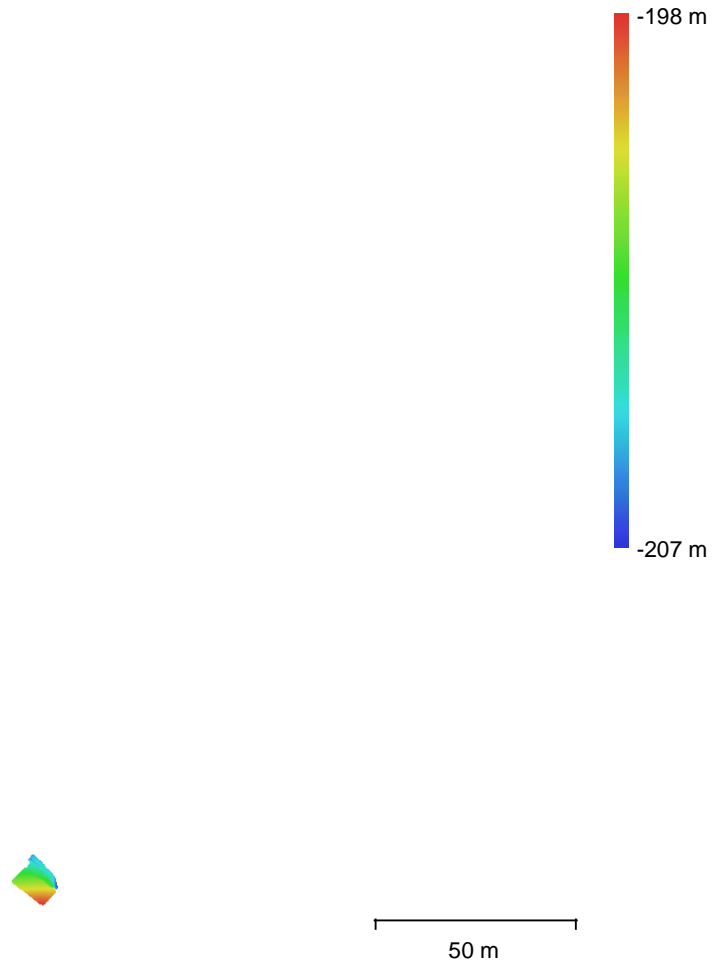


Fig. 3. Reconstructed digital elevation model.

Resolution: unknown  
Point density: unknown



# Processing Parameters

## General

Cameras	28
Aligned cameras	28
Markers	4
Scale bars	2
Coordinate system	Local Coordinates (m)
Rotation angles	Yaw, Pitch, Roll

## Point Cloud

Points	4,826 of 15,253
RMS reprojection error	0.169691 (1.33096 pix)
Max reprojection error	0.892138 (16.1198 pix)
Mean key point size	7.9935 pix
Point colors	3 bands, uint8
Key points	No
Average tie point multiplicity	4.59569

## Alignment parameters

Accuracy	Highest
Generic preselection	Yes
Reference preselection	No
Key point limit	40,000
Tie point limit	4,000
Exclude stationary tie points	Yes
Guided image matching	No
Adaptive camera model fitting	No
Matching time	53 seconds
Matching memory usage	4.38 GB
Alignment time	55 seconds
Alignment memory usage	57.20 MB

## Optimization parameters

Parameters	f, cx, cy, k1-k3, p1, p2
Adaptive camera model fitting	Yes
Optimization time	1 seconds
Software version	1.7.2.12070
File size	1.23 MB

## Depth Maps

Count	28
<b>Depth maps generation parameters</b>	
Quality	Ultra High
Filtering mode	Mild
Processing time	16 minutes 30 seconds
File size	232.87 MB

## Dense Point Cloud

Points	4,222,939
Point colors	3 bands, uint8
<b>Depth maps generation parameters</b>	
Quality	Ultra High
Filtering mode	Mild
Processing time	16 minutes 30 seconds
<b>Dense cloud generation parameters</b>	
Processing time	10 minutes 43 seconds

Software version	1.7.2.12070
File size	128.28 MB
<b>Model</b>	
Faces	841,602
Vertices	421,922
Vertex colors	3 bands, uint8
Texture	2,560 x 2,560, 4 bands, uint8
<b>Depth maps generation parameters</b>	
Quality	Ultra High
Filtering mode	Mild
Processing time	16 minutes 30 seconds
<b>Reconstruction parameters</b>	
Surface type	Arbitrary
Source data	Dense cloud
Interpolation	Enabled
Strict volumetric masks	No
Processing time	2 minutes 36 seconds
Memory usage	2.26 GB
<b>Texturing parameters</b>	
Mapping mode	Generic
Blending mode	Mosaic
Texture size	2,560
Enable hole filling	No
Enable ghosting filter	No
UV mapping time	3 minutes 26 seconds
UV mapping memory usage	590.64 MB
Blending time	4 seconds
Blending memory usage	2.11 GB
Software version	1.7.2.12070
File size	42.38 MB
<b>System</b>	
Software name	Agisoft Metashape Professional
Software version	1.7.2 build 12070
OS	Windows 64 bit
RAM	15.95 GB
CPU	Intel(R) Core(TM) i5-6600K CPU @ 3.50GHz

# Gamla skogsby

Gamla skogsby model report  
20 April 2021



# Survey Data

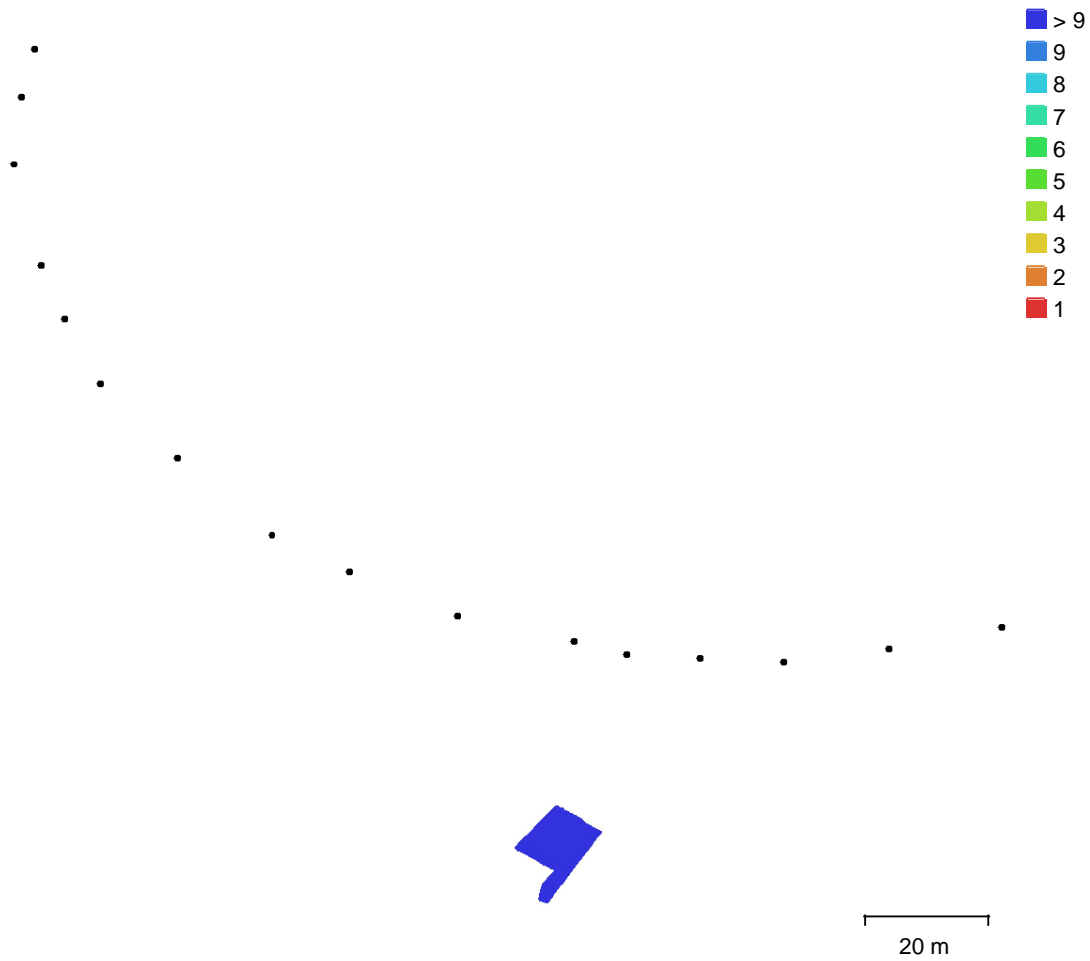


Fig. 1. Camera locations and image overlap.

Number of images:	48	Camera stations:	16
Flying altitude:	181 m	Tie points:	2,439
Ground resolution:	6.05 mm/pix	Projections:	18,985
Coverage area:	101 m <sup>2</sup>	Reprojection error:	1.73 pix

	Resolution	Focal Length	Pixel Size
II, TAMRON SP 90mm F/2.8 Di VC USD MACRO1:1 F017 (90mm)	6240 x 4160	90 mm	3.79 x 3.79

Table 1. Cameras.

# Camera Calibration

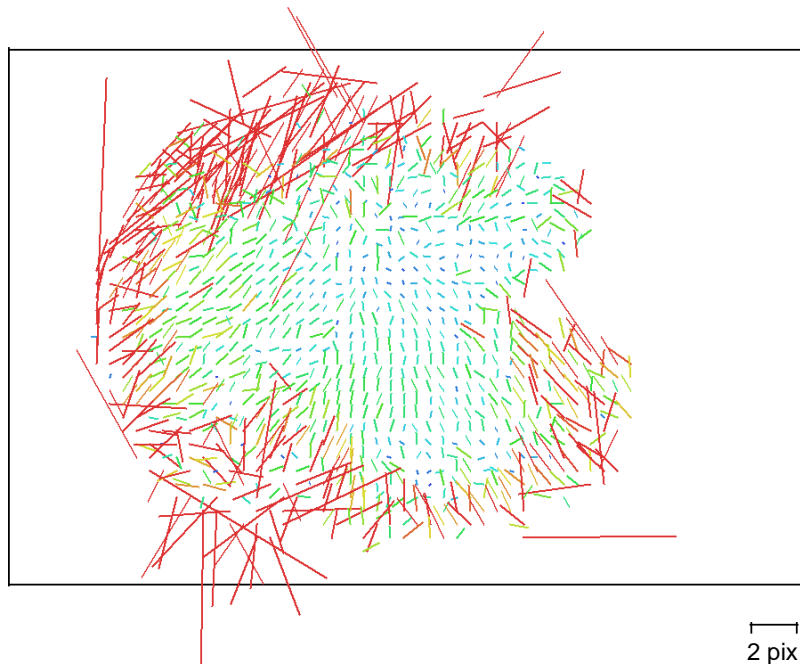


Fig. 2. Image residuals for Canon EOS 6D Mark II, TAMRON SP 90mm F/2.8 Di VC USD MACRO1:1 F017 (90mm).

## Canon EOS 6D Mark II, TAMRON SP 90mm F/2.8 Di VC USD MACRO1:1 F017 (90mm)

48 images

Type	Resolution	Focal Length	Pixel Size
Frame	<b>6240 x 4160</b>	<b>90 mm</b>	<b>3.79 x 3.79 <math>\mu\text{m}</math></b>

	Value	Error	F	Cx	Cy	K1	K2	K3	P1	P2
F	<b>29854.9</b>	3.1e+02	1.00	0.13	-0.11	-0.30	0.17	-0.10	0.06	0.91
Cx	<b>30.45</b>	18		1.00	0.34	-0.02	0.03	-0.04	0.35	0.05
Cy	<b>223.194</b>	1.3e+02			1.00	-0.10	0.09	-0.08	0.39	0.05
K1	<b>0.089711</b>	0.21				1.00	-0.92	0.84	-0.05	-0.27
K2	<b>29.6246</b>	68					1.00	-0.97	0.05	0.13
K3	<b>-1754.39</b>	6.3e+03						1.00	-0.04	-0.06
P1	<b>0.00825692</b>	0.00033							1.00	0.18
P2	<b>-0.132749</b>	0.0027								1.00

Table 2. Calibration coefficients and correlation matrix.

# Scale Bars

<b>Label</b>	<b>Distance (m)</b>	<b>Error (m)</b>
point 1_point 2	4.97072	-0.0292826
point 3_point 4	3.04408	0.044079
<b>Total</b>		<b>0.0374195</b>

Table 3. Control scale bars.

# Digital Elevation Model

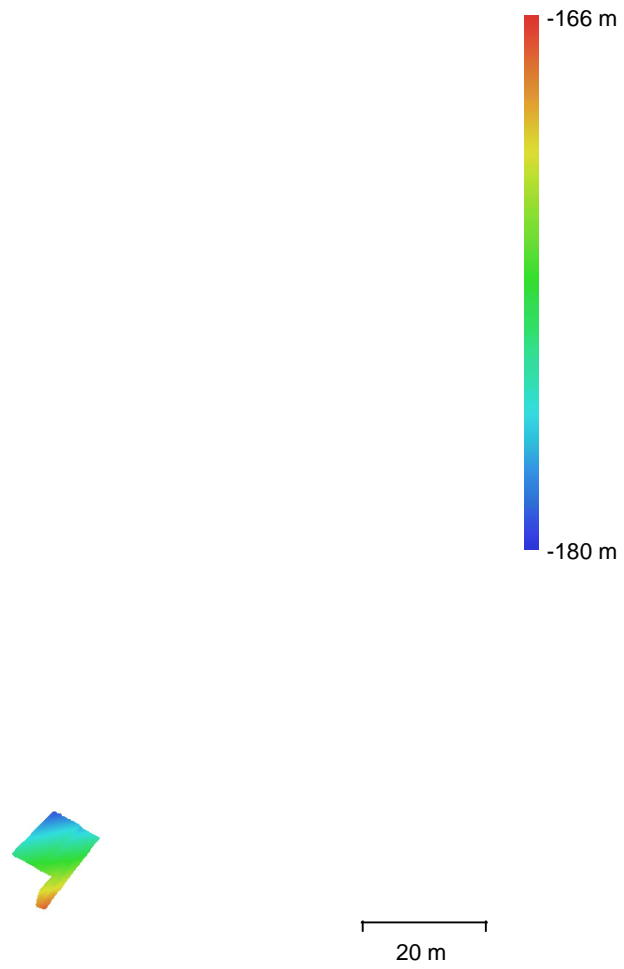


Fig. 3. Reconstructed digital elevation model.

Resolution: unknown  
Point density: unknown

# Processing Parameters

## General

Cameras	48
Aligned cameras	16
Markers	4
Scale bars	2
Coordinate system	Local Coordinates (m)
Rotation angles	Yaw, Pitch, Roll

## Point Cloud

Points	2,439 of 10,444
RMS reprojection error	0.174636 (1.73463 pix)
Max reprojection error	0.592495 (14.6045 pix)
Mean key point size	9.82864 pix
Point colors	3 bands, uint8
Key points	No
Average tie point multiplicity	6.13194

## Alignment parameters

Accuracy	Highest
Generic preselection	Yes
Reference preselection	No
Key point limit	40,000
Tie point limit	4,000
Filter points by mask	Yes
Mask tie points	Yes
Exclude stationary tie points	Yes
Guided image matching	No
Adaptive camera model fitting	No
Matching time	27 seconds
Matching memory usage	3.98 GB
Alignment time	13 seconds
Alignment memory usage	12.75 MB

## Optimization parameters

Parameters	f, cx, cy, k1-k3, p1, p2
Adaptive camera model fitting	Yes
Optimization time	1 seconds
Software version	1.7.2.12070
File size	1.06 MB

## Depth Maps

Count	16
-------	----

## Depth maps generation parameters

Quality	Ultra High
Filtering mode	Mild
Processing time	7 minutes 51 seconds
File size	270.58 MB

## Dense Point Cloud

Points	4,718,877
Point colors	3 bands, uint8

## Depth maps generation parameters

Quality	Ultra High
Filtering mode	Mild
Processing time	7 minutes 51 seconds



<b>Dense cloud generation parameters</b>	
Processing time	5 minutes 28 seconds
Software version	1.7.2.12070
File size	247.36 MB
<b>Model</b>	
Faces	943,774
Vertices	473,367
Vertex colors	3 bands, uint8
Texture	2,560 x 2,560, 4 bands, uint8
<b>Depth maps generation parameters</b>	
Quality	Ultra High
Filtering mode	Mild
Processing time	7 minutes 51 seconds
<b>Reconstruction parameters</b>	
Surface type	Arbitrary
Source data	Dense cloud
Interpolation	Enabled
Strict volumetric masks	No
Processing time	3 minutes 11 seconds
Memory usage	2.46 GB
<b>Texturing parameters</b>	
Mapping mode	Generic
Blending mode	Mosaic
Texture size	2,560
Enable hole filling	No
Enable ghosting filter	No
UV mapping time	3 minutes 28 seconds
UV mapping memory usage	620.56 MB
Blending time	4 seconds
Blending memory usage	2.13 GB
Software version	1.7.2.12070
File size	47.19 MB
<b>System</b>	
Software name	Agisoft Metashape Professional
Software version	1.7.2 build 12070
OS	Windows 64 bit
RAM	15.95 GB
CPU	Intel(R) Core(TM) i5-6600K CPU @ 3.50GHz
GPU(s)	AMD Radeon (TM) R9 Fury Series (Fiji)

# Falsterbo

Falsterbo model report

20 April 2021



# Survey Data

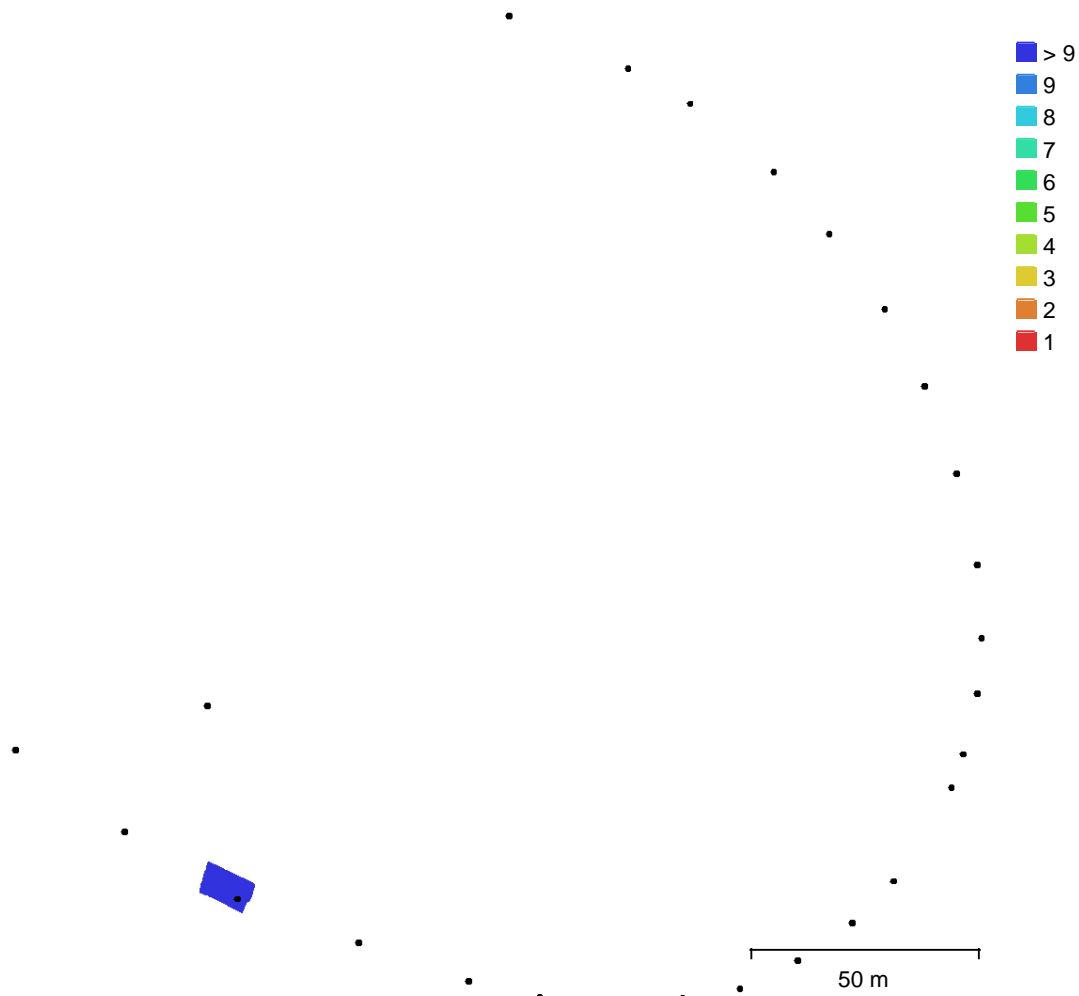


Fig. 1. Camera locations and image overlap.

Number of images:	42	Camera stations:	26
Flying altitude:	205 m	Tie points:	3,301
Ground resolution:	6.29 mm/pix	Projections:	10,858
Coverage area:	78.9 m <sup>2</sup>	Reprojection error:	2.87 pix

	Resolution	Focal Length	Pixel Size
II, TAMRON SP 90mm F/2.8 Di VC USD MACRO1:1 F017 (90mm)	6240 x 4160	90 mm	3.79 x 3.79

Table 1. Cameras.

# Camera Calibration

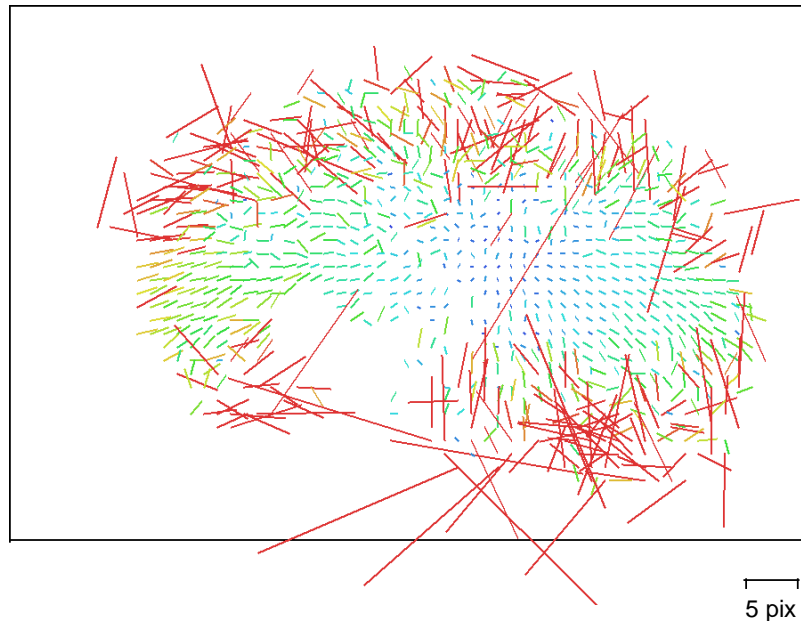


Fig. 2. Image residuals for Canon EOS 6D Mark II, TAMRON SP 90mm F/2.8 Di VC USD MACRO1:1 F017 (90mm).

## Canon EOS 6D Mark II, TAMRON SP 90mm F/2.8 Di VC USD MACRO1:1 F017 (90mm)

42 images

Type	Resolution	Focal Length	Pixel Size
Frame	<b>6240 x 4160</b>	<b>90 mm</b>	<b>3.79 x 3.79 <math>\mu\text{m}</math></b>

	Value	Error	F	Cx	Cy	K1	K2	K3	P1	P2
<b>F</b>	<b>32617.3</b>	6.5e+02	1.00	-0.22	-0.20	-0.06	0.17	-0.11	-0.30	0.51
<b>Cx</b>	<b>-184.444</b>	3.3e+02		1.00	-0.11	0.51	-0.56	0.35	0.74	-0.22
<b>Cy</b>	<b>133.565</b>	3.3e+02			1.00	-0.14	0.23	-0.24	-0.20	0.46
<b>K1</b>	<b>0.665185</b>	0.72				1.00	-0.90	0.82	0.23	-0.21
<b>K2</b>	<b>-103.957</b>	1.8e+02					1.00	-0.96	-0.47	0.27
<b>K3</b>	<b>4266.5</b>	1.3e+04						1.00	0.29	-0.24
<b>P1</b>	<b>0.00445525</b>	0.0068							1.00	-0.18
<b>P2</b>	<b>0.0346453</b>	0.0087								1.00

Table 2. Calibration coefficients and correlation matrix.

# Scale Bars

<b>Label</b>	<b>Distance (m)</b>	<b>Error (m)</b>
point 1_point 2	4.86103	-0.138973
point 3_point 4	4.17812	0.178122
<b>Total</b>		<b>0.159751</b>

Table 3. Control scale bars.

# Digital Elevation Model

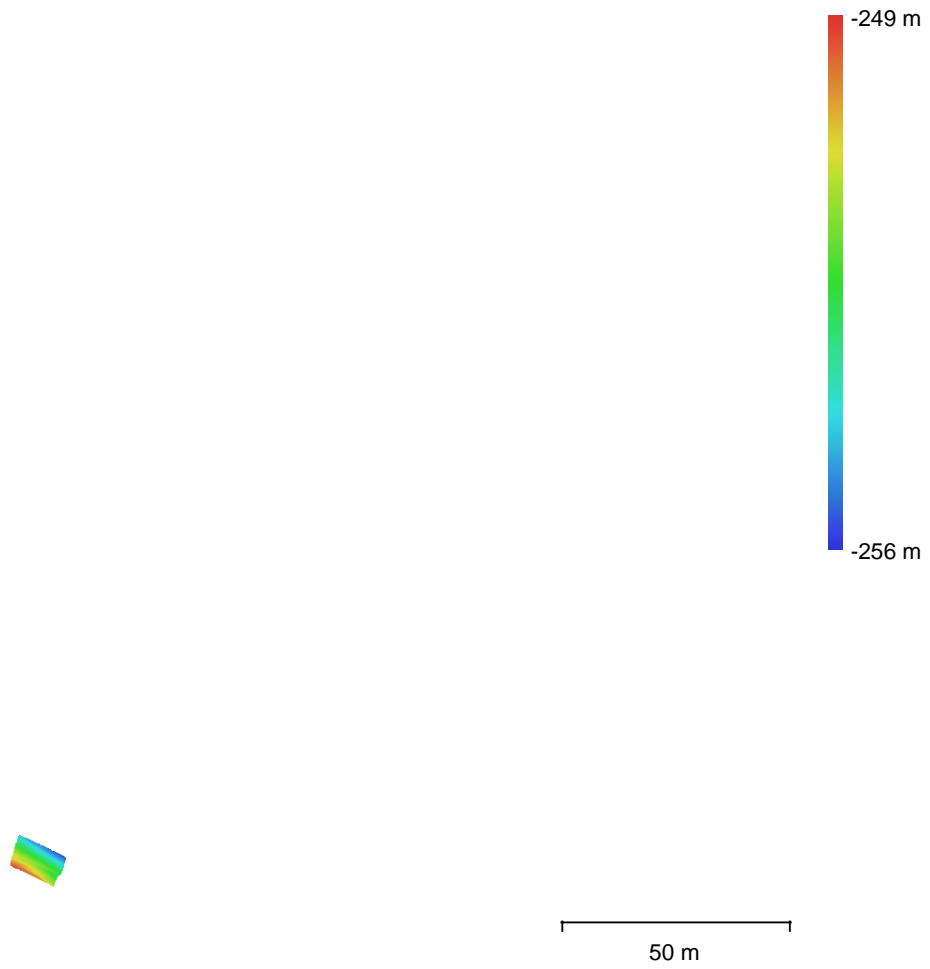


Fig. 3. Reconstructed digital elevation model.

Resolution: unknown  
Point density: unknown

# Processing Parameters

## General

Cameras	42
Aligned cameras	26
Markers	4
Scale bars	2
Coordinate system	Local Coordinates (m)
Rotation angles	Yaw, Pitch, Roll

## Point Cloud

Points	3,301 of 6,964
RMS reprojection error	0.252294 (2.86816 pix)
Max reprojection error	1.22185 (27.8039 pix)
Mean key point size	11.8538 pix
Point colors	3 bands, uint8
Key points	No
Average tie point multiplicity	3.48708

## Alignment parameters

Accuracy	Highest
Generic preselection	Yes
Reference preselection	No
Key point limit	40,000
Tie point limit	4,000
Filter points by mask	Yes
Mask tie points	Yes
Exclude stationary tie points	Yes
Guided image matching	No
Adaptive camera model fitting	No
Matching time	59 seconds
Matching memory usage	4.93 GB
Alignment time	8 seconds
Alignment memory usage	14.43 MB

## Optimization parameters

Parameters	f, cx, cy, k1-k3, p1, p2
Adaptive camera model fitting	Yes
Optimization time	0 seconds
Software version	1.7.2.12070
File size	480.67 KB

## Depth Maps

Count	17
-------	----

## Depth maps generation parameters

Quality	Ultra High
Filtering mode	Mild
Processing time	4 minutes 54 seconds
File size	126.76 MB

## Dense Point Cloud

Points	3,837,388
Point colors	3 bands, uint8

## Depth maps generation parameters

Quality	Ultra High
Filtering mode	Mild
Processing time	4 minutes 54 seconds

<b>Dense cloud generation parameters</b>	
Processing time	2 minutes 58 seconds
Software version	1.7.2.12070
File size	138.65 MB
<b>Model</b>	
Faces	758,030
Vertices	379,824
Vertex colors	3 bands, uint8
Texture	2,560 x 2,560, 4 bands, uint8
<b>Depth maps generation parameters</b>	
Quality	Ultra High
Filtering mode	Mild
Processing time	4 minutes 54 seconds
<b>Reconstruction parameters</b>	
Surface type	Arbitrary
Source data	Dense cloud
Interpolation	Enabled
Strict volumetric masks	No
Processing time	2 minutes 26 seconds
Memory usage	1.80 GB
<b>Texturing parameters</b>	
Mapping mode	Generic
Blending mode	Mosaic
Texture size	2,560
Enable hole filling	No
Enable ghosting filter	No
UV mapping time	4 minutes 34 seconds
UV mapping memory usage	438.86 MB
Blending time	4 seconds
Blending memory usage	2.06 GB
Software version	1.7.2.12070
File size	38.98 MB
<b>System</b>	
Software name	Agisoft Metashape Professional
Software version	1.7.2 build 12070
OS	Windows 64 bit
RAM	15.95 GB
CPU	Intel(R) Core(TM) i5-6600K CPU @ 3.50GHz
GPU(s)	AMD Radeon (TM) R9 Fury Series (Fiji)